공학박사 학위논문

Therapeutic Agent Coating on Structure Modified Metallic Bio-implant Surface to Improve Biological Activity

생체 활성 증진을 위한 개질 된 표면 구조를 지닌

금속 임플란트 표면 치료제 코팅

2017 년 2 월

서울대학교 대학원

재료공학부

김성원

Abstract

Therapeutic Agent Coating on Structure Modified Metallic Bio-implant Surface to Improve Biological Activity

Sungwon Kim

Department of Materials Science and Engineering

Seoul National University

Metallic implants have been widely used because of its excellent mechanical, chemical and biological stability for numerous surgical applications such as orthopedic implants, dental implants, and cardiovascular stents. However, due to the complicate biological environment in human body, the additive biological functions are desired to achieve successful cure by the metallic implants for several applications. Therapeutic agent delivery for biomedical metallic implant have received attention as a promising strategy to achieve enhanced bioactivity and additive biological functions. Therefore, various type of delivery platforms have been developed and investigated to provide desirable properties to the metallic

implants, including polymeric coating, nano-porous ceramic coating, and chemical surface modifications.

In this study, we introduced a target-ion induced plasma sputtering (TIPS)-treated surface as a platform for the delivery of therapeutic agent on metallic implant surface. A mechanically stable porous surface on metal implant created by TIPS treatment have been studied for the delivery of various type of therapeutic agent such as growth factors, antimicrobial agent, and antiproliferatvie drugs for dental and cardiovascular stent application.

Firstly, the TIPS-treated surface was applied on Ti surface to deliver the growth factor and antimicrobial agent for the improved performance of dental implant. Dental implant is the most extensively used device to substitute of problematic teeth. The dental implant is generally composed of fixture, abutment, and crown. Since the role of fixture is fixation of dental implant by being embedded in and interlocked with the jawbone, enhancement of osseointegration is required for fixture part. Therefore, bone morphogenetic protein-2 (BMP-2) was applied on the sandblasting with large grit and acid-etching (SLA) Ti surface treated with TIPS (SLA/TIPS) with optimum condition (1200 V, 10 min) for the increased BMP-2 loading efficiency. The loading efficiency enhancement were confirmed by loading and release test, and the biological effectiveness was assess by in vitro cell test using MC3T3-E1 cells. The biological activity of BMP-2 loaded SLA/TIPS surface showed significant enhancement in terms of attachment and differentiation of cells, and the osseointegration enhancement was proved by *in*

vivo animal test using dog mandible model. This study demonstrated that the BMP-2 delivery by SLA/TIPS surface is effective for the enhancement of bioactivity of dental fixture. For the abutment part, antimicrobial property is important, thus we coat the nano-scale silver (Ag) on TIPS treated Ti surface by conventional sputtering process on TIPS-treated surface varying the sputtering time form 10 s to 120 s. The antibacterial properties and the cytotoxicity of different content of Ag was evaluated using *Escherichia coli* and L929 fibroblast cells. The antibacterial activity was very effective regardless of the Ag content, but the cytotoxicity was increased as the Ag content increased. Only 10 s (TIPS-Ag10) sample didn't show the cytotoxicity in terms of cell viability. This study proved that the ultrasmall content of Ag on TIPS nano-structure can provide the additive antimicrobial property avoiding the cytotoxic effect of nano-scale Ag for dental abutment application.

In the second study, TIPS surface was introduced on Co-Cr surface for the delivery of antiproliferative agents for polymer-free drug eluting stent application. To overcome the problem of in stent restenosis, drug eluting stent containing the antiproliferative drug was invented. The conventional drug eluting stent has polymeric coating layer for the stable loading, and sustained release of antiproliferative drug. However, the polymeric coating layer on the stent surface has been found to be a critical reason for late stent thrombosis which is a very dangerous side-effect. For this reason, the delivery of antiproliferative agent having stable loading and sustained release property without polymer coating is desirable. Paclitaxel which is a kind of antiproliferative drug was loaded on the TIPS-treated

Co-Cr surface varying substrate bias (800 V and 1600 V). The loading stability under deformation was tested by strain test using Instron, and the drug on TIPS-treated surface was stably remained without delamination by mechanical anchoring effect. The release behavior of paclitaxel was also prolonged by the TIPS-treated surface. In the case of 800 V, the release behavior sustained until 21 days, and 1600 V sample showed further prolonged release behavior even until 28 days. The effectiveness of remained drug was evaluated by *in vitro* test using vascular smooth muscle cell. The attachment and proliferation was strongly inhibited by remained paclitaxel on 1600 V sample even after 21 days of release. Thus, the *in vivo* animal test using atherosclerosis rabbit model was conducted using bare Co-Cr stent, paclitaxel loaded bare Co-Cr stent and paclitaxel loaded 1600 V TIPS-treated Co-Cr stent. The restenosis was effectively inhibited by paclitaxel delivery by 1600 V TIPS-treated Co-Cr stent, compared to bare Co-Cr stent and paclitaxel loaded Co-Cr stent.

Keywords: Therapeutic agent, Bone morphogenetic protein (BMP), Silver, Paclitaxel, Delivery, Nanoporous, Dental implant, Drug eluting stent

Student number: 2011-20628

Contents

List of Tables

List of Figures

stenosis around Bare, Bare-PTX, and TIPS-PTX stents, and the (c) segmental and (d) total average I/M ratio round each stent (*P<0.05 compared to other two groups, #P<0.05 compared to Bare-PTX, &P<0.05 compared to Bare)

Chapter 1.
Introduction

1.1. Metallic bio-implants and the limitation

Metals have been widely used as materials for biomedical implant from the beginning of 20th century [1]. The metals used as implant material such as titanium (Ti), cobalt-chromium alloy (Co-Cr), and stainless steel (SUS) have excellent mechanical and chemical properties [2, 3]. The excellent mechanical stability (high strength, stiffness and toughness) of the metals contributes to reducing risk of implant failure caused by unpredictable external force. The chemical stability is associated with the biological reaction, which can disturb the human metabolism, in human body. Since the metals have excellent chemical stability, threatening body reactions such as immunogenic responses can be prevented [3]. Based on these properties, biological stability of the metals were verified by numerous *in vitro*, *in vivo* studies, and clinical studies [4-7]. Thus, metallic implants have been extensively used for commercial medical implant applications, which include dental implants, orthopedic implants, and vascular stents as shown in Figure 1.1.

Although metals have outstanding properties as biomedical implants, risk of implant failure caused by infection or side-effect is not completely solved especially for people suffering from metabolic predicament resulting from diabetes or old ages [8, 9]. To overcome the limitation, people have been tried to achieve fast tissue regeneration because risk of implant failure is significantly diminished after complete healing of adjacent tissues of implants. Thus, approaches to improve the healing rate, have been continuously conducted [10, 11]. In general, biological properties of metallic implants are strongly affected by the surface characteristics,

so that surface coating technique is a very reliable approach to modulating the biological property of metallic implants [12, 13]. Coating of bioactive materials such as hydroxyapatite, bioactive glass, or modulation of surface roughness has been conducted to achieve fast tissue regeneration [13-15]. The risk of implant failure was significantly decreased by these techniques. However, the bioactivity of those materials was not sufficient, furthermore, several biological problems could not be solved only by enhancing bioactivities. Consequently, various type of therapeutic agents to achieve high bioactivity or additive biological activities should be applied to the metallic implants.

1.2. Therapeutic agents for biomedical metallic implants

Reasons of biological problems after implant surgery are not only affected by the bioactivity of metallic implant but also affected by individual human metabolism. Even though people had same implant surgery with identically bioactive implant, the risk of implant failure could be different, because the metabolic ability of individual person is totally different. People who are old aged or suffering from metabolic syndrome have higher risk of implant failure, because their tissue regeneration rate and level of immunity are not sufficient as mentioned above [8, 9]. Therefore, it is necessary that implant has additive function appropriate to the condition of each patient, for instance, antimicrobial property for patient who has low level of immunity, and higher bioactive property for patient who has deficient healing rate.

Therapeutic agent is a kind of substance with a beneficial and desirable effect when consumed or applied and it includes antimicrobial agents, growth factors, antiproliferative agents and so on [16-18]. Applying of therapeutic agents on metallic implant is a promising way to prevent the risk of implant failure because various therapeutic agents which have various biological functions appropriate for the condition of patients are present. The functions of each therapeutic agent for biomedical metallic implants are listed below:

1.2.1. Growth factors.

Fast tissue regeneration is one of the most important goals to achieve successful implant surgery. Most biological problems are not considered if the adjacent tissues are completely regenerated, then, risk of implant failure is significantly decreased. To improve the healing rate of tissue, delivery of bioactive agent which can stimulate cells and tissues around implant is a very effective strategy [19, 20].

Growth factors play an important role for regulating cellular processes including cell attachment, proliferation, and cellular differentiation . Applying additional growth factors around implant stimulates the target tissue regeneration, leading to fast tissue regeneration after implant surgery. Various growth factors such as transforming growth factors (TGFs), fibroblast growth factors (FGFs), platelet-derived growth factor (PDDF) and bone morphogenetic proteins (BMPs) have been widely researched about their stimulating properties to cellular processes through *in vitro* and *in vivo* [21-23]. Among various growth factors, BMPs are verified as the most effective agent for the osteogenic tissue regeneration. BMP-2, especially, is well known for its excellent osteoinductive property, which intensely affects to the differentiation of mesenchymal stem cells to osteoblasts [24, 25]. However, several studies failed to achieve the enhanced tissue regeneration property because of the failure in terms of adjusting the amount of BMP-2 [26]. Therefore, the fast bone tissue regeneration can be achieved by local delivery of BMP-2 on implant surface with sufficient loading amount for dental or orthopedic

implant applications.

1.2.2. Antimicrobial agents

Risk of infection caused by microbial including bacteria, fungi, and virus adhesion surrounding implants is one of the serious concerns after implant surgery, especially for dental implant application. A number of bacteria are always living in oral environment, thus, implant site is very vulnerable to the bacteria infection after surgery [27, 28]. The bacteria infection is attributed to the bacteria adhesion and colonization, and it interferes the healthy tissue regeneration around implants [29, 30]. The phenomenon, consequently, is directly associated with implant failure.

Antimicrobial agent is a kind of therapeutic agents that kill bacteria or inhibit the growth and reproduction of bacteria. Antimicrobial agents comprise antibiotics (Penicillin, vancomycin, and aminoglycoside), fluoride, iodine, silver, and quaternary ammonium compounds. The applying of antimicrobial agent to the implant surface enables to prevent the bacteria infection, which can lead to implant failure. Among various antimicrobial agents, silver is considered to be an attractive agent due to its non-specific bactericide, which affects to broad spectrum of bacteria, and the stability in the physiological environment [27, 28]. However, silver also has cytotoxic property to human cells with high concentration [31, 32]. In this regard, the delivery with appropriate amount is one of the key factor to achieve successful implant surgery to apply the antimicrobial agent to metallic implant.

1.2.3. Antiproliferative agents

Antiproliferative agent is a substance used for inhibition of abnormal cell proliferation. One of the main uses of antiproliferative drugs is treatment of tumor, but these drugs are also used for biomedical implant applications [33, 34]. Drug eluting stent generally uses the antiproliferative drug to prevent in-stent restenosis (which means re-occlusion of blood vessel after stent surgery) problem caused by abnormal over growth of vascular smooth muscle cells [35]. Various antiproliferative drugs have been researched for the drug eluting stent application including paclitaxel, sirolimus, and tacrolimus [36-38]. Among various drugs, paclitaxel is the one of the most intensively researched drug about its property to prevent restenosis problem by *in vitro* and *in vivo* [39-41]. In the case of stent application, the delivery of antiproliferative drug should consider the sustained release property at least 21 days, and the immunogenic response to the blood and vessel [42]. Therefore, the proper delivery platform to achieve both properties is necessary for the application.

1.3. Local delivery platforms for therapeutic agents

Local delivery technique is one of the most beneficial strategies to apply the therapeutic agent effectively in other to overcome the limitation of general metallic implants. The most convenient technique for the local delivery for metallic implant is coating the therapeutic agent on the implant surface. However, direct coating of therapeutic agent on metallic implant has limitation. The amount control is not effective for the clinical surgery. The stability of coated agents is too weak so that the agents are not well delivered to the implant site. Agents are released too fast, thus the delivered agents are not able to show its effect. Therefore, delivery platforms for the stable agent delivery are essential. Several types of platforms for therapeutic agent delivery on metallic bio-implant surface are listed below:

1.3.1. Polymer coating on implants

The most widely used delivery platform for therapeutic agent is polymeric coating layer on the metallic implant surface. Therapeutic agents are incorporated in biocompatible polymers including synthetic polymers and natural polymers, and coated on the metallic implant surface. The polymeric coating layer provides loading stability, and controlled release of therapeutic agents in constant doses, consequently, the delivered agents by polymer coating platforms have enhanced the implant properties effectively. Numerous researches using polymeric coating layer as a delivery platform of therapeutic agent for metallic bio-implants have been reported [43-46].

For the growth factor delivery application, Schmidmaier et al. have developed IGFs and TGFs containing poly($_{D,L}$-Lactide) coating on Ti and SUS wires [47]. The stability and the release characteristics of growth factors contained in polymer layer were evaluated by *in vitro* and *in vivo*. The stability of growth factors remained until 42 days, and the release was sustained more than 42 days. BMP-2 is also delivered with polymeric coating layer. Han et al. have also conducted a BMP-2 encapsulated chitosan coating on Ti surfaces, and evaluated the biological properties by *in vitro* and *in vivo* [48]. The chitosan encapsulating BMP-2 coated Ti showed sufficient loading amount and sustained release more than 25 days. By local delivery of BMP-2 using chitosan coating, the cell proliferation property and differentiation properties was significantly increased at *in vitro* test using bone marrow stem cells. The *in vivo* result tested with rabbit demonstrated that the strong osteoinductivity of chitosan encapsulating BMP-2 coated implant.

The delivery of antimicrobial agents has been also conducted. GhavamiNejad et al. have developed a silver nanoparticle immobilized polydopamine coating on Ti surface to achieve antimicrobial property [49]. Stably immobilized silver nanoparticles in polydopamine coated on Ti showed sufficient antibacterial efficacy, tested by bacterial inhibition test using *Escherichia coli* and *Staphylococcus aureus* bacteria. Ammar et al. have also developed silver nanoparticle containing polymer coating for biomedical implant application. Poly-$_{L}$-lactic acid (PLLA), which is a biodegradable, biocompatible synthetic polymer, coating layer was used as a delivery platform of silver nanoparticles for stable delivery [50]. The antimicrobial efficiency of silver nanoparticles depending on the loading amount has been

evaluated with plate counting method using *Escherichia coli* and *Staphylococcus aureus*, resulting in high antimicrobial rate above 500 ppm of silver. The cytotoxicity of silver nanoparticle contained in PLLA coating layer was assessed using HeLa cells, resulting in the biocompatibility is remained until 700 ppm of silver, but most of cells were dead on 5000 ppm specimen.

For the stent application, antiproliferative drug delivery with polymeric coating layer has extensively researched. Kothwala et al. have investigated the properties of the antiproliferative paclitaxel loaded in biodegradable polymer coated on SS 316 LVM stent [51]. Poly ($_{D,L}$-Lactide)-co glycolide, Poly-($_{L}$-lactide)-co carpolactone, Poly-($_{L}$-Lactide) coating layers were used as a delivery platform for paclitaxel, and the release behavior was sustained more than 38 days. Jabara et al. have also studied the paclitaxel eluting stent delivered by biodegradable polymeric coating layer [52]. The release behavior was monitored until 140 days, and the sustained release behavior was observed. The effectiveness of paclitaxel was evaluated with the *in vivo* pig model. They found that paclitaxel eluting stent reduced the restenosis in 1 month and it showed minimal inflammation level.

Despite the beneficial properties of polymeric coating layer in terms of very stable and sustained delivery of therapeutic agents, polymer coating layer has been limited to be used for several biomedical implant applications. First, polymer coating layer is not used for dental implant application anymore because the lack of adhesion of polymer to living tissues can lead to mechanical implant failure, and the adverse immunological reactions are also reported about polymer coating for

dental applications [53]. Secondly, in the case of stent application, polymer coating layer is considered as one of the main reason of late stent thrombosis which is critically associated with the urgent death of patient. The hypersensitivity and inflammatory responses of polymer coating layer causes the late stent thrombosis [54, 55]. Recently, other types of platforms for therapeutic agent delivery are continuously researched to substitute the polymeric coating without those problems including hypersensitivity, inflammatory response.

1.3.2. Ceramic coating on implants

One of the most intensively investigated delivery platform to substitute polymer coating layer is ceramic coating layer, especially, having nano-scale porous layer such as anodized aluminum oxide layer (AAO), anodized Ti oxide (ATO) layer, and nano-structured hydroxyapatite coating [19, 56, 57]. The nano-structured ceramic coating layer provides the sufficient storage room for the therapeutic agent with a number of pores on the surface, and also provides sufficient surface area, thus enough amount of therapeutic agents can be coated on the surface [56]. Furthermore, the mechanical anchoring effect from rough surface of nano-structured ceramic coating layer makes the therapeutic agent more stable on the implant surface [58, 59]. Since the nano-structured surface has more bioactive properties, the synergetic effect between surface property and therapeutic agent can be achieved. Several researches using the ceramic coating layer as a delivery platform of therapeutic agent have been conducted.

For dental application, Bae et al. have developed anodic oxidized nanotubular Ti implant to enhance BMP-2 delivery [19]. Since the TiO_2 nanotubular structure provided improved hydrophilicity and sufficient storage room to deliver the BMP-2, higher amount of BMP-2 were loaded on the nanotubular surface with dispersed pattern. The loaded BMP-2 showed sustained release until 21 days, and the enhanced cell differentiation was confirmed using MC3T3-E1 cells. Additionally, Huh et al. have investigated the effect of BMP-2 delivered by anodized Ti surface by *in vivo* animal test [60, 61]. The assessment of biological property as dental implant was intensively conducted with *in vivo* rabbit model and beagle model. In the case of rabbit model, BMP-2 coated anodized Ti implants showed significant higher bone gain at 4 w and 8 w compared to uncoated one, and in the case of beagle model BMP-2 coated anodized Ti implants presented the enhanced bone level.

The antimicrobial agent delivery with ceramic coating layer have been developed. Carmona et al. have developed silver nano-particle contained hydroxyapatite coating on Ti alloy applied by atmospheric plasma spray method for dental application [62]. The antibacterial and cytotoxicity were investigated with 0.5, 1, 3, and 5 % of nano-silver contents in hydroxyapatite coating layer. The antibacterial efficiency was assessed with *Escherichia coli*, *Staphylococcus aureus*, and *Pseudomonas aeruginosa* strains and the hydroxyapatite coating with 1 % and higher layer showed above 99 % antibacterial rate. In the case of cytotoxicity, higher proliferation rate and the least DNA damage was observed on 1 % silver containing hydroxyapatite coating. Mei et al. have investigated that the silver

incorporated TiO_2 nanotube layer fabricated by silver plasma immersion ion implantation on anodized surface of Ti for dental application [27]. In this research, the silver amount was controlled by modulating the voltage during plasma immersion ion implantation technique. Silver incorporated at 1 kV voltage showed excellent antimicrobial properties to oral pathogens, but no cytotoxicity on epithelial cells and fibroblast cells was observed on 1kV voltage specimen.

For the stent application, the ceramic coating layer as a delivery platform of antiproliferative drug has been very importantly researched to solve the thrombosis problem. Giessen et al. have reported the hydroxyapatite coated stent for polymer-free sirolimus, which is a antiproliferative drug, eluting stent [63]. They coat the stent with 600 nm thickness of rough hydroxyapatite layer, followed by sirolimus coating, varying the amount of 25, 50, and 100 μg. The drug efficiency of sirolimus coated on hydroxyapatite coating layer was evaluated by *in vivo* swine model. The restenosis was not much changed according to the drug amount, but all the values showed similar level with the polymer coated drug eluting stent. Furthermore, the genesis of fibrinoids, which can be a marker of increasing in stent restenosis, was significantly lower than polymer coated drug eluting stent. Wieneke et al. have fabricated and evaluated the nanoporous stent coating for delivery of tacrolimus, which is also a kind of drug to suppress the smooth muscle cell activity [64]. The stent surface was covered with anodized aluminum oxide layer, and tacrolimus was coated on the anodized surface by dipping method. They checked the property of the stent with *in vivo* rabbit model. The tacrolimus loaded stent showed lower restenosis level, and inflammation score compared to bare metal stent.

However, the limitation of ceramic coating layer have been found in the field of dental implant and stent applications. The major issues of the limitation of ceramic coating layer are its brittle nature and weak bonding strength between metallic implant and coating layer. These issues cause coating fracture and delamination during or after implanting surgery. In the case of dental application, the delamination of coating layer strongly affects to the loosening of implant, then, second surgery should be under consideration, and the fractured debris of ceramic coating layer are also relevant to the formation of adverse response of surrounding tissues [65, 66]. The adverse effect of debris from coating layer was also reported for stent application. Kollum et al. have reported that the particle debris from anodized coating layer interfere the antiproliferative effect of tacrolimus [67]. In the research, the particle debris were observed in the vessel wall surrounding the ceramic coated stent. The particle debris generate the serious luminal stenosis regardless of the presence of antiproliferative drug. Based on these reports, development of mechanically stable, non-polymeric delivery platform for therapeutic agents is necessary to overcome the limitations of existing platforms.

1.3.3. Other techniques

Except the two types of platforms, other approaches have been researched for the stable delivery of therapeutic agents. That is delivery using chemically modified surface. The representative chemical modification is using self-assembled monolayer [68]. The self-assembled monolayer can capture the drug chemically.

The other chemical modification technique is just using the chemical adhesion property of drug itself to material surface. They coated the paclitaxel, which has high adsorbing property to certain materials, on Co-Cr substrate directly without using any platforms, but with very small amount which can bind to the surface chemically [69]. Even though those techniques prolongs the release behavior even up to 70 days, the total amount of loaded drug was too small compared to conventionally used drug eluting stents, at which amount may not be effective *in vivo* situation.

1.4. Target-ion plasma sputtering as a delivery platform of therapeutic agents

1.4.1. Target-ion induced plasma sputtering (TIPS) treatment

In our previous researches, we have introduced a novel nano-porous surface structure on metallic implant surface fabricated by target-ion induced plasma sputtering (TIPS) treatment [70]. The TIPS-treated surface was fabricated by sputtering process using conventional direct current magnetron sputter. Sputtering is one of the most well-known coating technique for the deposition of various metals and ceramics onto the surface of other materials. The coating principle of conventional sputtering is briefly descibed in Figure 1.2. A gaseous plasma, generally argon (Ar), accelerate the ions from the plasma into target material, then, the target atoms ejected from the ion bombardment. The ejected atoms flies form the target and impacted to the substrate, and deposited. However, In the case of TIPS process, the applied substrate bias is abnormally high negative compared with conventional sputtering process. The high negative bias induces the ion implantation of target ion and the ion beam erosion of substrate at the same time, where the nano-scale patterns are fabricated following the mechanism of ion beam erosion technique [71, 72]. However, additionally, the local sputtering yield are manipulated by implanted target material on substrate because of the sputtering yield difference between target material and substrate material. Unlike conventional ion beam erosion technique, this difference of local sputtering yield enables the tuning of pattern size from nanoscale to microscale in TIPS treatment.

1.4.2. Desirable properties of delivery platforms

Therapeutic agent delivery platform for biomedical metallic implants should be (a) biocompatible (the platform impedes the effect of therapeutic agent or make adverse effect if it is not biocompatible), (b) non-polymeric material (immunological disadvantages of polymer nature should be avoided), and (c) mechanically stable (the adverse effect from the debris of coating layer by fracture or delamination from the implant surface should be prevented). Additionally, if the structure of platform is controllable, it is possible to achieve additional effect such as enhanced bioactivity, or modulated release behavior.

1.4.3. Properties of TIPS as a delivery platform.

TIPS surface possesses the desirable properties as a delivery platform. First, it is biocompatible because the incorporated target material on the surface of implant by TIPS treatment is tantalum which has good biocompatibility, and the biological activity enhancement by TIPS treatment on Ti surface is already reported by our previous research [73]. Additionally, it is not a polymeric material so that the problems caused by polymer nature such as the hypersensitivity and immunogenic responses are not considered. Second, the nano-porous TIPS surface is mechanically stable because the nano-porous layer is not a coating layer which can be delaminated, but an etched substrate itself. The evidence is presented in the cross-sectional image of TIPS treated metal substrate (Figure 1.3 (a)). Noticeable

interface between substrate and porous layer is not observed, and the strain test results also support the stability of TIPS-treated porous layer (Figure 1.3 (b)). Even after 16 % strain, only a few cracks of struts were observed without any delaminated debris. Third one is the controllability of the pore-structures including the pore-width, pore-length, and pore-depth as shown in Figure 1.4. By the modulating the pore size, the behavior of loaded agent such as its release behavior would be controlled.

1.4.4. Aim of this study

In this study, we have tried to apply the TIPS-treated surface as a delivery platform of therapeutic agents for two different biomedical (dental implant and drug eluting stent) applications.

For the dental application, the TIPS-treated surface was applied for two components of dental implants, which are fixture and abutment. In the case of fixture part, we delivered BMP-2 by simple dipping technique on the TIPS-treated commercial Ti fixture which is modified with sandblasting with large grit and acid etching (SLA) process for enhanced osseointegration, consequently, the enhancement of loading amount, and bioactivity was intensively evaluated. In the case of abutment part, we delivered nano-structured silver by coating with sputtering on TIPS-treated Ti surface to assign antimicrobial effect. The effects of silver to the bacteria and soft-tissue cells depends on the coated Ag amount was investigated to find optimum silver coating condition for balanced activity of anti-

bacteria property and biocompatibility.

For the stent application, we delivered paclitaxel on TIPS-treated porous Co-Cr stent for stable loading even during stent expansion, and sustained release to achieve the successful suppression of in stent restenosis problem. The loading stability, and release behavior was investigated, and the biological activity of loaded drug was assessed by *in vitro* cell test and *in vivo* rabbit model.

Figure 1.1. Various types of metallic implants for biomedical applications

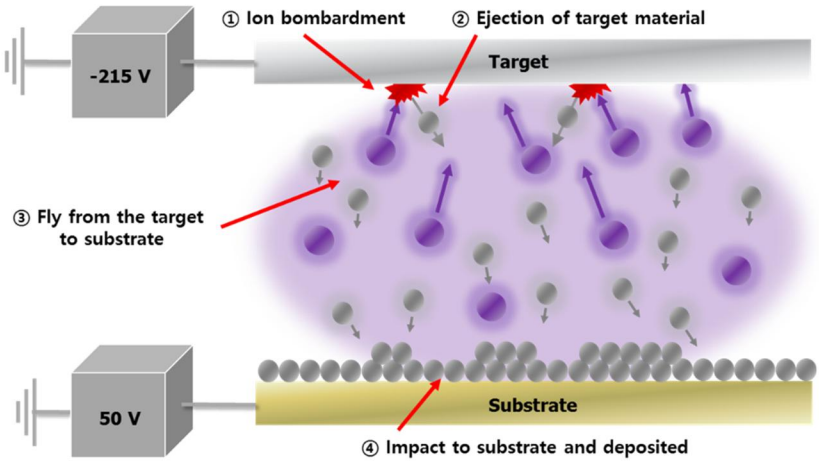

Figure 1.2. Schematic image of the deposition principle for conventional sputtering technique

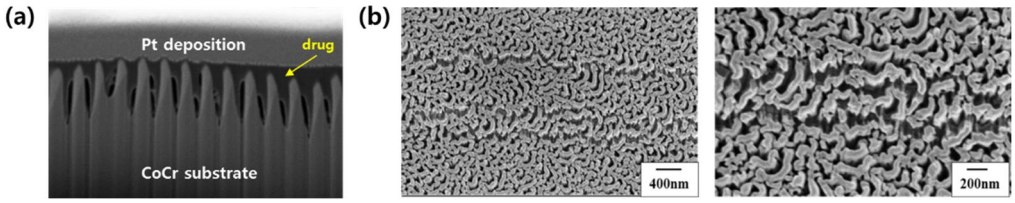

Figure 1.3. (a) The typical cross-sectional morphology of TIPS-treated Co-Cr surface, and (b) the surface morphology of TIPS-treated Co-Cr surface after 10% of strain

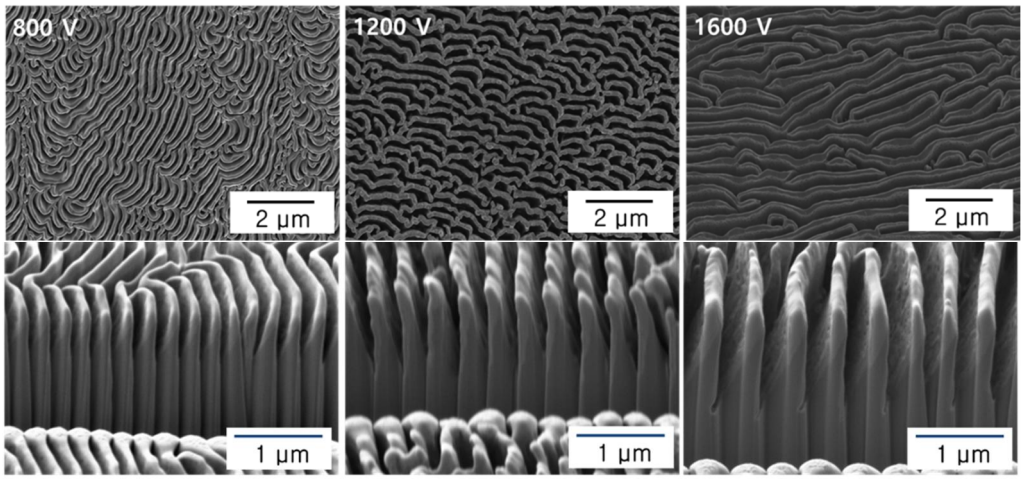

Figure 1.4. Structure changes of the TIPS-treated Co-Cr surface depending on the substrate bias

Chapter 2.

Growth Factor and Antimicrobial Agent Delivery on TIPS-treated Ti Surface for Dental Application

In this chapter, the studies focus on the improvement of dental implant ability by additive biological activity. Dental implant is the most extensively used device to substitute of problematic teeth. The dental implant is generally composed of fixture, abutment, and crown. The role of fixture is fixation of dental implant by being embedded in and interlocked with the jawbone. For this part, enhanced osseointegration property, which refers to the mechanical and chemical integration between the implant surface and living bone tissue, is most important issue so that delivery of growth factors, which can induce new bone formation, on fixture is applicable. The abutment is a part of dental implant placed on fixture part, connecting with the gum. The role of this part is supporting and securing for the placement of crown on the fixture part. However, the site between gum and abutment part can be a critical path for bacterial infection. Therefore, delivery of antibacterial agent on abutment is a promising strategy to reducing the failure rate of dental implant surgery. Here in, we treated the titanium with TIPS technique to create nano-porous surface, and delivered rhBMP-2 for fixture part, and Ag nano-particles for abutment part, respectively, and the biological properties were discussed.

2.1. Growth factor delivery on dental fixture

2.1.1. Introduction

Titanium (Ti) has been widely used as a dental implant for teeth reconstruction due to its high specific strength, endurance limit, and reasonable biocompatibility [3]. A native oxide layer on the topmost surface of Ti provides

good biological tolerance for bones growing without any corrosion or toxic reaction. This finally allows the formation of an intimate contact between the living bone and Ti surface [74]. For practical applications as a dental fixture, various surface modification techniques are employed to achieve successful osseointegration. These techniques mainly focus on the alteration of Ti surface chemistry and/or topography [10, 11]. For example, sandblasting with large grit and acid-etching (SLA) treatment has become the most widely used technique because of its successful performance in numerous clinical cases [75-77]. Micro- and submicro-scale surface roughness of SLA-treated Ti possesses a large surface area and empty spaces for mechanical anchoring with adjacent bones [78, 79]. However, Ti itself cannot meet increasing clinical demands such as enabling early implant fixation and guaranteeing the consistent success of surgical procedures without reference to patient circumstance. People suffering from metabolic syndromes such as diabetes are in danger of implant loss, which is caused by reduced angioneogenesis in early stages of bone healing and delayed bone reconstruction [8, 9].

Bioactive molecules such as extracellular protein, Arg-Gly-Asp (RGD) peptide, and growth factors have been introduced as a supplement to improve the insufficient biological performance of biomaterials and modulate neighboring cell/tissue reactions [19, 80, 81]. In particular, recombinant human bone morphogenetic protein-2 (rhBMP-2) is a well-known bioactive molecule and a powerful inducer of early differentiation events in mesenchyme stem cells leading to bone formation [24, 25]. Therefore, for decades, many researchers have

continued to apply rhBMP-2 on the surface of dental implants through various surface modification techniques [20, 25, 82]. For maximizing clinical effectiveness in biomolecule treatment, the application of a biocompatible polymer to the implant surface assists in stably loading a specific amount of rhBMP-2 onto the implant. Several studies have examined the polymer coating layer as a versatile carrier for controlling the release rate and duration of incorporated BMPs through modification of its structures [43, 83]. However, in the dental implant application, polymer coating is no longer used because of its poor mechanical stability. During the implant surgery, severe wearing is occurred between the implant surface and adjacent bones, which can easily tear the polymer coating layer and cause unpredictable immune response [53].

To achieve successful rhBMP-2 delivery from the dental implant surface, a polymer-free biomolecule delivery system of dental implant is essential. Among the various surface and coating technologies, creating a nanoporous surface layer, which provides sufficient empty storage on the surface, can enhance the loading amount and stability of rhBMP-2 on the implant surface. In previous studies, several ceramic nano-structured coatings, such as anodized TiO_2 and nano-hydroxyapatite coating layers, have been introduced for the efficient delivery of drugs and biomolecules onto the Ti surface [56, 57]. The desired amount of BMPs can be loaded just prior to the medical device operation through a simple dipping process. Therefore, there is no conflict of issues about the contamination or denaturation of pre-loaded BMPs. However, the weak interfacial bonding strength between the implant and ceramic coating layers causes severe failure in dentistry,

e.g., the delamination of the coating layer directly leads to the fixation loosening of a dental implant [65, 66].

Recently, we introduced the Ta target-ion induced plasma sputtering (TIPS) technique to create a bioactive nanoporous layer on the Ti substrate. Since nanopore formation is based on the Ta ion etching process, the fabricated nanoporous layer is considered to be a part of the substrate, composing 90% of it. In contrast, only a small portion of the implanted Ta exists on the surface [70]. Based on the superior feasibilities of the TIPS-treated metal surface, here in, we use this nanoporous surface layer as a rhBMP-2 delivery system on the SLA-Ti surface. We examine the improved efficiency of rhBMP-2 loading with a TIPS-treated SLA-Ti implant (SLA/TIPS) by observing the loading morphology of rhBMP-2 and measuring the loading amount of rhBMP-2. The enhanced osseointegration of the rhBMP-2-loaded SLA/TIPS surface is evaluated with SLA, rhBMP-2-loaded SLA (SLA-BMP), SLA/TIPS, and rhBMP-2-loaded SLA/TIPS (SLA/TIPS-BMP) via *in vitro* cell test and *in vivo* animal tests conducted on a dog model.

2.1.2. Experimental procedure

Surface modification

An SLA/TIPS surface was created by target-ion (Ta) induced plasma sputtering (TIPS) on a commercially used SLA-Ti sample (Dentium Co. Ltd., Korea), with micro-scale roughness, using a direct-current (DC) magnetron sputter (Ultech Co. Ltd., Korea). The SLA-Ti sample with a diameter of 10 mm and thickness of 2 mm was fabricated by SLA followed by etching with a hydrochloric acid solution [84]. The SLA-Ti sample was ultrasonically cleaned three times with ethanol, 10 min each, before being placed in a vacuum chamber as a substrate. The vacuum chamber was then pumped down to 5×10^{-4} Pa using a rotary pump and a diffusion oil pump. Subsequently, the sample was sputtered with a Ta target (purity 99.99%; Kojundo, Japan) under varying a negative-bias voltage and time (800 V to 1600 V and 5 min to 30 min) to find optimum condition, maintaining the working pressure at 2.4 Pa with high-purity (99.999%) Ar gas flow. The target power was 60 W and additional heat was not applied during the sputtering process.

Preparation of protein-coated samples

Biomolecules including green fluorescent protein (GFP) and rhBMP-2, produced by *Escherichia coli* (*E.coli*), were used to examine the protein coating efficiency of the SLA/TIPS surface. GFP was used to visualize the protein loading property of each sample. To coat the SLA- and SLA/TIPS-Ti samples with GFP, they were immersed in a protein solution with a concentration of 100 μg/ml for 30 min in a 37 °C incubator and dried under sterilized conditions. rhBMP-2 was also

used to compare the amount and release behavior of the protein coated on each sample The samples were coated with rhBMP-2 via immersion in two different concentrations of the rhBMP-2 solution (1 and 750 μg/ml) for 30 min in the 37 °C incubator and dried under sterilized conditions.

Surface characterization

The surface morphology of SLA- and SLA/TIPS-Ti samples, uncoated and coated with rhBMP-2 (1 and 750 μg/ml), were investigated through field emission scanning electron microscopy (FE-SEM; SUPRA 55 VP, CARL ZEISS, Germany). The rhBMP-2-coated samples were completely dried and coated with a Pt coater before observation by FE-SEM. The hydrophilicity of SLA- and SLA/TIPS-Ti surface was examined by sessile drop method. Distilled water drop was applied onto each surface and photographed with a CCD camera which is connected to a goniometer. The contact angle was calculated by an analysis program (imageJ).

Investigation of protein-coated surfaces

The GFP loading ability of each surface was visualized by a confocal laser scanning microscope (CLSM; FluoView FV1000, Olympus, Japan). The rhBMP-2 amount coated on each sample was measured using UV spectroscopy (UV-1700, Shimadzu, Japan). To quantify the amount of rhBMP-2 coated on each sample, the samples were dipped in 5 ml of sterilized DPBS and gently sonicated for 15 min to dissolve the entire rhBMP-2 on the samples. Subsequently, the absorbance values of rhBMP-2-dissolved solutions were measured by UV spectroscopy at 220 nm,

and then, converted by a calibration curve. The calibration curve was prepared by measuring the optical absorbance values of rhBMP-2 in 0.010–20 μg/ml DPBS. The obtained curve showed a linear relationship between the absorbance values and rhBMP-2 concentration. Thus, each absorbance value was directly converted to the amount of rhBMP-2 in each solution. The release behavior of rhBMP-2 was also monitored using UV spectroscopy by measuring the absorbance values of the released rhBMP-2 at 220 nm. The rhBMP-2-loaded SLA- and SLA/TIPS-Ti samples were immersed in 1 ml of PBS in 10 ml vials, which were then placed in the oven under the temperature of 37 °C. The rhBMP-2-released solutions were extracted at predetermined times, i.e., 6 h, 1 day, 2 days, 4 days, and 7 days, and replaced with fresh DPBS. The optical absorbance values of the extracted solutions were measured by UV spectroscopy and converted to the rhBMP-2 amount by the calibration curve. Subsequently, the cumulative releases of rhBMP-2 on each sample were presented.

***In vitro* cell test**

The *in vitro* biocompatibility of the rhBMP-2-coated SLA/TIPS-Ti s was evaluated using an MC3T3-E1 cell, which is a pre-osteoblast cell (MC3T3-E1; ATCC, CRL-2593, Rockville, MD, USA). To distinguish and specify the effect of surface structure and rhBMP-2, four types of samples including SLA, SLA-BMP, SLA/TIPS, and SLA/TIPS-BMP were chosen for the *in vitro* cell test. The pre-incubated cells were seeded onto the samples at a density of 3×10^4 cells/ml for the cell attachment test and 1×10^4 cells/ml for cell proliferation and differentiation

tests. For cell culturing, the alpha minimum essential medium (α-MEM; LM008-53, WELGENE Inc., Korea), supplemented with 10% fetal bovine serum (FBS; Gibco®, USA) and 1% Pen Strep, was used as the culturing medium, and the cells were incubated in a humidified incubator with 5% CO_2 at 37 °C.

After seeding and 30 min of incubation, the attached cell morphologies on each sample were observed by a scanning electron microscope (SEM; JSM-5600, JEOL, Japan). Prior to the SEM observation, the cells on the samples were fixed with 2.5% glutaldehyde for 10 min, followed by dehydration in graded ethanol (70%, 95%, and 100%). The samples were immersed in hexamethyldisilazane for 10 min, and then, air dried. Cell proliferation was examined using three samples (n = 3) for each condition by an MTS assay after three and seven days of culturing. The cultured cells were reacted with 3-(4, 5-dimethlthizaol-2-yl)-5-(3-carboxymethoxyphenyl)-2-(4-sulfophenyl)-2H-tetrazolium (MTS; Promega, Madison, USA) for 2 h. The formazan product was quantified by Micro-reader (Model 550; Biorad, USA) at 490 nm wavelength. The differentiation of cells on each sample (n = 4) was evaluated by ALP assay after 12 days of culturing. For the ALP test, the culturing medium was replaced with a new medium containing 10 mM of β-glycerophosphate and 50 μg/ml of ascorbic acid after 1 day of seeding. The ALP activity, which indicates the degree of cell differentiation, was measured by quantifying the level of p-nitrophenol (pNP) converted from p-nitrophnyl phosphate in the presence of ALP during reaction. The pNP level was measured by Micro-reader at 405 nm wavelength. The ALP activity was calculated by a

standard curve prepared by measuring the absorbance values of bovine serum albumin at 0.2–1.2 mg/ml concentration.

In vivo animal test

An *in vivo* experiment was performed to ensure the osseointegration enhancement of SLA/TIPS-BMP-Ti as a dental implant in a dog mandible model. Two types of samples, including SLA-BMP- and SLA/TIPS-BMP-Ti screws, were chosen for the experiment. rhBMP-2 was coated on sterilized SLA- and SLA/TIPS-Ti screws with dimensions of 3 ø × 5 mm by dipping in a rhBMP-2 dissolved solution with a concentration of 0.75 mg/ml for 30 min in a 37 °C incubator, and then, dried under sterilized conditions (n = 4). The amounts of rhBMP-2 loaded on SLA- and SLA/TIPS-Ti screws were 7 and 11 µg, respectively.

Mongrel dogs (9 months old, male, weight range of 25 ± 5 kg) were used for the *in vivo* experiments. During the first surgery, their premolars and first molar of the lower jaws were extracted for suitable implantation sites. Screw implantation was performed two months after the extraction, which is a sufficient time for complete bone healing. General and local anesthesia were performed. Alveolar ridges were trimmed to produce a flat ridge before screw implantation. Then, SLA-BMP- and SLA/TIPS-BMP-Ti screws were implanted on the trimmed implantation sites with a trephine drill and sutured carefully.

The mongrel dogs were scarified eight weeks after the implantation surgery. Screws surrounded by adjacent tissues were extracted and fixed with 10% neutral formaldehyde for 7 days. The screws were resin (Technovit 7200 VLS, Kulzer,

Germany) blocked after rinsing with water and dehydrating in ethanol. Screw resin blocks were sectioned and stained with Goldner's trichrome and haematoxylin-eosin. The digital images of the stained sections of the resin blocks were observed by Axioskop microscopy (Olympus BX51, Olympus, Japan). Bone-to-implant contact (BIC) ratio and bone regeneration percentage were calculated using a digital image analysis program (ImageJ).

Statistical analysis

All experimental results were expressed in the form of mean ± standard deviation. The statistical value was calculated using t-test and a one-way analysis of variance (ANOVA) after the normality test by Shapiro-Wilks test. A p-value of less than 0.05 was considered to be statistically significant ($*p < 0.05$).

2.1.3. Results and discussion

Since the TIPS treatment is based on the etching process, the micro-scale roughness can be reduced as the treatment time and substrate bias increased. In order to find optimum surface structure, treatment was performed varying treatment time and substrate bias voltage (5 to 30 min and 800 to 1600 V). The micro- and nano-scale morphology observed by FE-SEM at each treatment condition are arranged in Figure 2.1.1. After 30 min of treatment, the nanopores are uniformly created but micro-roughness is almost disappeared regardless of the substrate bias. On the other hand, the nanopores were not uniformly fabricated after 5 min of treatment even though the micro-structure are well remained. In the case of 10 min treatment samples, the micro-structure are well remained without 1600 V sample. However, the depth of pores at 800 V sample is less than 100 nm which is not sufficient to provide additional storage room for rhBMP-2 loading while the 1200 V sample shows sufficient pore depth (>500 nm) as shown in Figure 2.1.2.(a) and (b) Therefore, the 1200 V substrate bias with 10 min of treatment time was chosen for the optimum condition for this study.

Surface characterization

Figures 2.1.3 shows the surface topographic images of SLA- and SLA/TIPS-Ti samples. The SLA-Ti surface demonstrates a typical micro-scale-roughened surface with sharp edges and submicro-scale pits (Figure 2.1.3(a)). After 10 min of TIPS treatment, severe surface etching by Ta ions under an extremely high

substrate bias voltage of 1200 V substantially changes the surface topography compared with the smooth surface (Figure 2.1.3(b)), but a brief TIPS treatment preserves the micro-scale roughness of SLA-Ti (Figure 2.1.3(b) and (c)). As shown in the inset of Figure. 2.1.3(b), nanoscale pores with diameters ranging from 50 to 200 nm are uniformly formed following the micro-scale roughness. A nanoporous structure with around 500 nm depth exhibits an excellent structural unity with the substrate and there is no noticeable boundary between the surface nanostructure and Ti substrate. Hence, a mechanically stable and undetachable nano-scale porous layer is developed on the SLA-Ti surface (Figure 2.1.3(d)).

The hydrophilicity of SLA- and SLA/TIPS-Ti is characterized by measuring the contact angle of distilled water, as shown in Figure 2.1.4. The SLA-Ti surface exhibits typical near hydrophobicity with a contact angle of 88°, which is generally caused by surface topography. On the other hand, the SLA/TIPS-Ti surface shows a significantly decreased wetting angle of 37°. The blunted surface morphology of SLA/TIPS combined with the distinct surface nanoporous structures improve the hydrophilicity of the SLA surface.

rhBMP-2 solutions with two concentrations (1 and 750 μg/mL) are used as coating solutions to demonstrate the effectiveness of rhBMP-2 coating for the *in vitro* cell test and *in vivo* animal test, respectively. The results of each rhBMP-2 concentration are in agreement with other investigations according to the biological effectiveness of BMP concentration *in vitro* and *in vivo* [26, 60, 61, 85, 86]. After dip-coating of SLA- and SLA/TIPS-Ti, coated rhBMP-2 is clearly observed on each surface, as marked with yellow arrows in Figure 2.1.5. As the concentration

of BMP solution increases, the coated amount of rhBMP-2 increases on both Ti samples. Note that there is a huge difference in the amount of rhBMP-2 on SLA- and SLA/TIPS-Ti surfaces despite the same dipping conditions. For the case of low concentration, SLA-treated Ti is barely covered with BMP, and even under high concentration condition, the morphology of a typical SLA surface, which is not covered with BMP, is observed in Figure 2.1.5(a) and (c). In contrast, the SLA/TIPS surface shows a thicker coating layer and better surface coverage of rhBMP-2 with a uniform dispersion state following the nanoscale pores under both dip-coating conditions (Figure 2.1.5(b) and (d)).

Furthermore, in the high magnification image (the inset of Figure 2.1.5(d)), nanoscale pores of the SLA/TIPS surface are filled with rhBMP-2, which means that the nanoscale porous structures are used as storage spaces for BMP loading on the Ti surface. The coating amount and dispersion state of rhBMP-2 are strongly affected by the surface properties of morphology and hydrophilicity [19, 56]. During the dip-coating process, compared with SLA-Ti, a better hydrophilic SLA/TIPS-Ti surface is formed by improving the wettability using the rhBMP-2 solution. The nanoporous surface structure immobilizes and solidifies rhBMP-2 on the surface through nanoanchoring effects. According to the mechanical interlocking mechanism, the adhesion strength can be enhanced by increasing the interfacial bonding area, while shrinkage of the solidified BMP does not occur until the anchoring parts are pulled out [58, 59].

Protein affinity

Prior to measuring the rhBMP-2 amount coated on each sample, the biomolecule ability on SLA- and SLA/TIPS-Ti is examined by observing the green fluorescence of the attached GFP on the surface using CLSM. GFP is generally used as a biomolecule for examining the protein affinity of biomaterials through visualization of their amount and distribution in CLSM observation, because the coating state of GFP can directly represent that of other proteins including rhBMP-2 [87, 88]. In Figure 2.1.6, the green fluorescence signal is uniformly deposited on both SLA and SLA/TIPS surfaces without any microscopic aggregation; however, their intensities are substantially different with naked eyes. The improved hydrophilicity and nanoporous structure allow for a larger amount of GFP to coat the SLA/TIPS surface; therefore, a higher amount of rhBMP-2 can be uniformly coated on the SLA/TIPS surface.

The actual coated amount of rhBMP-2 on each surface and its release behavior are confirmed using a UV spectrophotometer, as shown in Figure 2.1.7. Even when using the same concentration of rhBMP-2 solution as designed for *in vitro* and *in vivo*, the coated amount significantly differs between the SLA and SLA/TIPS surfaces, which is in good agreement with SEM and CLSM results. In the cases of low and high concentrations of rhBMP-2 solution, the SLA/TIPS surface shows 38% and 63% higher rhBMP-2 coated amounts, respectively, compared with the SLA surface (Figure 2.1.7(a)). The coated layer of rhBMP-2 on both surfaces is fully released in the release medium and there is no substantial difference in the releasing duration of the samples (Figure 2.1.7(b)). Although the coated BMP exhibits a fast release behavior due to its high solubility in the water-

based release medium, the high coating efficiency of rhBMP-2 on SLA/TIPS surface is notable, due to the high cost of rhBMP-2 for dentistry applications. For a successful clinical performance, a large amount of rhBMP-2 is necessary due to its short *in vivo* half-life, which is caused by its fast enzymatic degradation [89]. However, the superior rhBMP-2 coating efficiency of the SLA/TIPS surface provides a competitive advantage, which implies using a less concentrated rhBMP-2 solution for the dip-coating process. In addition, the desired amount of BMP for each patient can be carefully estimated with the required concentration and loaded just prior to the implant in the surgery process.

***In vitro* cellular response**

The *in vitro* biocompatibility is evaluated in terms of initial cell attachment, proliferation, and osteogenic differentiation of a preosteoblast cell (MC3T3-E1). To distinguish between the effects of surface structure and rhBMP-2, four types of samples, including SLA, SLA-BMP, SLA/TIPS, and SLA/TIPS-BMP, are chosen for the *in vitro* cell test. Figure 2.1.8 shows the representative initial cell adhesion morphologies for surface structures with 30 min of culturing. The cell on the SLA-Ti sample barely presents the spread attachment feature. A few filopodia are slightly stretched on the sharp tips of the SLA surface structure, and most parts of the cell mass remain spherical (Figure 2.1.8(a)). On the other hand, the surface nanostructures on SLA/TIPS-Ti substantially enhance the cell spreading area with flat and tightly adhered morphology, and a strongly interacted filopodia with a nanoporous surface structure is observed in the high magnification images (Figure

2.1.8(c)), which is well matched with a previous study of TIPS-treated flat Ti surfaces [73]. A surface nanostructure with excellent hydrophilicity provides a favorable surface environment for cell attaching, because of its similar size scale compared to the cell adhesion molecules and easy accessibility. A comparison of the SLA- and SLA/TIPS-Ti samples, both coated with rhBMP-2, shows substantially enhanced initial cell adhesion behavior with wider spreading areas and active filopodia formation (Figure 2.1.8(b) and (d)). These positive effects of rhBMP-2 on initial cell adhesion are due to its unique ability of stimulating the integrin synthesis and regulating the organization of cell adhesion molecules for rapid spreading and filopodia formation [90, 91].

The viability and osteogenic differentiation of cells on each sample are investigated by MTS assay and ALP activity, respectively, as shown in Figure 2.1.9. After 3 days of culturing, the SLA/TIPS-Ti samples (SLA/TIPS and SLA/TIPS-BMP) show slightly higher viability levels compared with the SLA-Ti samples (SLA and SLA-BMP); however, there is no significant difference. By increasing the culturing time up to 7 days, all samples show significantly increased proliferation values and the differences between the samples' surface structures substantially increase (Figure 2.1.9(a)). Generally, cell viability tendency is strongly affected by the surface structure rather than the presence or absence of rhBMP-2, and sometimes even decreased with BMPs [92, 93]. A strong induction of rapid osteoblast differentiation in rhBMP-2 can down-regulate the cell cycle progression for proliferation by suppressing the expression of cyclin-dependent protein kinases (Cdks). This plays an important role in activating the cell cycle to

the next phases [94]. Therefore, there is a slight decrease in the cell viability values on the sample with BMP compared with the same surface structure without BMP. However, in the ALP activity values obtained after 12 days of culturing, both rhBMP-2-coated surfaces show significantly increased ALP activity compared with their bare counterparts, as shown in Figure 2.1.9(b). For the SLA/TIPS-BMP-Ti sample, the highest ALP activity value is shown due to a synergic effect of surface nanostructure and a large amount of rhBMP-2 coated on the surface.

***In vivo* animal test**

Based on the *in vitro* cellular response, rhBMP-2-coated SLA- and SLA/TIPS-Ti samples are fabricated using screw shapes to evaluate the clinical performance in a dog mandible model (Figure 2.1.10(a)). After TIPS treatment, the color of the Ti screw changes from gray to matte black uniformly, which means that the nanoporous surface structure is uniformly generated on the implant surface [70]. Eight weeks after the surgery, the implanted samples are extracted with adjacent tissues and treated by following the procedure for histological observation. Figure 2.1.10(b)–(e) clearly shows the screw-shaped Ti implants and stained adjacent tissues with different magnifications; unstained parts (black) are implants, and the mineralized and un-mineralized tissues are stained as blue and red, respectively. The bone remodeling procedure in both samples originates from the lateral walls of the adjacent trabecular bone and inhomogeneously fills in the defect areas in the radially inward direction. In addition, all histological images show no inflammatory reaction, such as inflammatory granulations around implant surfaces

[95]. However, the formation of mineralized new bones and filling of the defect spaces show distinct differences between the samples; it is clearly observed that the bone-to-implant contact area and regenerated bone volume in the defect sites are improved at the SLA/TIPS-BMP-Ti screw, as shown in Figure 2.1.10(d) and (e). In addition, the higher portion of mineralized bone (blue) is observed at the SLA/TIPS-BMP-Ti screw.

The percentages of BIC and regenerated new bone volume (NBV) are quantified through an image analysis program, as presented in Figure 2.1.11. Both BIC and NBV levels are significantly increased at the SLA/TIPS-BMP-Ti screw compared with the SLA-BMP one. The bone healing at the SLA/TIPS-BMP-Ti screw is attributed to the synergetic effect of surface structure and the large amount of rhBMP-2 coated on the surface. The nanoporous surface structure can enhance the cell proliferation and differentiation, and enough amount of rhBMP-2 further enhances early cellular adhesion and differentiation. Therefore, these *in vivo* experimental results validate that the multi-scale surface SLA/TIPS-Ti is a promising modified surface for delivering rhBMP-2 efficiently and enhancing the osseointegration of implant in dentistry.

2.1.4. Conclusion

In this study, to improve the biological performance of Ti implants, a l arge amount of rhBMP-2 was successfully coated on the SLA/TIPS-Ti surfac e. The distinct nanoporous surface structure with excellent structural unity pr ovided a sufficient storage space on the Ti surface, which resulted in the en hancement of rhBMP-2 coating capacity. *In vitro* cellular responses indicated that the rhBMP-2-coated Ti surfaces significantly stimulated the initial cell at tachment and differentiation. Moreover, the nanoporous surface structure of S LA/TIPS-Ti substantially enhanced cell proliferations. The improving effect o f nanoporous surface structure and rhBMP-2-coated layer on the SLA/TIPS-T i surface was further confirmed by an *in vivo* animal test. The SLA/TIPS-B MP-Ti evaluations exhibited higher quantitative results for BIC and NBV co mpared with SLA-BMP Ti. These results prove the high efficiency of rhBM P-2 coating on the SLA/TIPS surface, making it a good candidate for dental implants to improve osseointegration.

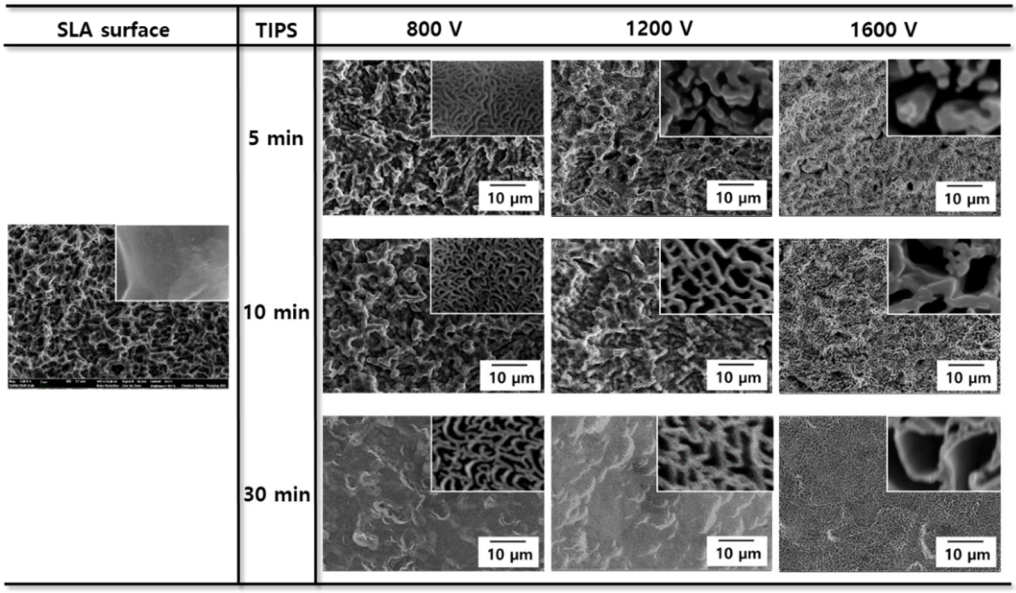

Figure 2.1.1. Surface morphology change depending on the substrate bias and treatment time

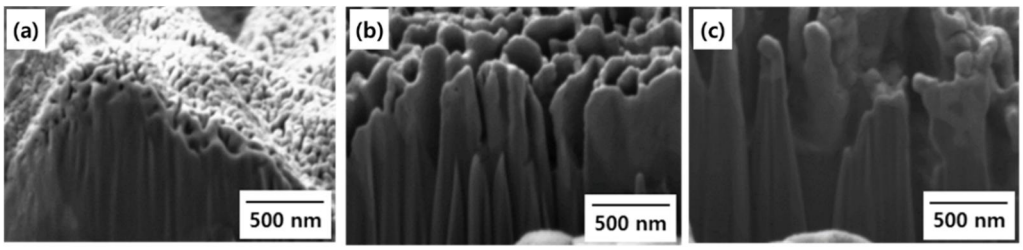

Figure 2.1.2. The cross-sectional images of (a) 800 V, (b) 1200 V, and (c) 1600 V TIPS-treated SLA surface for 10 min

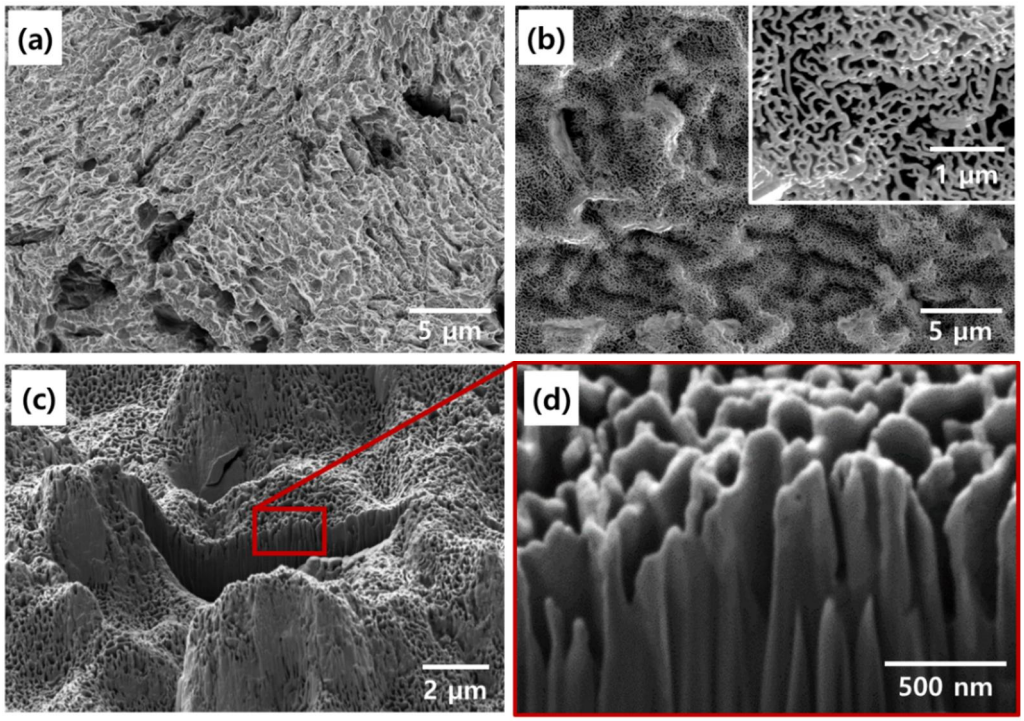

Figure 2.1.3. Typical surface morphology of (a) SLA-Ti surface, and (b) optimized SLA/TIPS-Ti surface. The cross-sectional images of SLA/TIPS-Ti surface with (c) low magnification and (d) high magnification

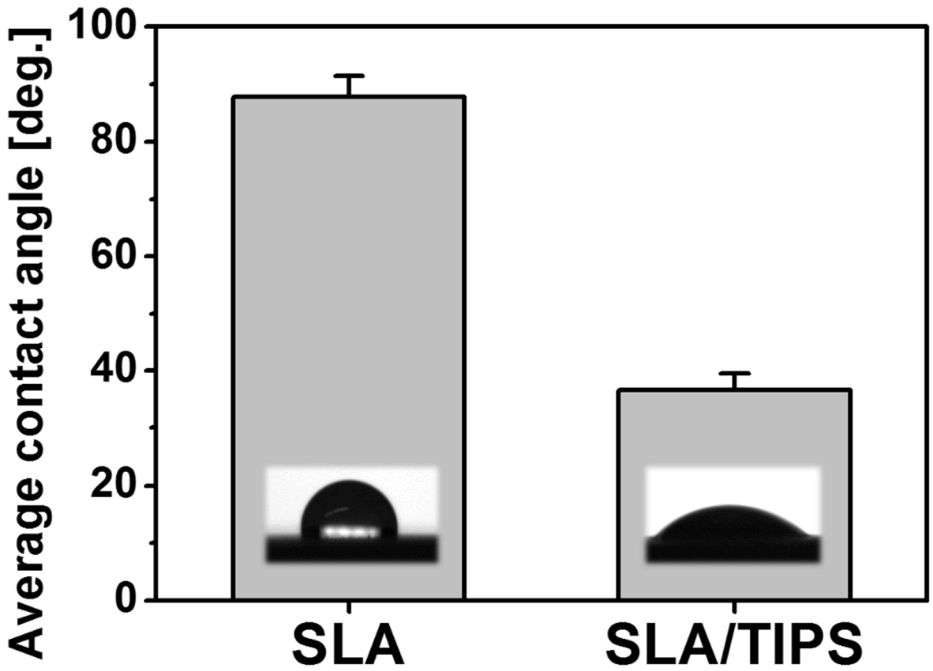

Figure 2.1.4. Contact angle of SLA and SLA/TIPS surface

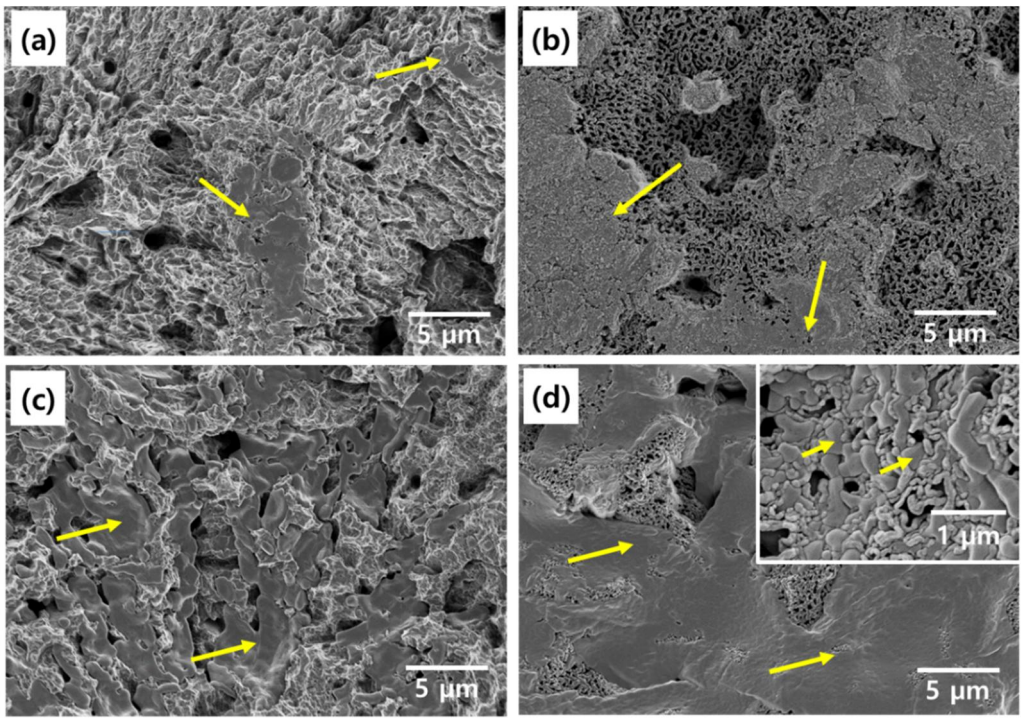

Figure 2.1.5. The typical morphology of low concentration (1 μg/ml) rhBMP-2 loaded (a) SLA and (b) SLA/TIPS with and high concentration (750 μg/ml) rhBMP-2 loaded (c) SLA and (d) SLA/TIPS

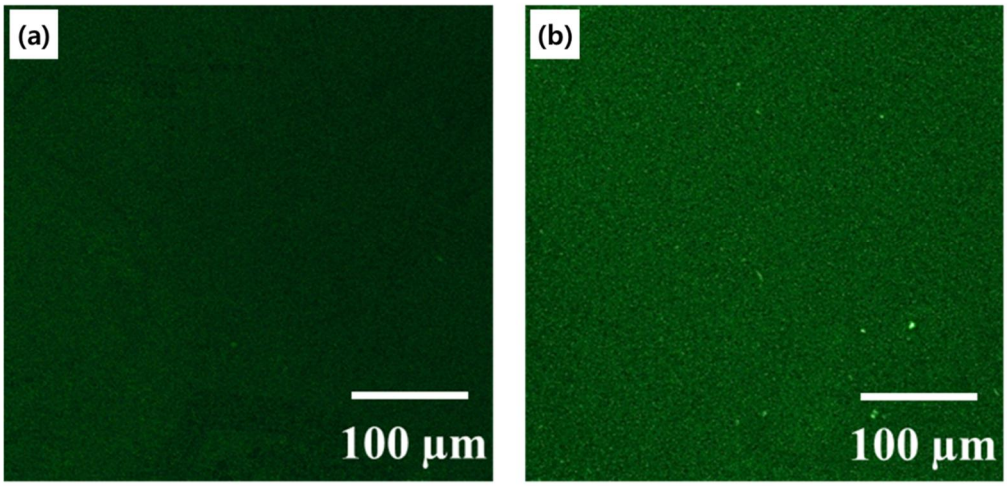

Figure 2.1.6. CLSM image of GFP loaded (a) SLA and (b) SLA/TIPS surface

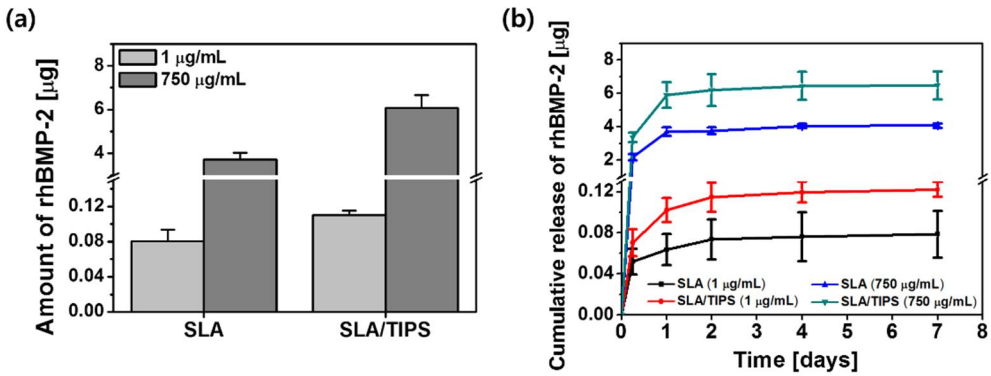

Figure 2.1.7. (a) The loading amount of rhBMP-2 on each surface and (b) the release behavior

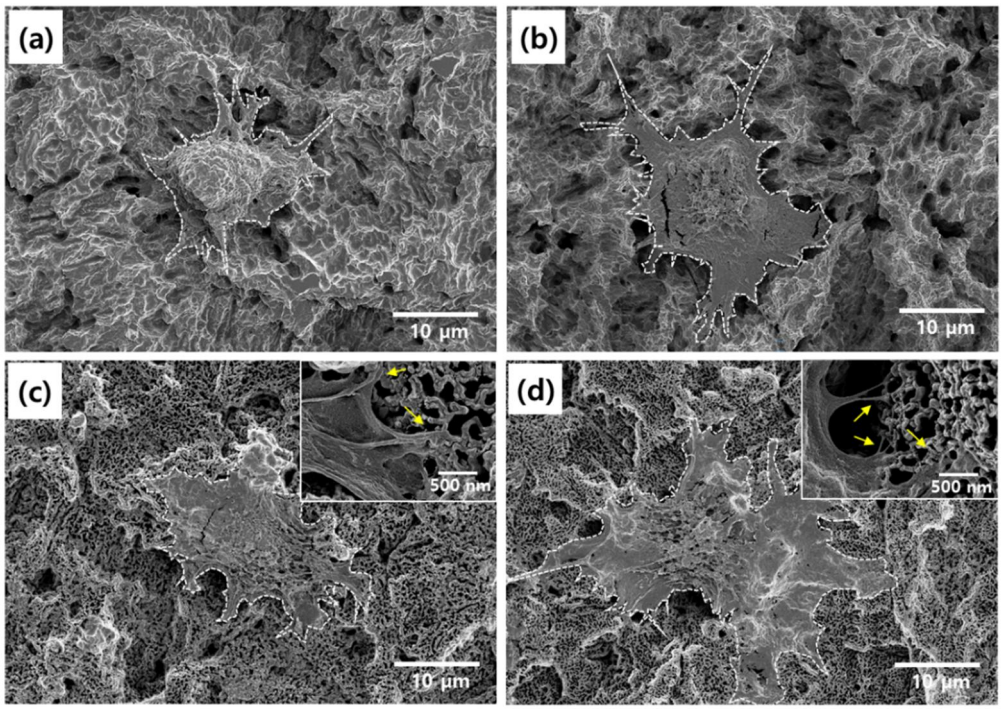

Figure 2.1.8. Typical MC3T3-El cell morphology on (a) SLA, (b) SLA-BMP, (c) SLA/TIPS, and (d) SLA/TIPS-BMP after 30 min of culture

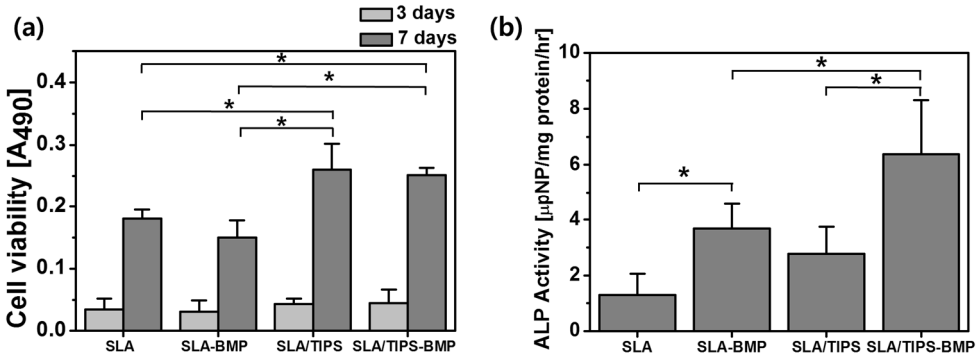

Figure 2.1.9. (a) The MC3T3-E1 cell proliferation after 3 and 7 days of culture on each surface evaluated by MTS assay, and (b) The cell differentiation property of each surface after 12 days of culture by ALP activity test

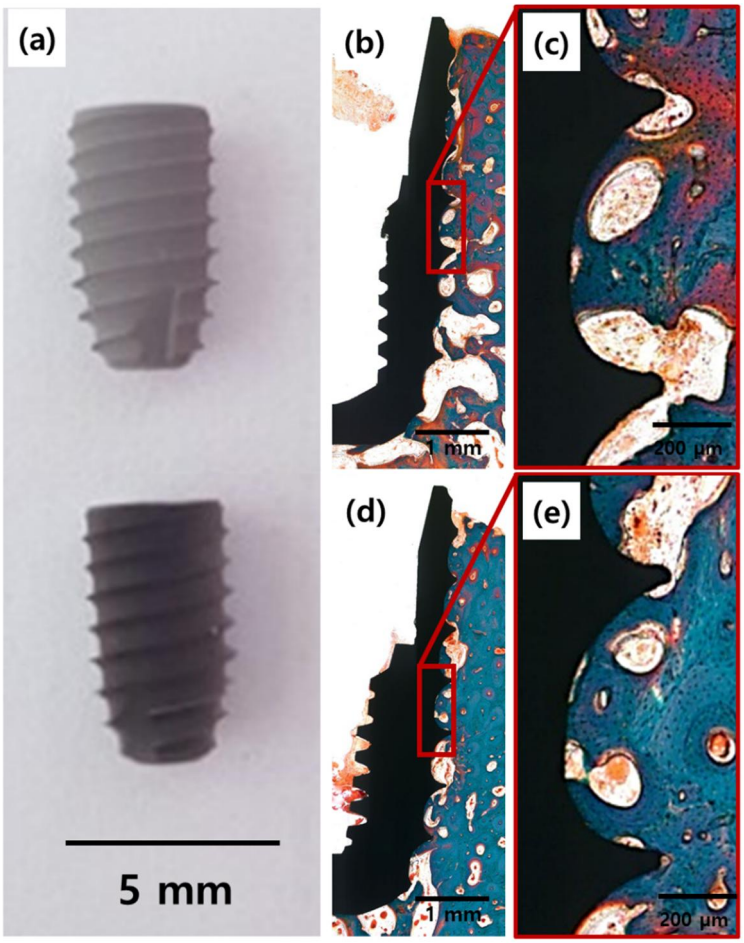

Figure 2.1.10. (a) The optical morphology of samples prepared for *in vivo* animal test, and the histological image of (b-c) SLA-BMP, and (d-e) SLA/TIPS-BMP after 8 week of implantation

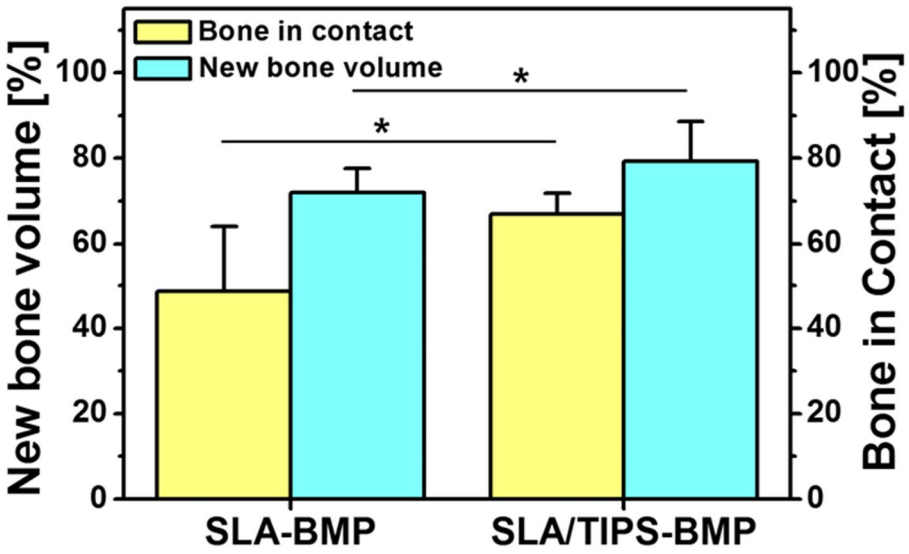

Figure 2.1.11. The statistical graph of the formation bone in contact (BIC) and new bone volume (NBV)

2.2. Antimicrobial agent delivery on dental abutment

2.2.1. Introduction

Infection related with dental implants is an important issue for the successful implant surgery [27]. Mostly, infection associated with the dental implant is come from the bacteria adhesion and colonization on the implant material, but the titanium and its alloys, which are generally used material for dental implant, has highly suitable for the bacterial colonization and biofilm formation [29, 96, 97]. Furthermore, oral environment is always exposed to numerous living bacteria. For these reasons, the implanted site is very weak to the bacteria infection, especially, the transgingival abutment of dental implant can be a root for bacterial admittance [27, 28]. To overcome the problem, strategies to deliver antibiotics such as vancomycin, streptomycin, and gentamicin have been tried [98, 99].

Recently, the appearance of pathogens which are highly resistant to antibiotics has raised the concern about other type of antibacterial agents such as silver (Ag), fluorine, and copper. Among these various antibacterial agents, Ag has been focused as a fascinating material due to its broad spectrum antibacterial property even against pathogens that is resistant to conventional antibiotics, and its good stability in physiological environment [27, 28]. Ag nano-particle, especially, is considered as the most recommended form of Ag because of its higher activity with large surface area. Vigorous researches have already demonstrated that the strong effectiveness of nanoscale Ag to kill or inhibit the bacterial growth [100-102]. Several mechanisms about the antibacterial activity of Ag have been announced.

Firstly, the antibacterial activity is strongly associated with the direct interaction between Ag nanoparticle and bacteria cell membrane including the membrane disruption and penetration, resulting in the bacterial death [103]. Furthermore, Ag nanoparticles induce the formation of free radicals, which cause the damage on the bacterial membrane and production of reactive oxygen species (ROS). The ROS influences to the bacterial DNA by the formation of superoxide anion, hydroxyl radical, and singlet oxygen, leading to oxidative damage [104]. In addition, the sliver ions released from the nanoparticles also affect to the bacteria. The ions penetrate into the bacteria through ion channels without damages to the cell membrane, and the ions attack the ribosome, enzymes, proteins, and DNA, which are essential for the bacteria cellular process [105].

However, the cytotoxicity of free Ag nanoparticle to mammalian cells has been found which is associated with the inhibition of cell viability rather than cell death [106]. The ultrasmall Ag nano-particles (< 100 nm) having high mobility can penetrate the mammalian cell membrane, where the nanoparticles affects to the DNA of cells, and the excessive Ag ions released from the Ag nano-particles can also damage to the cell DNA, resulting in the inhibition of cell viability [107]. Therefore, the delivery of nano-scale Ag with immobilized form with appropriate contents have been researched. The nanoparticle penetration effect can be blocked by immobilization of Ag, thereby, the cytotoxicity of Ag can be controlled by modulating the Ag ion concentration, which is adjusted by the contents of immobilized Ag. Recently, *in vitro* studies have reported about delivery of immobilized nano-scale Ag, demonstrating the strong antibacterial effect without

mammalian cell cytotoxicity [28, 30, 108].

Recently, we introduced the target-ion induced plasma sputtering (TIPS) treatment to create a mechanically stable and bioactive nanoporous layer on the Ti substrate, which is formed based on Ta ion etching [70, 73]. We, here in, created immobilized nano-scale Ag by 2nd coating using conventional sputtering prcoess on TIPS-treated Ti surface to deliver the nano-scale Ag for dental abutment application. Since Ag was deposited following the bioactive nanoporous structure of TIPS-treated surface, nano-scale Ag was easily obtained just by sputtering process. In this study, Ag content was the key parameter for the balance of antimicrobial activity and mammalian cell cytotoxicity. Figure 2.2.1 depicts the concept of this study. The cell viability of Ti surface is enhanced by TIPS-treatment, where the cell viability will decrease as the Ag content increased, while the bacterial activity will rapidly increase as the Ag content increase. Since the Ag content is easily modulated by sputtering time, the antimicrobial property with *Escherichia coli* and mammalian cell viability with fibroblast cells was evaluated varying the sputtering time (10, 30, and 120 s) to achieve effective antimicrobial activity without diminishing the cell viability of Ti for dental abutment application.

2.2.2. Experimental procedure

Creation of nano-structured surface.

A nano-structured surface was formed by target-ion (Ta) induced plasma sputtering (TIPS) on a Ti (grade 4) sample using a direct-current (DC) magnetron sputter (Ultech Co. Ltd., Korea). The Ti samples with a dimensions of 10 × 10 × 2 mm^3 were polished with 200–2000 grit SiC abrasive paper, and cleaned ultrasonically before being placed in a vacuum chamber as a substrate. The vacuum chamber was then pumped down to 5×10^{-4} Pa using a rotary pump and a diffusion oil pump. Finally, the plate was sputtered with a Ta target (purity 99.99%; Kojundo, Japan) under a negative-bias voltage of 1200 V for 30 min, maintaining the working pressure at 2.4 Pa with high-purity (99.999%) Ar gas flow. In the process, the target power was maintained at 60 W and no additional heat was applied.

Immobilization of nano-scale Ag

Immobilization of nano-scale Ag was performed by commercial sputtering process with direct-current magnetron sputter (Ultech Co. Ltd., Korea) on TIPS-treated Ti surface. The TIPS-treated Ti samples were cleaned ultrasonically, and located in a vacuum chamber, followed by being pumped down to 5×10^{-4} Pa using a rotary pump and a diffusion oil pump. Subsequently, the sample was sputtered with a Ag target (purity 99.99%; Kojundo, Japan) under negative-bias voltage of 50 V, and target power of 1.25 kW, varying the coating time (10, 30 and

120 s). The working pressure was maintained at 2.4 Pa with high-purity (99.999%) Ar gas flow, and additional heat was not applied during the sputtering process.

Surface characterization

The surface morphology of bare, TIPS-treated and Ag immobilized-TIPS(TIPS-Ag)-treated (10, 30, and 120 s) Ti samples were examined through field emission scanning electron microscopy (FE-SEM; SUPRA 55 VP, CARL ZEISS, Germany). The cross-sectional image were observed using FE-SEM assisted by focused ion beam (FE-SEM/FIB, AURIGA, CARL ZEISS, Germany). The chemical composition of each sample was investigated by energy dispersive spectrometry placed in FE-SEM (EDS/FE-SEM; SUPRA 55 VP, CARL ZEISS, Germany). The hydrophilicity of bare, TIPS-, TIPS-Ag-treated(10, 30, 120 s) was evaluated by sessile drop method. Distilled water trop was applied onto each surface and photographed with a CCD camera. The contact angle was calculated by an analysis program (ImageJ).

Ag ion release behavior

The Ag immobilized samples were immersed in 10 mL of PBS in 37 ℃ oven for 7 days. The release medium was extracted at predetermined times (1, 3 and 7 days), and changed to fresh medium. The extracted mediums containing Ag ions released from each specimen were examined by inductively coupled plasma mass spectrometry (IPC-MS; ELAN6100/NexION 350D, PerkinElmer, USA).

Subsequently, the cumulative release curves of Ag ions from each samples were presented.

Antimicrobial activity test

E.coli BL21(DE3) (*E.coli*; ATCC, PTA-5073, Rockville, MD, USA) strain was stored at -80°C deep-freezer in Luria-Bertani broth (LB broth; BD Difco™, 244620, USA) containing 50 % sterile glycerol. Seed culture was performed with 50 μl of the strain into 3 ml of new LB medium, followed by culturing for 12 h. After culturing, the bacteria suspension was diluted to a concentration of $4x10^5$ CFU/ml with new LB medium, and 100 μl of diluted suspension was introduced onto the surface of bare, TIPS-, and TIPS-Ag(10, 30, and 120 s)- treated Ti samples. The bacteria suspensions inoculated on each sample were incubated in 37°C oven for 12 h.

For the plate counting method, the samples were rinsed by 1 ml of PBS at once after incubation, and the rinsed samples were transferred into 3 ml of fresh PBS in 15 ml of sterilized tube, respectively. The tube containing bacteria incubated on samples were, then, vortexed for 1 min to detach all bacteria from the surface of samples. The viable bacteria in the PBS were examined by standard serial dilution and spreading on LB agar plate. The agar plate was incubated in 37°C for 15 h, and the colony images were obtained by digital camera.

For the SEM observation to examine the bacteria morphology on each surface, bacteria on the samples were fixed with 2.5% glutaldehyde for 10 min, followed by dehydration in graded ethanol (70%, 95%, and 100%). Subsequently, the samples

were immersed in hexamethyldisilazane for 10 min, and then, air dried. Prior to the observation, the samples were coated with a Pt coater.

In vitro biocompatibility test

The *in vitro* biocompatibility of TIPS-Ag (10, 30, 120 s) samples was evaluated using a fibroblast cell line (L929; derivative of strain L, Mus musculus, mouse). Five different samples including Bare, TIPS- TIPS-Ag(10, 30, and 120 s)-treated Ti were chosen for the *in vitro* cell test. The pre-incubated cells were seeded onto the samples at a density of 5×10^4 cells/ml for the cell attachment test and 1×10^4 cells/ml for cell proliferation tests. For cell culturing, the alpha minimum essential medium (α-MEM; LM008-53, WELGENE Inc., Korea), supplemented with 10% fetal bovine serum (FBS; Gibco®, USA) and 1% Pen Strep, was used as the culturing medium, and the cells were incubated in a humidified incubator with 5% CO_2 at 37 °C.

After 12 h of incubation, the attached cell morphologies on each sample were observed by a FE-SEM (FE-SEM; SUPRA 55 VP, CARL ZEISS, Germany). Prior to the SEM observation, the cells on the samples were fixed with 2.5% glutaldehyde for 10 min, followed by dehydration in graded ethanol (70%, 95%, and 100%). The samples were immersed in hexamethyldisilazane for 10 min, followed by drying in air. Cell proliferation was examined using three samples (n = 3) for each condition by an MTS assay after 2 and 5 days of culturing with changing culture medium every day. The cultured cells were reacted with 3-(4, 5-dimethlthizaol-2-yl)-5-(3-carboxymethoxyphenyl)-2-(4-sulfophenyl)-2H-

tetrazolium (MTS; Promega, Madison, USA) for 2 h. The formazan product was quantified by Micro-reader (Model 550; Biorad, USA) at 490 nm wavelength.

Statistical analysis

All experimental results were expressed in the form of mean ± standard deviation. The statistical value was calculated using t-test and a one-way analysis of variance (ANOVA) after the normality test by Shapiro-Wilks test. A p-value of less than 0.05 was considered to be statistically significant ($*p < 0.05$).

2.2.3. Results and discussion

Surface characterization

Figure 2.2.2 shows topographic images of bare, TIPS-, TIPS-Ag(10, 30, and 120 s)-treated Ti surfaces. Bare Ti surface shows smooth surface with several scratches by the grinding texture (Figure 2.2.2(a)). After 30 min of TIPS treatment nanopores with 100–300 nm size are uniformly created on Ti surface, where the wall thickness of pores are 50-100 nm (Figure 2.2.2(b)). After 10 s of Ag sputtering, the changes of overall pore structure are almost negligible, however, the roughness of pore walls were slightly changed as shown in Figure 2.2.2(c). The wall morphology change is because Ag was deposited on the pore wall. The wall morphology change was continuously more noticeable as the deposition time increased from 10 s to 120 s. The thickness of pore wall is getting thicker as presented in Figures 2.2.2(d) and (e). Since the Ag was deposited following the structure of nanoscale pore walls, the scale of deposited Ag also showed nanoscale, which is the effective scale to achieve antimicrobial activity. The cross-sectional image of 120 s is presented in Figure 2.2.2(f) which is representative cross-sectional images of all Ag deposited specimen. In the image, the depth of pore was 900 nm with the aspect ratio of 1:5–1:8, and the Ag was mostly deposited on the top of pore walls. In the case of physical-vapor deposition, the deposition was affected by the substrates pore structure such as pore size and aspect ratio. When the surface has high aspect ratio, the deposition does not occur uniformly, concentrating on the top of the structure. The pores fabricated by TIPS treatment with high voltage of 1200 V have high aspect ratio, thus, most of Ag were

deposited following the pore wall structure.

The chemical composition of each surface was evaluated by EDS analysis. The atomic concentrations of Ag on each specimen are listed in Table 2.2.1. The concentration of Ag is dramatically increased from 0.28 at% to 5.43 at% as the deposition time increased. The tendency is well matched with the tendency of Ag thickness increase in FE-SEM images in Figure 2.2.2. The EDS mapping data of TIPS-Ag120 (Figure 2.2.3) confirms that the Ag deposition is concentrated on the top of pore walls. The Ti atoms are mostly observed inside the pores (Figure 2.2.3(b)), while the Ag atoms are mostly detected on the top of pore walls as show in Figure 2.2.3(c).

The hydrophilicity of the specimens was examined using sessile drop method. The contact angle of bare, TIPS, and TIPS-Ag (10, 30, and 120 s) surfaces were presented in Figure 2.2.4. The contact angle of bare Ti was sharply decreased from 61º to 6º after TIPS treatment. After 10 s Ag deposition, the contact angle increased to 33º because of compositional change of top surface. Ag generally has high contact angle values (~95º) so that the deposited Ag particles on the top of pore walls increase the contact angle value. For this reason, the contact angle values are steadily increased, as the content of Ag on the surface increased.

Ag ion release behavior

The Ag ion release behaviors of TIPS-Ag(10, 30, and 120 s)-treated Ti samples were monitored as shown in Figure 2.2.5. The samples were immersed in

PBS in 37°C oven until 7 days, and the concentration of released Ag ions were evaluated by ICP-MS. The release amount of Ag ions, and the release rate, expectably, increased with the immobilized Ag content on surface. The concentration of Ag ions is closely related with the efficiency of antibacterial activity and cellular responses of mammalian cells, the high concentration of Ag ion release such as TIPS-Ag120 sample can inhibit not only the bacterial activity but also the mammalian cell viability [107]. The relationship between the cellular response and the Ag ion release behavior will be discussed at *in vitro* cell test.

Antimicrobial activity test

The antimicrobial activity of bare, TIPS-, TIPS-Ag(10, 30, and 120 s)-treated Ti samples is estimated by plate counting method. After 12 h of *E.coli* culture on each surface, all the bacteria was detached from the surfaces and spreading was performed on agar plate. Figure 2.2.6 shows the representative optic images of agar plates with the colonies of *E.coli* after 15 h of incubation in 37°C oven. The numerous bacterial colonies were detected at bare and TIPS-treated Ti samples, and even more bacteria colonies were observed at TIPS-treated samples as presented in Figure 2.2.6(a) and (b). The TIPS structure has higher bioactivity and it would be also provide appropriate environment to bacterial growth. Similarly, the anodized TiO_2 nanotubes which has higher bioactivity also was reported that bacteria can grow better than bare Ti surface [27]. In the meantime, in the case of TIPS-Ag samples, bacterial colonies were not found regardless of the Ag contents

on the surface (Figure 2.2.69(c)-(e)). This means that almost all of the bacteria were inactivated or dead by the immobilized nano-scale Ag on TIPS nano-structure.

Bare, TIPS-, TIPS-Ag(10, 30, ans 120 s) Ti samples with 12 h of *E.coli* culture were examined using FE-SEM in order to observe the state of attached bacteria. Figure 2.2.7 present the typical morphologies of *E.coli* on each surface. The *E.coli* on bare and TIPS-treated Ti surface shows that they are maintaining their intact shape after 12 h of culture (Figure 2.2.7(a) and (b)). In contrast, bacteria on TIPS-Ag surfaces shows abnormal morphology. The yellow arrows are indicating the bacteria membrane which is bound to the Ag nano-structures and torn by the binding, and the morphologies looked like shrunken. The damage of bacteria membrane by contact is one of the strong antibacterial mechanisms of nano-structured Ag. Several researches also demonstrated that the contact killing effect by immobilized nano-scale Ag. The FE-SEM images demonstrates that the contact killing effect by disrupting bacteria membrane is a strong mechanism for the antibacterial activity of TIPS-Ag-treated Ti surfaces. These antibacterial test results confirm that the TIPS-Ag treatment has effective antibacterial activity regardless of the Ag contents.

***In vitro* cell test**

The *in vitro* biocompatibility was assessed by initial cell attachment and proliferation using a fibroblast cell line (L929) to find compromising condition in terms of cytotoxicity. The bare, TIPS-, TIPS-Ag(10, 30 and 120 s)-treated Ti

specimens were evaluated by *in vitro* cell test. Figure 2.2.8 shows the representative cell adhesion morphology on each treated surface after 12 h of culture. Unlike the bacteria, all the cells are maintaining their intact shape on all types of surfaces, even on the TIPS-Ag120 which has high Ag contents. Generally, mammalian cell membrane has higher resistance to the contact with nano-scale Ag compared to bacteria membrane. In this test, the culturing condition was exactly same with bacterial FE-SEM observation test, thus, the result supports that the higher resistance of mammalian cell membrane to the contact with nano-scale Ag. Furthermore, the spreading level of L929 cells on samples was similar except the TIPS-Ag120 sample. Since the bioactive TIPS nano-structure is mostly maintained at TIPS-Ag10, and TIPS-Ag30 (Figure 2.2.2(b)-(d)), the cell spreading property can be also influenced by the bioactive structural effect. The hydrophilicity increase compared to bare Ti also support the cell spreading results. The enhanced hydrophilicity, generally, improves the cell spreading, thus, the significantly enhanced hydrophilicity of TIPS-Ag10 and TIPS-Ag30 compared to bare Ti surface by TIPS structural effect can affects to the cell spreading property. However, TIPS-Ag120 showed worse cell spreading result compared to other samples (Figure 2.2.8(e)) although the hydrophilicity was slightly better than bare Ti surface. The result explains that higher amount of immobilized Ag affects to the cellular process. In the case of TIPS-Ag120, the Ag ion release rate is very fast compared to other samples (Figure 2.2.5). Since high concentration of Ag ion arrests the cell metabolism, the cell was not spread well on TIPS-Ag120.

The effect of Ag ion to the cell viability was investigated by the cell proliferation test using MTS assay as shown in Figure 2.2.9. After 2 days of culturing, there is no noticeable difference among samples. After 5 days, L929 cells were well significantly proliferated on all the samples, but the proliferation level was remarkably different. The TIPS treated sample, predictably, shows the highest cell viability value among samples. However, as the Ag content increases, the cell viability values reduced sharply. As mentioned, the high concentration of Ag ion damage to the mammalian cell DNA, and it has been continuously reported that the inhibition of cell viability by high concentration of Ag ions. The cell viability result demonstrate that the adverse effect of high Ag ion concentration to fibroblast cell, and the cytotoxicity can be controlled by the adjusting Ag content which is directly related with Ag ion concentration. In this result, the TIPS-Ag10 showed similar level of cell viability compared with bare Ti, although the viability was lower than TIPS-surface, indicating that the TIPS-Ag10 is not toxic to fibroblast cells. Based on the antimicrobial test and in vitro cell test results, the TIPS-Ag10 surface is the most balanced condition in terms of antimicrobial activity and cytotoxicity for the dental abutment application.

2.2.4. Conclusion

In this study, to achieve additive antimicrobial activity to Ti dental abutment, extremely small amount of nano-scale Ag was immobilized on TIPS-treated Ti surface by short time (10 s) sputtering process. The Ag was mostly immobilized on the top of nano-scale pore struts of TIPS treated surface without noticeable change of the bioactive nano-structure of TIPS surface. As the sputtering time increased, the Ag content on the silver increased, and higher amount of Ag ions was released. The antibacterial activity test indicated that immobilized nano-scale Ag on the top of TIPS-Ag surface kill the bacteria effectively by contact with bacteria membrane regardless of Ag content. The *in vitro* cell test demonstrated that the mammalian cell membrane has higher resistance to the contact with nano-scale silver compared to bacteria, but the silver ion affects to the cell viability in terms of proliferation. As the silver ion increased, the cell viability decreased after 5 days of culturing. However, TIPS-Ag10 showed similar level of cell viability with bare Ti sample after 5 days of culturing, meaning that the TIPS-Ag10 is not toxic to fibroblast. Based on results, TIPS-Ag10 has balanced activity in terms of antimicrobial activity and cytotoxicity to mammalian cells. Thus, the extremely small content of nano-scale Ag immobilized TIPS structure can be a good candidate for the enhanced property of dental abutment.

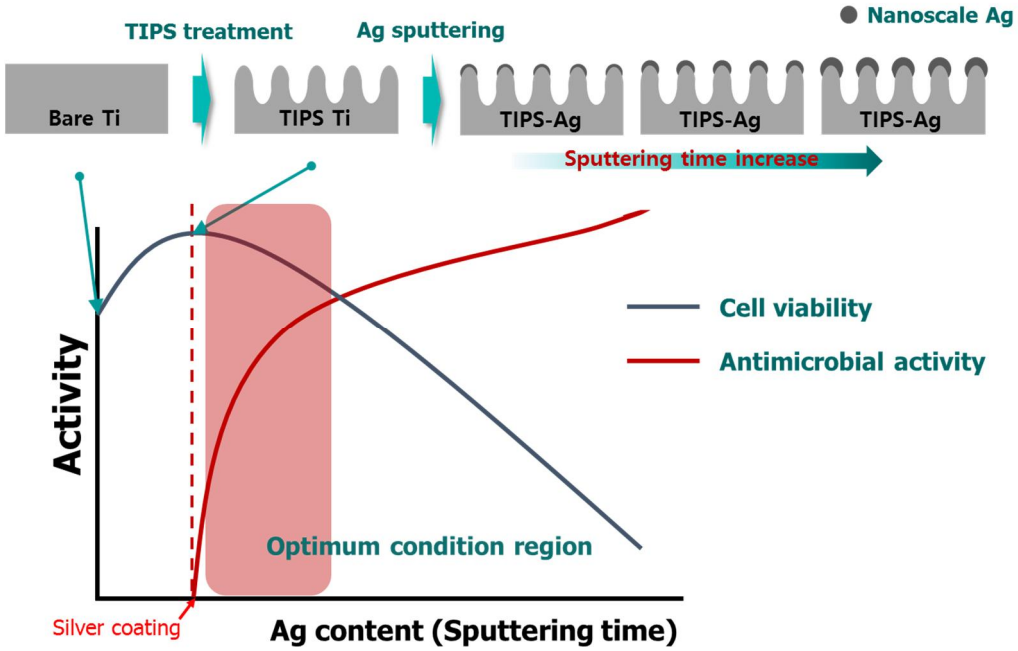

Figure 2.2.1. The schematic diagram of the concept of this study

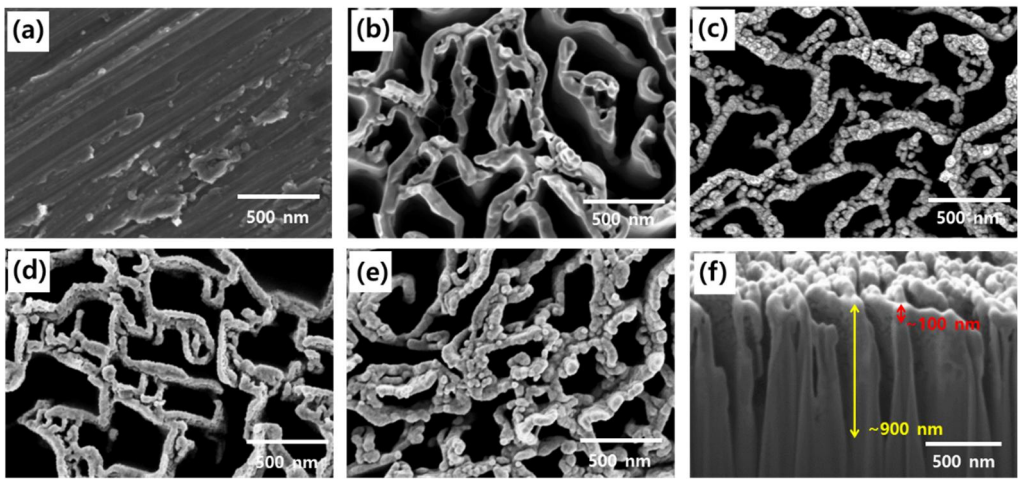

Figure 2.2.2. The typical morphologies of (a) bare, (b) TIPS, (c) TIPS-Ag10, (d) TIPS-Ag30, (e) TIPS-Ag120, and (f) the cross-sectional image of TIPS-Ag120

Table 2.2.1. Table of the atomic concentration on each surface detected by EDS analysis

Sample	Atomic concentrations (at%)				
	Ti	Ta	Ag	O	C
Pure Ti	95.74	–	–	–	4.26
TIPS	68.93	7.87	–	17.32	5.88
TIPS-Ag10	75.98	5.46	0.28	18.28	–
TIPS-Ag30	77.04	6.43	1.14	12.76	2.63
TIPS-Ag120	70.84	6.58	5.43	12.63	4.52

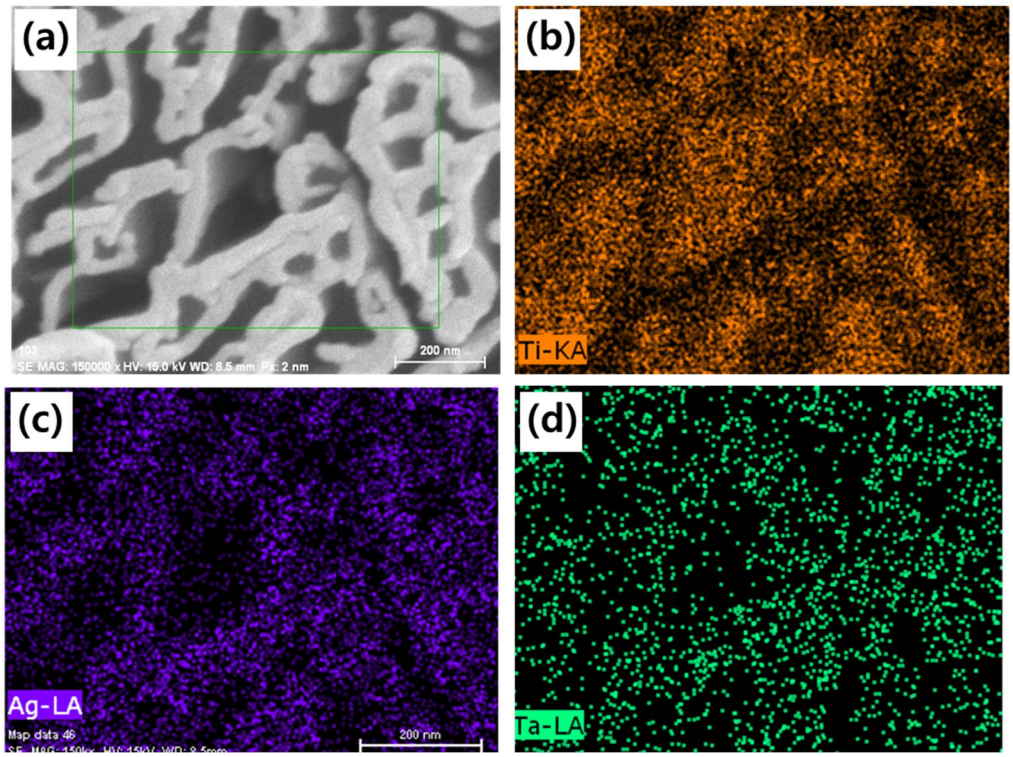

Figure 2.2.3. (a) FE-SEM image of TIPS-Ag120 for EDS mapping, and the mapping images of (b) Ti, (c) Ag, and (d) Ta atoms on TIPS-Ag120

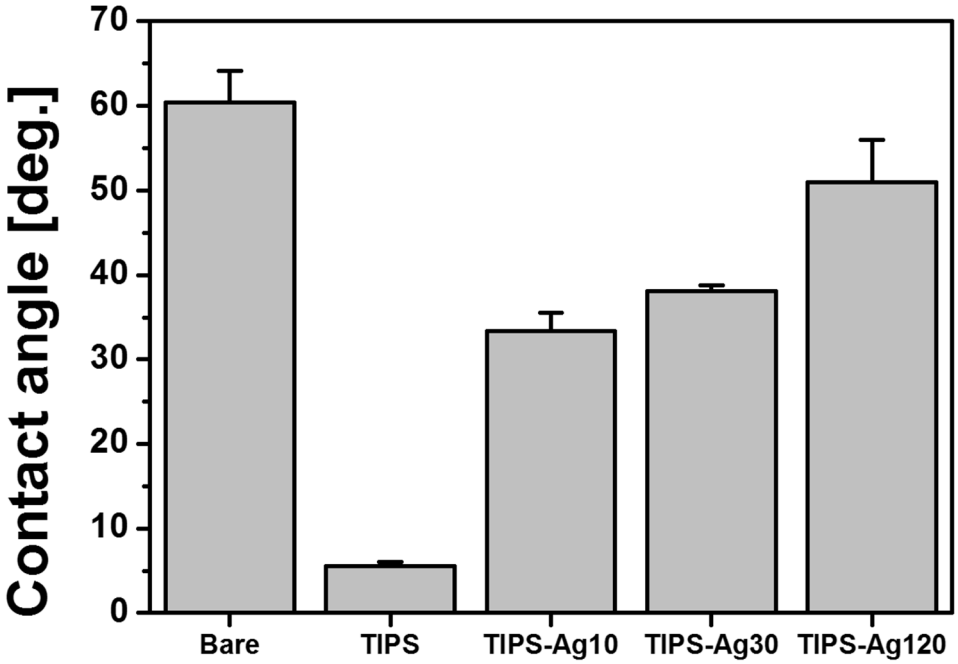

Figure 2.2.4. The contact angle values of bare, TIPS, TIPS-Ag, TIPS-Ag3, and TIPS-Ag120 surfaces

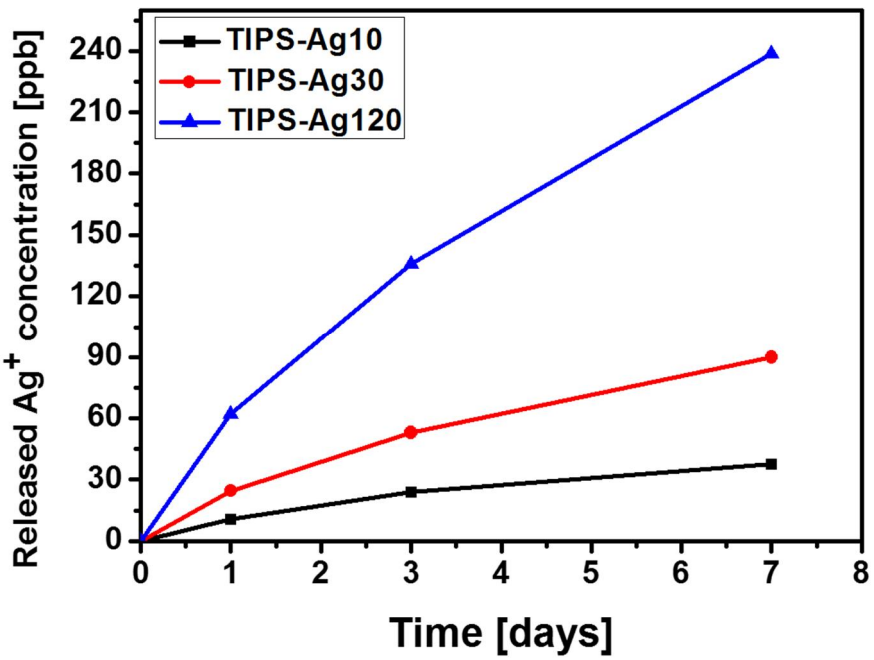

Figure 2.2.5. Release behavior of Ag ions form TIPS-Ag10, TIPS-Ag30, and TIPS-Ag120

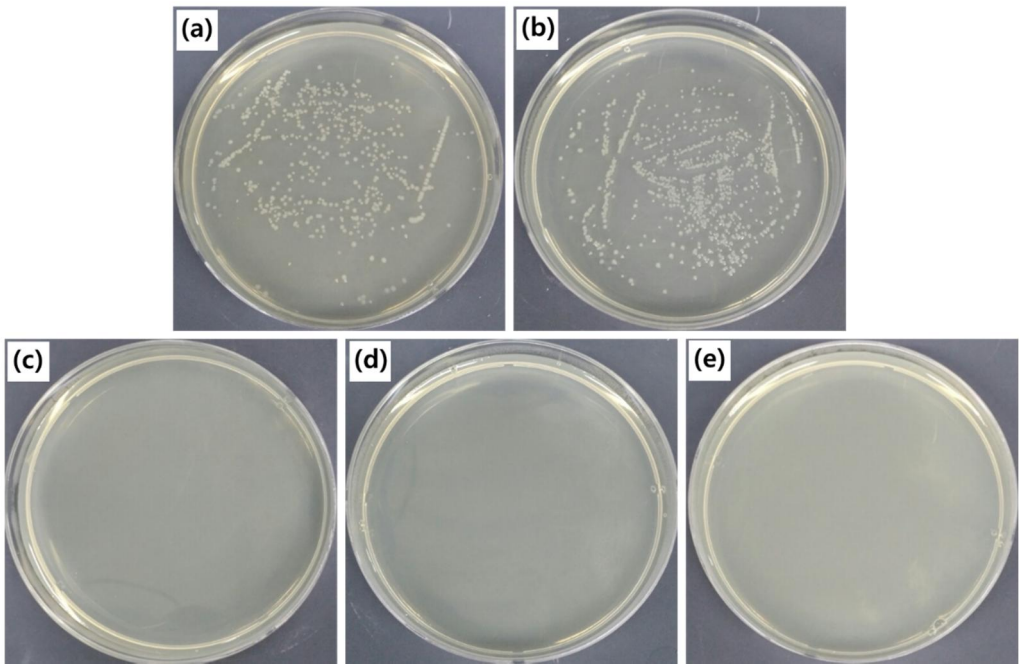

Figure 2.2.6. The bacterial colony formation from (a) bare, (b) TIPS, (c) TIPS-Ag10, (d) TIPS-Ag30, and (e) TIPS-Ag120 surface on agar plate by plate counting method after 12 h of culture on sample and 15 h of culture on agar plate

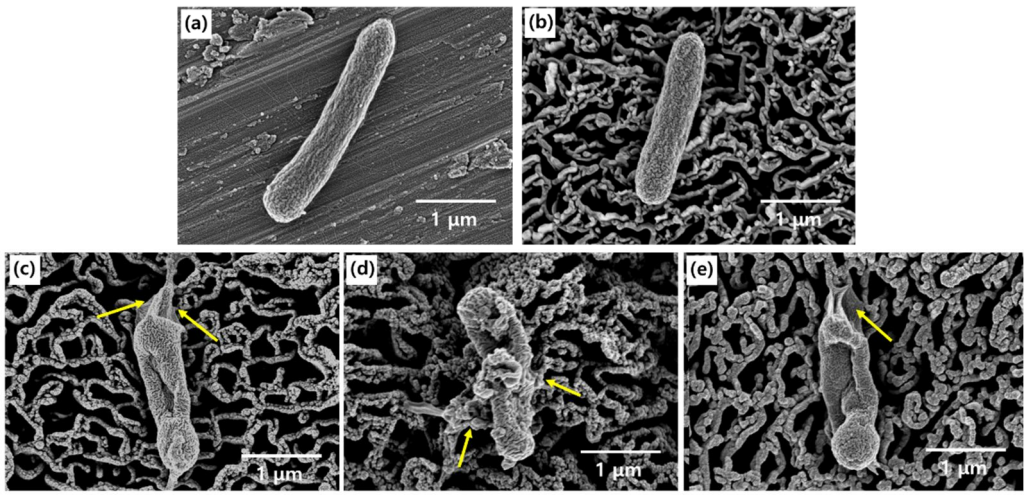

Figure 2.2.7. The typical bacteria morphology on (a) bare, (b) TIPS, (c) TIPS-Ag10, (d) TIPS-Ag30, and (e) TIPS-Ag120 after 12 h of culture

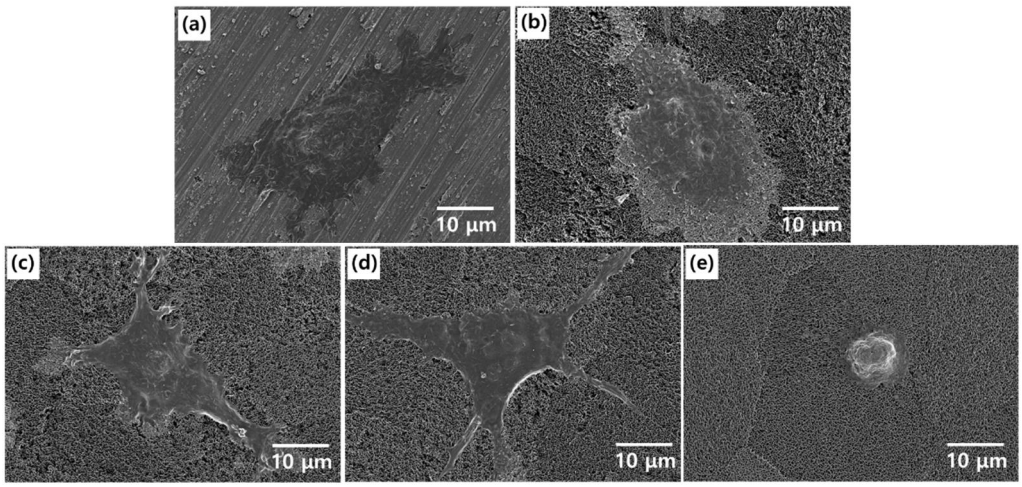

Figure 2.2.8. The typical morphology of L929 cells on (a) bare, (b) TIPS, (c) TIPS-Ag10, (d) TIPS-Ag30 and (e) TIPS-Ag120 surface after 12 h of culture

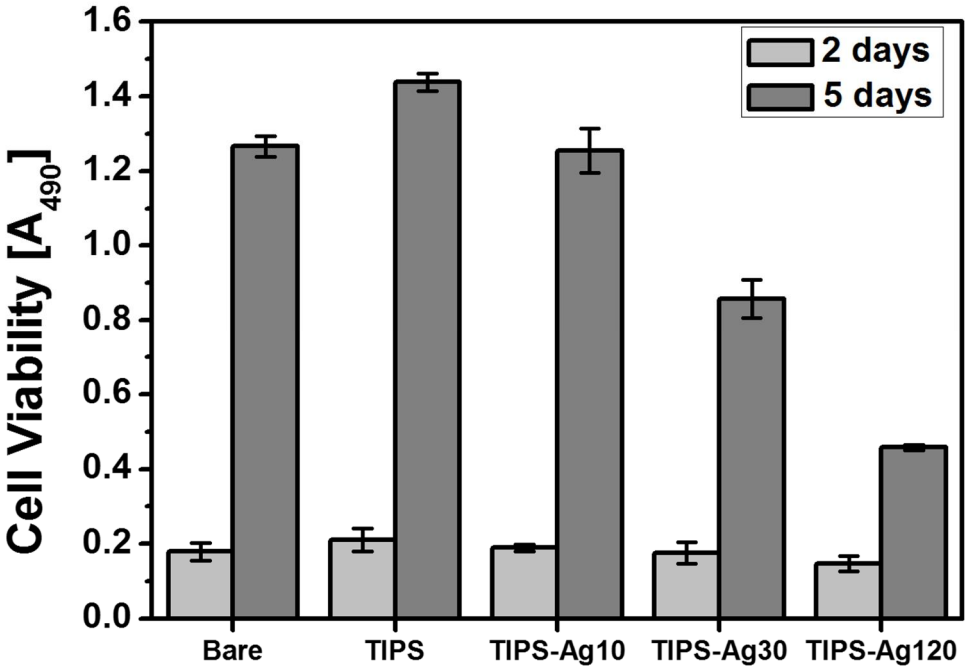

Figure 2.2.9. The L929 cell viability evaluated by MTS assay on bare, TIPS, TIPS-Ag10, TIPS-Ag30, and TIPS-Ag120 after 2 and 5 days of culturing

Chapter 3.

Antiproliferative Drug Delivery on TIPS-treated Co-Cr Surface for Stent Application.

In this chapter, the research concentrate on improvement of vascular stent ability by additive biological activity. Stent is a device developed for the treatment of coronary and peripheral artery disease. Bare metal stent is a first generated stent generally made of Co-Cr alloy and NiTi alloy. The invention of bare metal stent provide the innovative healing of various type of artery diseases including aneurysm, atherosclerotic plaques, and thrombus problem. Nevertheless, in stent restenosis problem was found from the patients who had the stent surgery, which is caused by the abnormal growth of vascular smooth muscle cell(VSMC) into blood vessel. To overcome the problem of in stent restenosis, drug eluting stent was invented which containing the antiproliferative drug for the inhibition of VSMC over-growth. The developed conventional drug eluting stent has polymeric coating layer for the stable loading, and sustained release of antiproliferative drug. However, the polymeric coating layer on the stent surface has been found to be a critical reason for late stent thrombosis which is a very dangerous side-effect directly associated with the patients' death after long period of stent surgery. For this reason, the delivery of antiproliferative agent having stable loading and sustained release property has been extensively researched. We, here in, treated the Co-Cr surface with TIPS technique to create nano- to submicro- porous structure, and delivered paclitaxel by incorporating in the TIPS surface to achieve the loading stability and sustained release property without polymeric layer. The loading stability and release behavior were assessed, and the biological properties were investigated *in vitro* and *in vivo*

3.1. Introduction

Bare metal stent was developed to overcome the limitation of high ratio of restenosis phenomenon after balloon angioplasty procedure, which is a technique to cure the various type of angiosis such as aneurysms, atherosclerotic plaques, and thrombus problems in blood vessel [109, 110]. Among various materials, cobalt-chromium (Co-Cr) alloys are widely used as bare metal stent material due to its excellent mechanical strength, flexibility, and radiopacity. The Co-Cr bare metal stent remarkably decreased the restenosis problem, and it was even more effective to more severe vascular disease compared to the balloon angioplasty procedure [111, 112]. However, the bare metal stent implantation was found to lead the other type of restenosis. Stent implantation, generally, cannot avoid the endothelium denudation and injury because of its high mechanical strength and strong force during expansion. The endothelium injury induces the growth factor release from activated platelets, resulting in the vascular smooth muscle cell (VSMC) over-growth into the blood vessel. The over-growth of smooth muscle cells followed by extracellular matrix synthesis and deposition leads to the re-occlusion of vessel, which is announced as in stent restenosis [113, 114].

To overcome the limitation of bare metal stent, drug eluting stent, which is containing the antiproliferative drug such as paclitaxel, sirolimus, and everolimus which can inhibit the abnormal over-growth of VSMC, has been introduced. The commercially used drug eluting stent usually have used the polymeric coating layer because the polymeric coating layer is promising for the loading stability and

desirable release of delivered drug on stent surface to inhibit the restenosis problem remarkably [115, 116]. However, a serious problem of present drug eluting stent has been found in various clinical cases, which is known as very late stent thrombosis. Actually, thrombosis is an inevitable problem after stent surgery, because of the injury on inner vessel wall, but it can be easily prevented by taking anti-thrombus drugs for certain period (1-3 months) after surgery. In general, the endothelium is completely recovered in 3 months after the implantation of bare metal stent, thus, no more thrombus formation occurs. On the contrary, the endothelium is not fully recovered for a longer period time, even after 1 year, after the implantation of the conventional drug eluting stent. Due to the un-recovered endothelium around stent, thrombus formation occurs urgently when patient quit taking anti-thrombus drug, resulting in the urgent cardiac death. Recently, the polymeric layer has been considered to be a major reason of the late thrombosis phenomenon due to its hypersensitivity inducing the prolonged inflammation, allergic reactions, and foreign body reactions. Hence, several techniques have been researched to deliver drugs having stable loading and sustained release properties without polymer coating [114, 117, 118].

The non-polymeric drug delivery platforms can be classified with two groups, chemical and physical modification techniques. The representative chemical modification is using self-assembled monolayer. The self-assembled monolayer can capture the drug chemically [41, 118]. The other chemical modification technique is just using the drugs' adhesion property to material surface. They coated the paclitaxel, which has high adsorbing property to certain materials, on Co-Cr

substrate directly without using any platforms, but with very small amount which can bind to the surface chemically. Even though those techniques prolong the release behavior even up to 70 days, the total amount of loaded drug was too small compared to conventionally used drug eluting stents, at which amount may not be effective *in vivo* situation. The physical modification of stents include reservoir, textured, and porous surfaces. The stents having porous surfaced with different scale of pores from nano- to macro-scale have been developed to deliver antiproliferative drug effectively. The micro-scale textured structure fabricated by sandblasting technique has showed good clinical performance. However, the micro-scopic surface treatment can affect to the mechanical property of thin stent struts [37, 55]. For example, the micropits can act as the stress concentrated defectv. In the case of nano-scale, several coating techniques including anodized porous layer, hydroxyapatite coating layer, and nano-porous metal coating have been introduced [119]. The *in vivo* effectiveness of delivered drug using nano-scale porous platforms coating layer has been also reported. However, the risk of coating layer on stent also reported which is associated with the delaminated coating debris [67]. The debris induced serious adverse effect during *in vivo* animal test. Based on the previous researches, it is promising that the mechanically stable nano- to submicro-scale porous surface can be a fascinating candidate as a delivery platform for antiproliferative drug on stent surface with stable loading and desirable release behavior, substituting polymeric coating layer.

Recently, we introduced target-ion induced plasma sputtering (TIPS) treatment to create mechanically stable nanoporous layer on Co-Cr substrate,

which is formed based on Ta ion etching. We, here in, introduced the nanoporous TIPS surface as a delivery platform of paclitaxel on Co-Cr surface. We investigated the loading stability by observing the morphology after certain amount of strain. The release behavior controllability varying the pore structure also examined by release test under 60 rpm shaking condition in PBS with 0.05% of Tween20. The efficacy of remained drug after release test was assess by *in vitro* cell tests after 7 and 21 days of release. Consequently, the in vivo performance of paclitaxel loaded Co-Cr stent with TIPS surface were evaluated by atherosclerosis rabbit model.

3.2. Experimental procedure

Surface modification

Porous surface on Co-Cr alloy was created by target ion (Ta) induced plasma sputtering (TIPS) by using direct current (DC) magnetron sputter (Ultech Co. Ltd, Korea). Co-Cr alloy samples with dimensions of $10 \times 10 \times 2$ mm^3 were polished with 400 – 2000 SiC abrasive paper, and cleaned by sonication in acetone, and ethanol three times for 10 min, respectively, and dried by air blowing. The cleaned Co-Cr substrate was located in vacuum chamber, and the chamber was pumped down to 5×10^{-4} Pa by rotary and diffusion oil pump. The Co-Cr substrate was then sputtered with Ta target (purity 99.99%; Kojundo, Japan) under a negative bias voltage of 800 V and 1600 V for 1 h without applying additional heat into the chamber. The working pressure during processing was sustained at 2.4 Pa with high-purity (99.999%) Ar gas flow, and the target power was 60 W.

Drug loading on substrates

All of the samples were cleaned by sonication in ethanol three times for 10 min each, and dried by air blowing, followed by drying in 70 °C oven for 1 h. After cleaning process, paclitaxel (Samyang genex, 99-100%, Ltd, Korea) was loaded on each substrate by dipping method. For the paclitaxel loading, the paclitaxel was dissolved in ethanol with 6 wt% concentration for bare Co-Cr, and 5 wt% concentration for TIPS treated Co-Cr samples to match the loading amount to 3 $\mu g/mm^2$. All the substrates were immersed in the ethanol solution inside a vacuum chamber (0.91 MPa) for 15 min, and dried in covered dish in 70 °C oven for 15 min.

Surface characterization

The surface morphology of bare, 800 V, 1600 V Co-Cr samples, unloaded and loaded with paclitaxel was investigated using field emission scanning electron microscopy (FE-SEM; SUPRA 55 VP, CARL ZEISS, Germany). The paclitaxel loaded samples were completely dried and coated with a Pt coater before observation by FE-SEM. The cross-sectional image of each sample was observed using FE-SEM assisted by focused ion beam (FE-SEM/FIB, AURIGA, CARL ZEISS, Germany).

Evaluation of drug stability

The loading stability of paclitaxel on Co-Cr samples against strain was evaluated by observing the surface morphology after certain amount of strain using tensile test machine (Instron) as presented in Figure 3.1(a). The strain rate was 10 mm/min and the total strain value was 12 % which is commonly occurs during stent expansion. The rod type samples with dimensions of 30 x 5 x 2 mm3 with saw like grip was used for the test as shown in Figure 3.1(b). The surface of center part of sample with dimensions of 10 x 5 mm2 which is marked with red rectangular box in Figure 3.1(b) was observed by scanning electron microscope (JSM6360, JEOL Techniques, Tokyo, Japan) and FIB (FE-SEM/FIB, AURIGA, CARL ZEISS, Germany) after strain test to figure the loading stability of drugs on each surface.

Release behavior of paclitaxel

To quantify the amount of paclitaxel coated on each sample, the samples were dipped in 10 ml of absolute ethanol and gently sonicated for 15 min to dissolve the entire paclitaxel on the samples. Subsequently, the absorbance values of paclitaxel dissolved solutions were measured by UV spectroscopy at 230 nm, and then, converted by a calibration curve. The calibration curve was prepared by measuring the optical absorbance values of paclitaxel in 0.10–50 μg/ml absolute ethanol. The obtained curve showed a linear relationship between the absorbance values and

paclitaxel concentration. Thus, each absorbance value was directly converted to the amount of paclitaxel in each solution.

The release behavior of paclitaxel was also monitored using UV spectroscopy by measuring the absorbance values of the released paclitaxel at 230 nm. The paclitaxel loaded bare, 800 V and 1600 V Co-Cr samples were immersed in 2 ml of PBS with 0.05% of Tween20 in 10 ml vials, which were then placed in the 60 rpm shaking oven under temperature of 37°C. The paclitaxel released solutions were extracted at predetermined times (0.25, 1, 3, 7, 14, 21 and 28 d) and replaced with fresh PBS with 0.05% of Tween20. Prior to measuring of optical absorbance values of the extracted solutions, the solutions were mixed with 2 ml of absolute ethanol to dissolve all of the paclitaxel released from the samples, then, the optical absorbance values of the extracted solutions were measured by UV spectroscopy and converted to the paclitaxel amount by a calibration curve. In this case, the calibration curve was obtained using similar method with previous calibration curve, but the medium was 1:1 mixed solution of PBS with 0.05% Tween20 and absolute ethanol. The obtained curve showed a linear relationship between the absorbance values and paclitaxel concentration. Subsequently, the % cumulative release curves of paclitaxel from each sample were presented.

In vitro cell test

The antiproliferative efficacy of remained drug after 7 and 21 days of release on bare, 800 V and 1600 V Co-Cr surface was evaluated by *in vitro* cell test using

vascular smooth muscle cell (VSMC; CC-2583, LONZA, Switzerland). To release the paclitaxel for cell test, all the samples before paclitaxel loading and 10 ml vials were sterilized by cleaned with ethanol 3 times for 10 min and dried, followed by sterilization with autoclave. The paclitaxel loading was performed on sterilized samples in cleaned vacuum chamber in clean bench and dried in cleaned 70°C oven for 15 min. The drug loaded samples were immersed in 2 ml of sterilized PBS with 0.05 % Tween20 in 10 ml sterilized vials. The release medium was changed with fresh sterilized PBS with 0.05% Tween20 at predetermined time (same with release test) in clean bench. After 7 days and 21 days of release, the samples were extracted from the vial, and transferred to 24 well, and rinsed with DPBS 5 times to clean up the Tween20 from the samples. Then, the samples were transferred to new 24 well.

The pre-incubated cells were seeded onto the samples at a density of 3×10^4 cells/ml for the cell attachment and cell proliferation tests. For the cell culturing, the SmBM medium (CC-3181, LONZA, Switzerland) supplemented with SmGM-2 bulletKit (CC-3181 & CC-4149, LONZA, Switzerland) was used as the culturing medium, and the cells were incubated in a humidified incubator with 5 % CO_2 at 37 °C.

After 1 day of culturing, the attached cell morphologies on each sample were observed by confocal laser scanning microscope (CLSM; Fluoview FV1000, Olympus, Japan). Prior to the CLSM observation, the cells were fixed with 4% paraformaldehyde solution diluted with PBS for 10 min, and washed with PBS 3

times. After that, cells were permeabilized with 0.1% Triton X-100 (Sigma-Aldrich, USA) diluted with PBS for 5 min, and then washed with PBS 2 times. Blocking the nonspecific site was performed with 1 % bovine serum albumin (BSA; albumin bovine, Sigma-Aldrish, USA), followed by staining of F-actin and nuclei of the cell with phalloidin (Alexa Fluor® 555 phalloidin, Invitrogen, USA) and 4',5-diamidino-2-phenylindole (DAPI; ProLong® Gold antifade reagent with DAPI, Invitrogen, USA), respectively.

Cell proliferation was examined using three samples (n = 3) for each condition by an MTS assay after three and seven days of culturing. The cultured cells were reacted with 3-(4, 5-dimethlthizaol-2-yl)-5-(3-carboxymethoxyphenyl)-2-(4-sulfophenyl)-2H-tetrazolium (MTS; Promega, Madison, USA) for 2 h. The formazan product was quantified by Micro-reader (Model 550; Biorad, USA) at 490 nm wavelength.

In vivo animal test

The *in vivo* animal test was carried out on 12 female New Zealand white rabbits. For the induction of atherosclerosis, rabbits were fed a diet containing 1% of cholesterol and 6% peanut oil. One week after feeding of high-cholesterol diet, balloon injury was performed at the iliac arteries. The balloon injury affects to the acceleration of atheroma formation inside desired artery. After artery injury, rabbits were continued on the high cholesterol diet for additional 4 weeks, then the diet

was changed to a diet with 0.025% of cholesterol for remaining of the *in vivo* study (Figure 3.2).

After 4 weeks of switching diet, stents were implanted. For the implantation, 24 bare Co-Cr stents with a 18 mm long, 2 mm in diameter, and 0.0025 inch strut thickness (Genoess, Korea) were prepared. Among 24 stents, 8 stents were TIPS-treated with 1600 V condition to create nano-porous layer on the stent surface. The paclitaxel was loaded on 8 bare Co-Cr stents and 8 TIPS-treated Co-Cr stents by dipping method with 10 wt%, and 9 wt% of paclitaxel solution, respectively, to load the 3 $\mu g/mm^2$ paclitaxel amount on each stent surface. The prepared samples (n = 8), then, were placed in the atheroma formed iliac artery. After the implantation, the diet with 0.025% cholesterol was continued additional 4 weeks until the animals were sacrificed (4 weeks of follow up).

After sacrifice, the stent inserted vessels were extracted and fixed with a 10% neutral formaldehyde solution for more than 3 days. Prior to the post-treatment of histological evaluation, all the vessels were evaluated with micro-tomography scanner (micro-CT; Skyscan 1173, Kontich, Belgium). For the micro-CT observation, the fixed vessels containing stent were transferred into tubes with the size of 3.5 mm diameter. Then, tubes were filled with contrast media which make the inside and surrounds of vessel radiopaque to distinguish the blood vessel in the CT images. After tomography with micro-CT, the vessels were cleaned with normal saline, and the post-treatment for histological analysis was performed. The fixed and cleaned vessel tissues were embedded in resin, followed by sectioning.

The resin block sections, then, were stained with Masson-Thrichrome and haematoxylin-eosin for the observation of restenosis level, and Carstairs staining method for the observation of fibrin deposition around the stent struts. The stained sections were observed using Axioskop microscopy (Olympus BX51, Olympus, Japan). Neo-intima thickness, and the degree of fibrin deposition was calculated from the images using a digital analysis program (ImageJ).

Statistical analysis

All experimental results were expressed in the form of mean ± standard deviation. The statistical value was calculated using t-test and a one-way analysis of variance (ANOVA) after the normality test by Shapiro-Wilks test. A p-value of less than 0.05 was considered to be statistically significant ($*p < 0.05$).

3.3. Results and discussion

Surface characterization

Figure 3.3 shows the topographic surface and cross-sectional images of bare, 800 V, and 1600 V Co-Cr surfaces observed with FE-SEM before paclitaxel loading. Bare Co-Cr surface shows smooth surface with several scratches by the grinding texture (Figure 3.3(a)). After 1 h of TIPS treatment with 800 V substrate bias, elongated nanopores with 100 – 150 nm width are uniformly created on Co-Cr surface where the depth of pores is 450 – 500 nm (Figure 3.3 (b) and (d)). In the case of 1600 V substrate bias TIPS treated Co-Cr surface, the pore width of elongated pores is 200 – 250 nm, where the pore depth is around 1.2 μm (Figure 3.3 (c) and (e)). For the TIPS treatment, the pore depth is closely affected by the local difference in sputtering yield and ion energy for etching. The pore depth is determined when the etching rate of Ta rich region and non-rich region become equilibrium state with sufficient time. Since the sputtering yield difference is proportional to the ion energy (substrate bias), the equilibrium state occurs deeper point, resulting in deeper pore creation.

After paclitaxel loading was performed, the surface morphologies were also observed by FE-SEM. Figure 3.4 present the surface and cross-sectional images after paclitaxel loading. The surface morphologies are almost same on all of the specimens, which shows all covered by paclitaxel uniformly (Figure 3.4 (a) - (c)). Paclitaxel was loaded without any crystallized phase which is easily detached during stent expansion. Figure 3.4 (d) – (f) shows that the cross-sectional images of

paclitaxel loaded samples. The paclitaxel layer shows darker gray color than Co-Cr substrate, and it is densely coated on each sample. The degree of drug infiltration into the porous surface is clearly observed by these cross-sectional images. Almost all of the portion of pores are fulfilled with paclitaxel with very small pore at the end of porous-structure (Figure (e) and (f)). Since the loaded drug into pores can provide the mechanical interlocking effect, the loading stability and prolonged release of drug are expected.

Loading stability of paclitaxel under strain

Stent is generally deformed during the implantation because expansion process is essential for stent surgery. However, the loaded drug can be delaminated by the deformation, and the delaminated drug can cause side effect at undesirable site by floating away in blood flow. In this regard, the loading stability of drug under strain is an important factor for drug eluting stent. The loading stability of paclitaxel under strain was performed as described as shown in Figure 3.1. The surface morphologies after 12 % strain of each sample are presented in Figure 3.5. In the low magnification images, a lot of delaminated regions are observed on paclitaxel coated bare Co-Cr surface, while no delamination was observed on 800 V and 1600 V Co-Cr surface (Figure 3.5 (a)-(c)). In the high magnification images, the delaminated regions on the bare Co-Cr sample expose the sample surface (Figure 3.5 (d)). The scratched surface formed by grinding is clearly observed at the delaminated region, indicating that the whole paclitaxel layer is delaminated

from the surface. On the contrary, paclitaxel layer on 800 V and 1600 V Co-Cr samples shows only crack formation without any delaminated regions (Figure 3.5 (e) and (f)). The reason of drug stability is expected because of the mechanical anchoring effect by the porous structure on the Co-Cr surfaces as described in Figure 3.1(c). The cross-sectional images of drug layer on each sample after strain test is presented in Figure 3.6. The cracked paclitaxel layer on bare Co-Cr surface is clearly delaminated and exposing the flat scratched surface, and even the attached paclitaxel layer also shows the gap between the drug layer and surface, meaning that the drug is not stably attached on the surface (Figure 3.6(a)). In contrast, the cracked paclitaxel layer on 800 V and 1600 V sample shows the tightly attached morphology on the porous layer. The mechanical anchoring effect of porous surface layer are well reported for the coating technology []. Here, since the infiltrated drugs are anchoring the whole drug layer tightly with the TIPS porous layer, no delamination occurs by the deformation. The anchoring effect of TIPS-treated surfaces provide the stable drug delivery even under the deformation for drug eluting stent application.

Release behavior of paclitaxel

The release behavior of paclitaxel in PBS with 0.05% Tween20 in 37°C shaking oven is monitored until 28 days as shown in Figure 3.7. To simulate the blood flow, spontaneous 60 rpm of shaking was performed during release test. The paclitaxel loaded on bare Co-Cr surface showed burst release behavior 80% of

paclitaxel is released in 6 h, and almost all of the paclitaxel was released in 7 days. In the case of paclitaxel loaded on 800 V Co-Cr surface, the release behavior prolonged until 21 days without rapid burst compared to bare Co-Cr sample. The paclitaxel loaded on 1600 V sample showed further sustained release behavior where the 20% of paclitaxel is still remained after 28 days. The sustained release behavior also associated with the mechanical anchoring effect of porous structure formed by TIPS treatment. The paclitaxel was not completely dissolved in PBS with 0.05% of Tween20 medium due to its hydrophobic nature. Thus, the release occurs with two mechanisms including small portion of dissolving in the medium and mechanical detachment from the surface. The portion of released amount is higher at mechanical detachment, thus the anchoring the drug by porous layer is very effective to prolong the drug release behavior of paclitaxel. The remained drug morphologies in pores are observed after 21 days of release as shown in Figure 3.8. Any trace of remained paclitaxel was not observed on bare Co-Cr surface after 21 days of release. However, the remained paclitaxel was observed in pores of the TIPS-treated 800 V and 1600 V Co-Cr surfaced after 21 days of release. The 800 V sample, especially, almost all of the drug were released at 21 days and no more release was observed at 28 days, the small amount of drugs were stuck in pores. The remained drug in pores would inhibit the VSMC growth.

***In vitro* efficiency of remained paclitaxel**

In vitro cellular response of VSMC to the remained paclitaxel after 7 and 21 days of release test were assessed in terms of cell adhesion, and cell proliferation as shown in Figure 3.9 and 3.10. The role of paclitaxel for stent application is inhibition of growth of VSMC, thus, the remained drug should suppress the cellular activity of VSMC. Based on the release behavior as shown in Figure 3.7, 7 days and 21 days were chosen for the test because almost all of the paclitaxel on bare and 800 V Co-Cr surfaces are released away at the point, respectively. Figure 3.9 shows the cell attachment (CLSM) after 1 day of culture, and proliferation (MTS) 3 days of culture VSMC on bare, 800 V, and 1600 V samples with remained paclitaxel after 7 days of release. The VSMC spreads and stretches well on the bare sample compared to other samples. Additionally, more attached cells were observed compared with other samples after one day of culture (Figure 3.9(a)). This is because most of the drug on bare Co-Cr surface was already released, resulting in insufficient inhibition of cellular activity. On the other hand, the cell morphology on the 800 V and 1600 V sample showed spherical shape without spreading, and the number of cells was much smaller than bare samples (Figure 3.9 (b) and(d)). The tendency was similar at 3 days of proliferation test by MTS assay. The VSMC on bare sample proliferate well compared to other two samples. The degree of proliferation of 800 V and 1600 V Co-Cr sample was similar level in MTS assay data. The remained drug amount on both samples are sufficient for suppressing the VSMC proliferation *in vitro*. After 21 days of release, the cellular responses of VSMC to the remained paclitaxel were evaluated with same protocols as shown in Figure 3.10. The VSMC spreads and stretches very well on the bare

sample after 1 day of culture like 7 days results (Figure 3.10(a)). The cells on the 800 V sample spreads a bit but it is not much (Figure 3.10(b). Even though the most of the drug were released from the surface, the drug inside pores (as shown in Figure 3.8(b)), still inhibit the initial cell spreading property. The 1600 V sample which is still containing sufficient remained drug prohibit the cell spreading very well, thus, the cell morphology is spherical even after 21 days of release (Figure 3.10(c)). The proliferation result after 3 days of culture are presented in Figure 3.10(d). The proliferation level of VSMC on the bare sample was much higher than other samples. Unlike the 7 days of results, the proliferation of 800 V sample was significantly higher than 1600 V sample. Even though the small amount of drugs were remained inside the pores, the amount was not sufficient to suppressing the proliferation compared to 1600 V sample. The *in vitro* results indicates that the remained drug on Co-Cr surface after certain period time of release can effectively suppress the proliferation of VSMC. Furthermore, 1600 V sample can suppress the growth of VSMC even after 21 days of release. Therefore, the 1600 V TIPS-treated Co-Cr surface can be a good candidate for the polymer-free drug eluting stent.

***In vivo* animal test**

The *in vitro* analysis demonstrated that the 1600 V TIPS treated Co-Cr surface shows the stable loading property and sustained release of paclitaxel more than 28 days, and the remained drug on the surface can inhibit the VSMC activity effectively. Based on the *in vitro* results, bare Co-Cr (Bare), bare Co-Cr with paclitaxel (Bare-PTX), 1600 V TIPS treated Co-Cr (TIPS-PTX) were chosen for

the *in vivo* animal test. The atherosclerosis model was used to examine the performance of stent in similar condition to the patients' vessel condition following the study protocol as presented in Figure 3.2.

The micro CT evaluation was performed for each specimen before the histological evaluation to estimate the degree of restenosis. The representative CT images of Bare, Bare-PTX, TIPS-PTX are presented in Figure 3.11(a-c). The white dots are the cross-section of stent struts, and the light gray area surrounded by struts are lumen area filled with contrast media. The black area between struts and lumen area is considered to be a neointima hyperplasia area. The neointima hyperplasia formed at TIPS-PTX inserted vessel shows much thinner thickness and small area compared to other two group of stent (Figure 3.11(c)). The percentage of area stenosis are quantified through an image analysis program, as shown in Figure 3.11(d). The area stenosis of Bare and Bare-PTX stents shows similar level, but the area stenosis of TIPS-PTX shows significantly low values. Since the stable loading and sustained release effect of TIPS-PTX can inhibit the SMC over-growth effectively as proved by *in vitro* cell test, the restenosis can be suppressed significantly. However, the micro CT images cannot indicate the neointima hyperplasia exactly, hence, the histological analysis was performed to confirm the effect of TIPS-PTX stent on neointima thickness. The representative histological images of vessels with each stent are presented in Figure 3.12. The trend is similar with micro-CT images. The neointima around the Bare and Bare-PTX stents shows similar thickness, but the TIPS-PTX shows much thinner thickness (Figure 3.12(c)). The stenosis level was quantified with an image analysis program. The stenosis

levels, and intima/media area ratio (I/M ratio) of proximal, medial, and distal part was compared segmentally, and the total average values were also statistically compared as shown in Figure 3.13. For all parts, the average value of area restenosis was decreased for TIPS-PTX stents, especially, in the case of medial part, the average value is significantly low compared to other two groups (Figure 3.13(a)). The total average values of stenosis also shows the significantly lowest level for TIPS-PTX stents (Figure 3.13(b)). The I/M ratio also shows the similar trend to the restenosis level. The TIPS-PTX stents presents the significantly low values of I/M ratio. These *in vivo* results demonstrate that the TIPS-treatment on stent surface can deliver the PTX effectively to the stent vessel, and the delivered drug can suppress the restenosis problem effectively.

This suggested that the ripple-structure formed by TIPS-treatment can be a effective drug carrier for stent application, and the TIPS-treated stent may be a promising candidate as a polymer-free drug eluting stent to substitute the polymer coated drug eluting stent.

3.4. Conclusion

In this study, the paclitaxel was delivered on TIPS-treated Co-Cr surface for the application of polymer-free drug eluting stent. The paclitaxel was well loaded inside the ripple structure created by TIPS-treatment. The loading stability was achieved by anchoring effect of ripple structure, and the enhancement of loading stability was evaluated by SEM observation after strain test. The drug loaded on ripple structure shows no delamination and stably anchored morphology. The sustained release property was also investigated. The paclitaxel on the bare Co-Cr surface shows burst release, and most of drugs were release after 7 days of release, but the paclitaxel loaded on TIPS-treated surface showed sustained release even after 28 days in the case of 1600 V treated Co-Cr surface. By the *in vitro* cell test, the effectiveness of remained drug on TIPS-treated surface was confirmed. Furthermore, the *in vivo* results demonstrated that the paclitaxel loaded on TIPS-treated Co-Cr stent shows effective restenosis inhibition property. Therefore, the TIPS-treated Co-Cr surface can be an excellent candidate for polymer-free drug eluting stent.

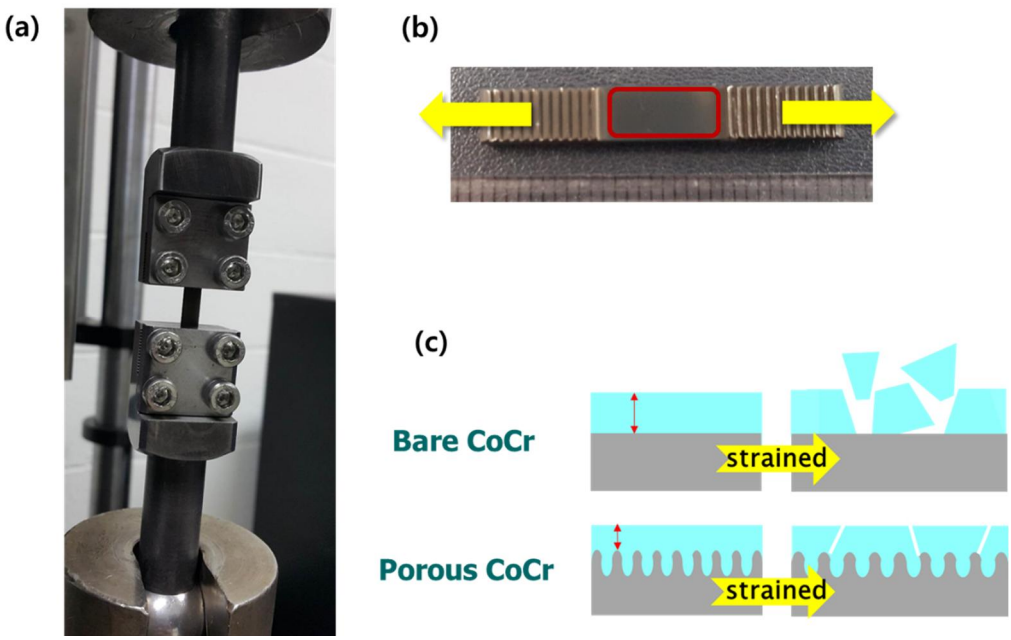

Figure 3.1. The optical image of (a) strain test by Instron machine, (b) the prepared specimen for strain test, and (c) the schematic diagram of mechanical anchoring effect of TIPS surface

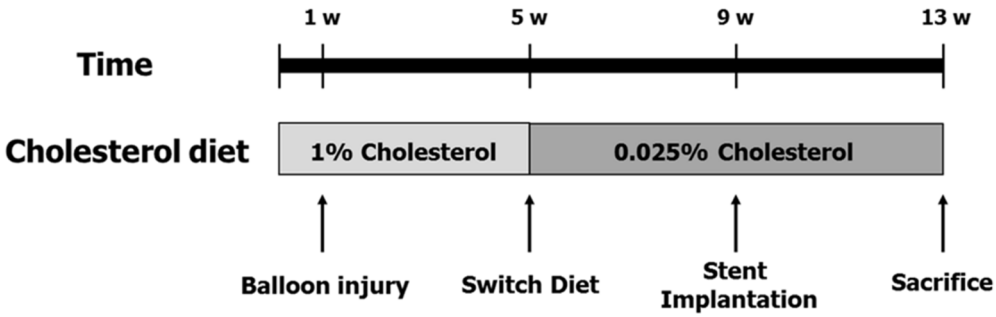

Figure 3.2. Study protocol for the atherosclerosis rabbit model for *in vivo* animal evaluation of stent performance

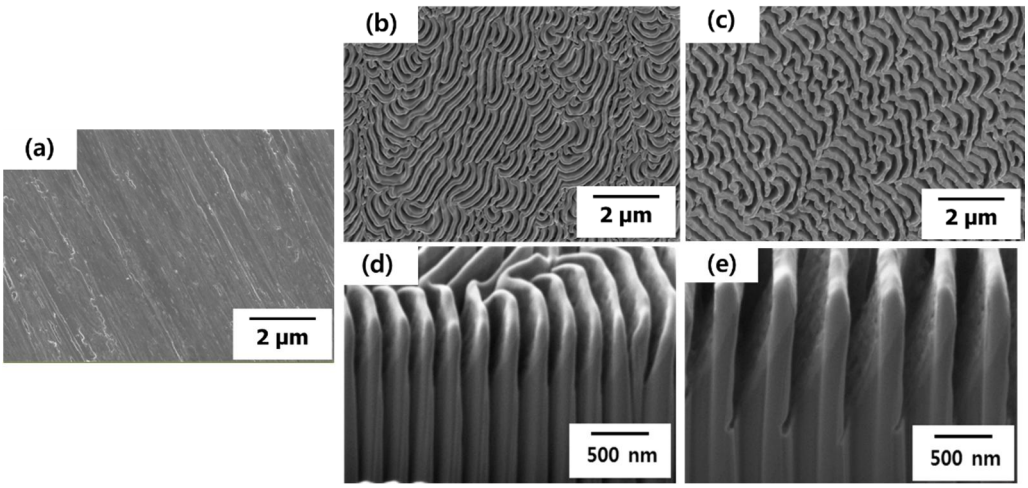

Figure 3.3. The typical surface morphology of (a) bare, (b) 800 V, and (c) 1600 V Co-Cr surface, and cross-sectional morphologies of (d) 800 V and (e) 1600 V Co-Cr surface

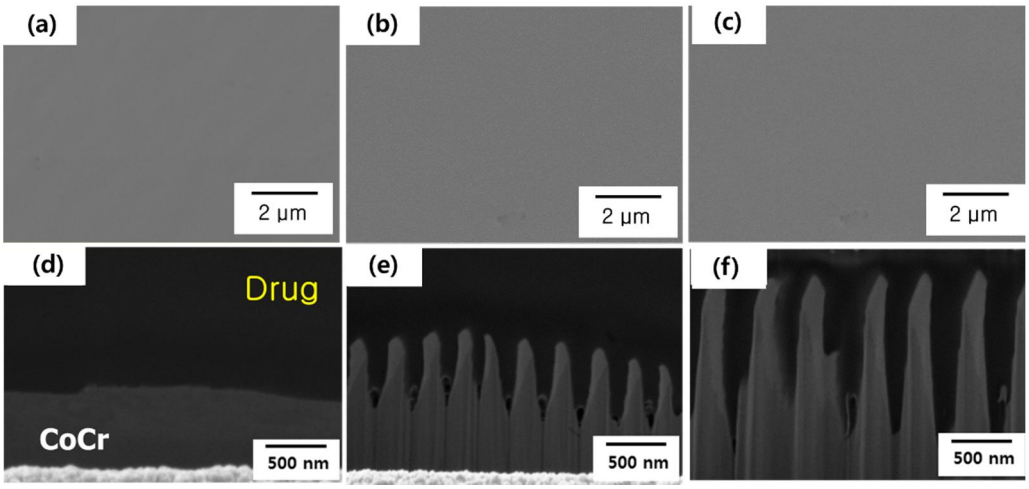

Figure 3.4. The typical surface morphology of (a) bare, (b) 800 V, and (c) 1600 V Co-Cr surface after paclitaxel loading, and (d-f) the cross-sections, respectably

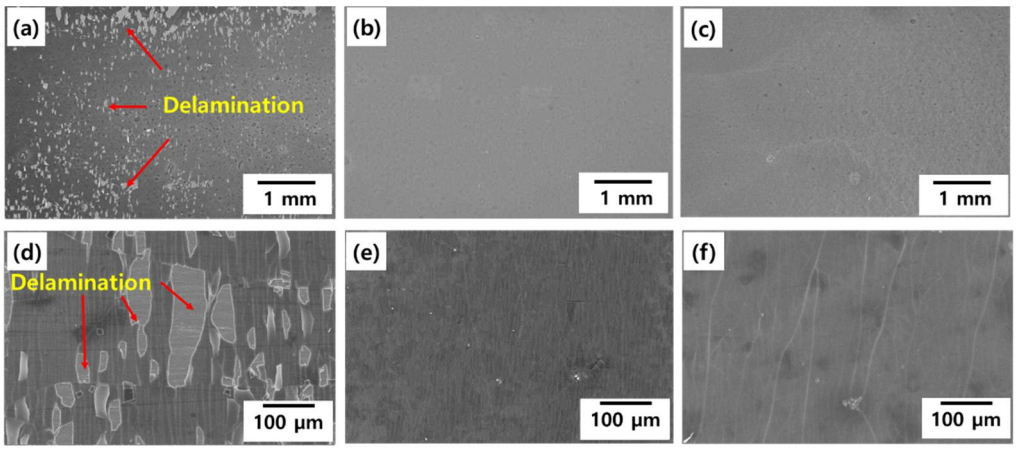

Figure 3.5. The morphology of paclitaxel on (a) bare, (b) 800 V, and (c) 1600 V after 12 % of deformation with low magnification (x20), and (d-f) the high magnification images, respectably

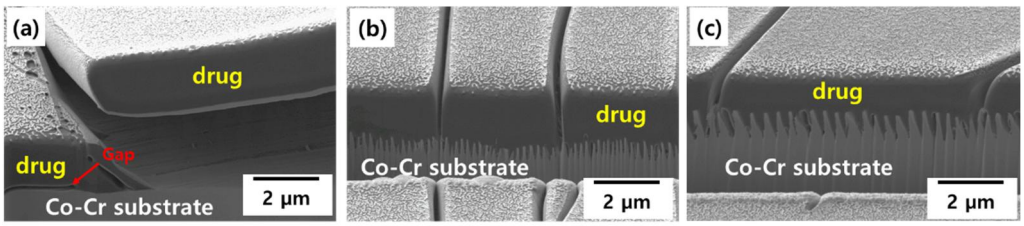

Figure 3.6. Cross-section images of paclitaxel layer on (a) bare, (b) 800 V, and (c) 1600 V Co-Cr surface after 12 % of deformation

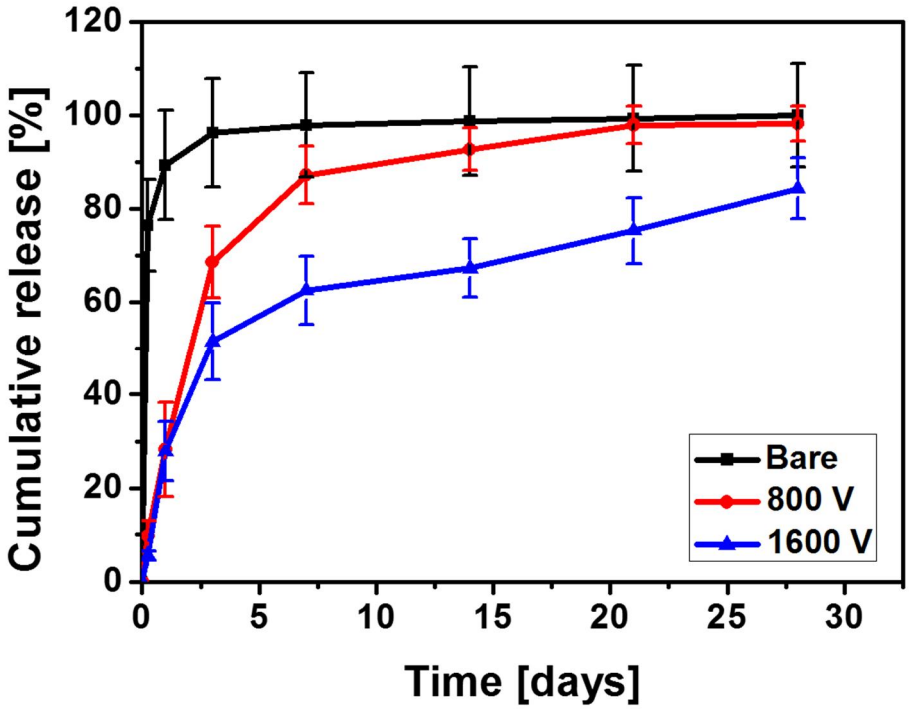

Figure 3.7. The cumulative release behavior of paclitaxel from bare, 800 V, and 1600 V surface in PBS with 0.05% of Tween20

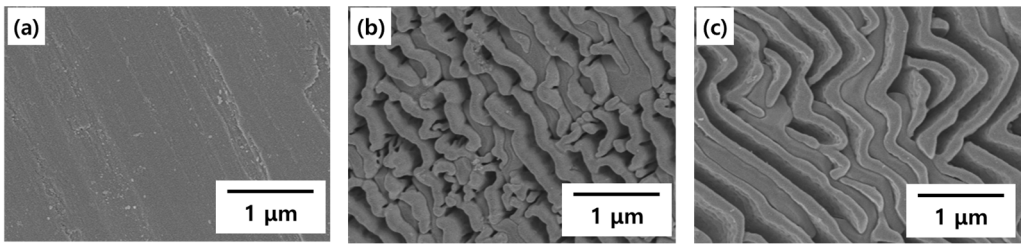

Figure 3.8. The surface morphology paclitaxel loaded (a) bare, (b) 800 V, and (c) 1600 V Co-Cr surface after 21 days of release

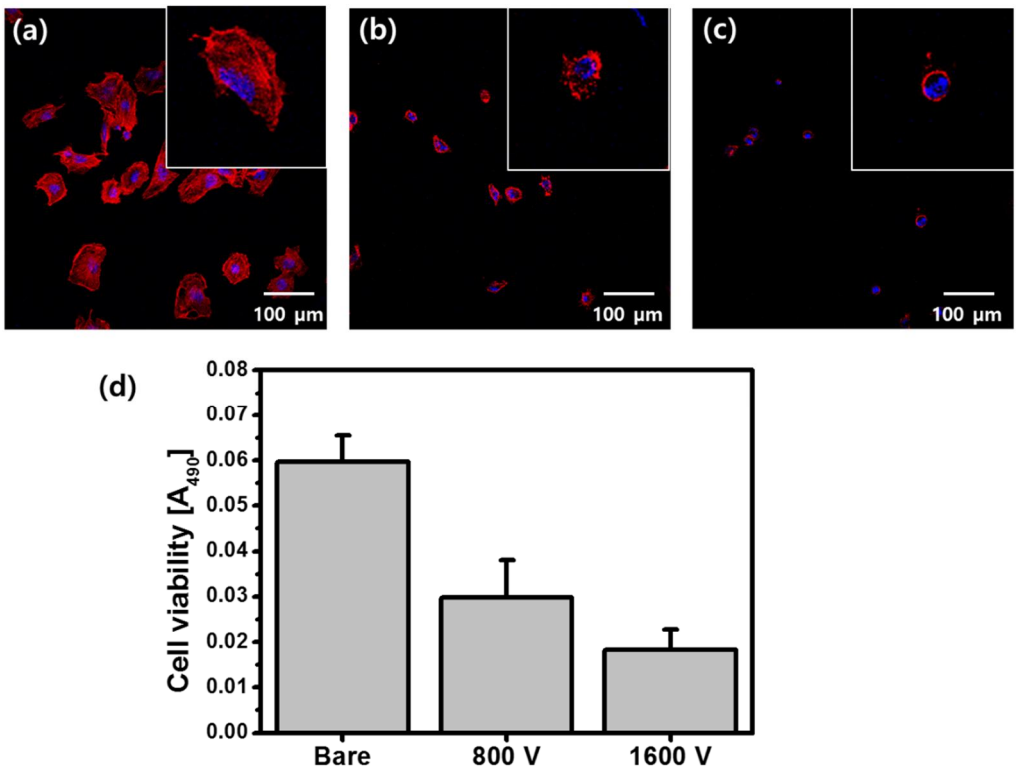

Figure 3.9. The CLSM image of VSMC (1 day) on paclitaxel loaded (a) bare, (b) 800 V, and (c) 1600 V after 7 days of release, and (d) the proliferation (MTS, 3 days) level of VSMC on each sample

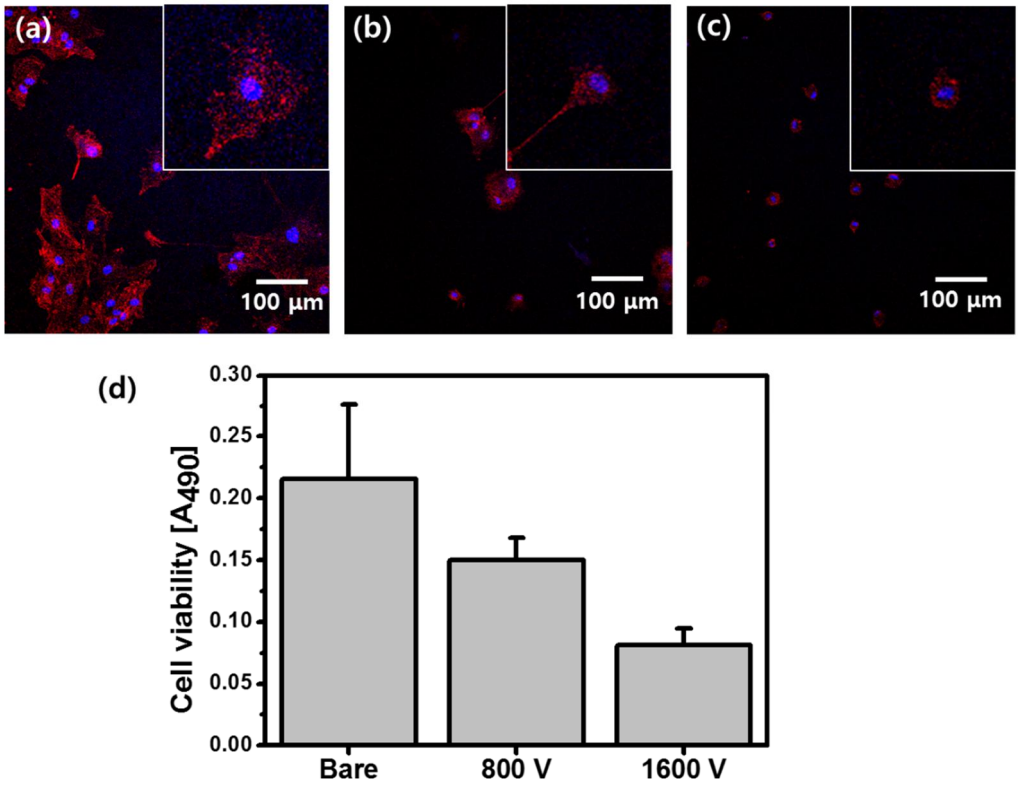

Figure 3.10. The CLSM image of VSMC (1 day) on paclitaxel loaded (a) bare, (b) 800 V, and (c) 1600 V after 21 days of release, and (d) the proliferation (MTS, 3 days) level of VSMC on each sample

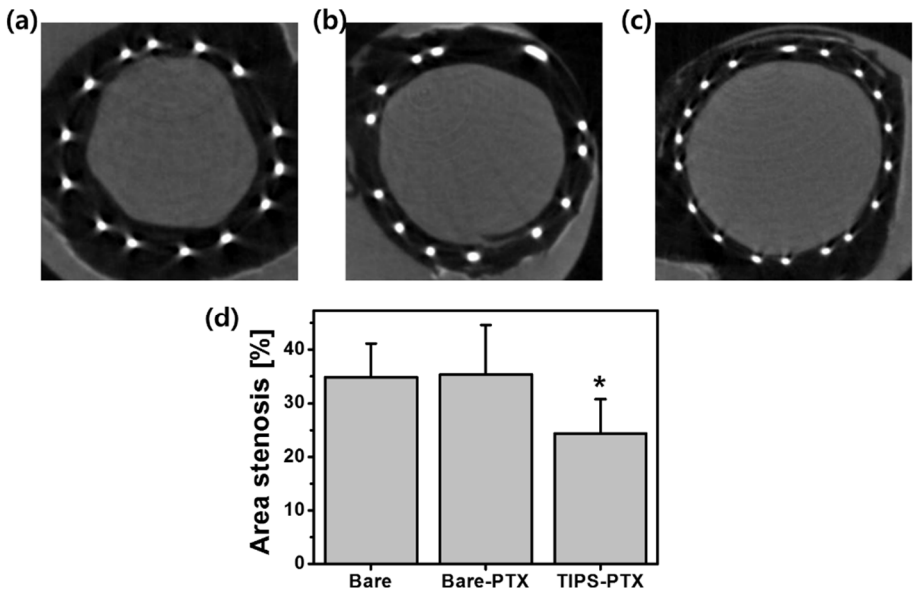

Figure 3.11. The micro CT image of (a) Bare, (b) Bare-PTX, and (c) TIPS-PTX stent inserted vessels, and the statistical graph of the area stenosis around each stent (*P<0.05 compared to other two groups)

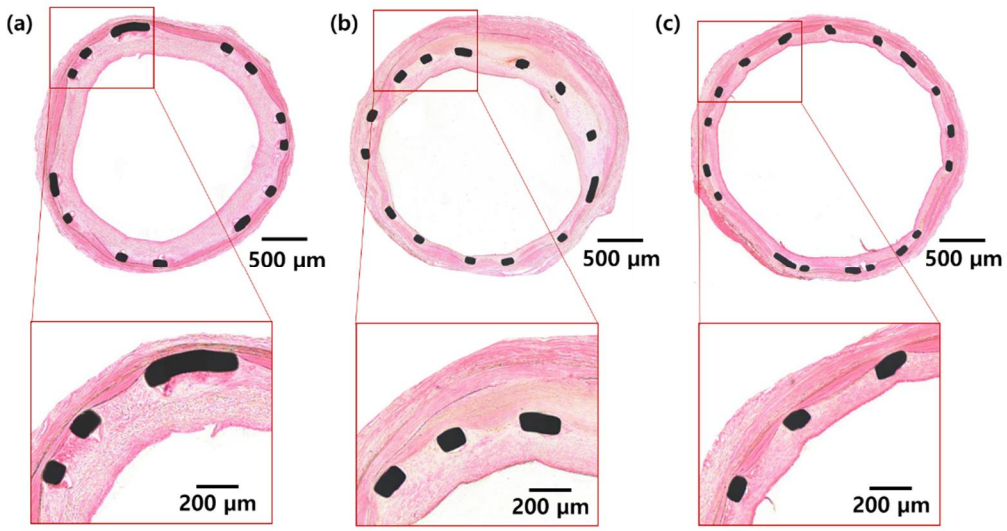

Figure 3.12. The histological image of (a) Bare, (b) Bare-PTX, and (c) TIPS-PTX stent inserted vessels with low and high magnification

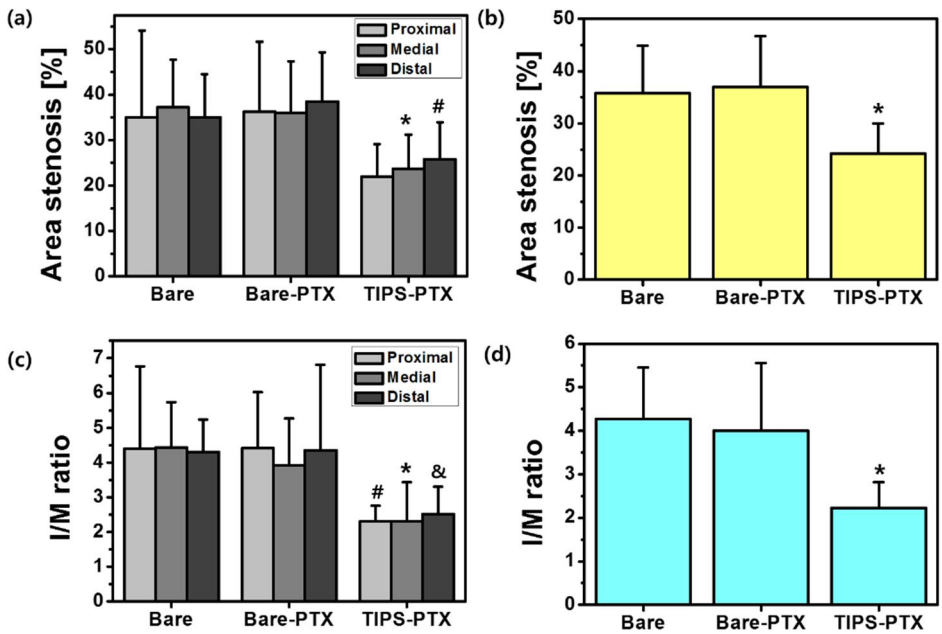

Figure 3.13. The statistical graphs of (a) segmental and (b) total average area stenosis around Bare, Bare-PTX, and TIPS-PTX stents, and the (c) segmental and (d) total average I/M ratio round each stent (*P<0.05 compared to other two groups, #P<0.05 compared to Bare-PTX, &P<0.05 compared to Bare)

Chapter 4.

Conclusion

In this thesis, we aimed to use target-ion induced plasma sputtering (TIPS) treated surface as a delivery platform for various type of therapeutic agent to achieve functionally improved metallic bio-implants. Since the TIPS-treated surface provides large surface area, and mechanically stable carrier layer, the surface deliver the various therapeutic agents very effectively.

Firstly, the TIPS-treated surface was introduced on the SLA-treated Ti surface for the rhBMP-2 delivery to enhance the osseointegration property of conventional dental fixture in chapter. 2. Compared to conventional SLA Ti surface, TIPS-treated SLA Ti (SLA/TIPS) surface delivered the larger amount of rhBMP-2 because of its hydrophilic property and sufficient storage room. The *in vitro* cell test indicated that the rhBMP-2 coated Ti surfaces significantly promoted the initial cell attachment and differentiation, and the nanoporous surface structure of SLA/TIPS-Ti substantially enhanced cell proliferation. Based on the *in vitro* results, BMP-2 coated SLA-Ti (SLA-BMP) and SLA/TIPS-Ti (SLA/TIPS-BMP) was further investigated with *in vivo* animal test. The SLA/TIPS-BMP screw exhibited higher quantitative values of bone in contact (BIC) and new bone volume (NBV) compared to SLA-BMP screws. The results demonstrated that the enhanced rhBMP-2 coating efficiency on SLA/TIPS surface can be a candidate for improved dental implants for enhanced osseointegration.

Further improve of dental implant, the nano-structured silver (Ag) coating was adopted on Ti surface to achieve additive antimicrobial activity of dental abutment. The extremely small amount of nano-scale Ag was immobilized on TIPS-treated Ti surface by short time (10 s) sputtering. The most Ag were immobilized on the top of nano-patterns of TIPS-treated Ti surface without noticeable change of cellular viability of TIPS surface. As the sputtering time increased, Ag contents increased, and the release Ag ions also increased. The antibacterial activity was not much affected by Ag contents, and all the Ag coated samples showed very high antibacterial activity. However, *in vitro* cell test shows that the cytotoxicity to the mammalian cells were significantly increased as the Ag content increased. In this study, the 10 s sputtering was indicated as the optimum condition because it showed the similar cell viability with bare Ti surface, and the very effective antibacterial activity. The nano-scale Ag coated TIPS Ti surface can be a good candidate for the dental abutment surface treatment to improve the success rate of implant surgery.

The rest of the study focused on the application of polymer-free drug eluting stent. The paclitaxel which is widely used drug for drug eluting application was delivered on the TIPS-treated Co-Cr surface. The TIPS-treated surface showed the ripple structure, and the paclitaxel was loaded inside the ripple structure very uniformly. The ripple structure anchored the

drug strongly, resulting in the stable drug loading against the deformation of substrate. Furthermore, the anchoring effect also affected to the drug release behavior, thus, the sustained release was achieved until 28 days. By the *in vitro* cell test, the effective inhibition of SMC proliferation by remained drug after 7 and 21 days of release was confirmed. Furthermore, in vivo animal test conducted on atherosclerosis rabbit model to prove the effectiveness of delivered paclitaxel on TIPS-treated Co-Cr stent. The micro-CT and histological results indicated that the paclitaxel delivered on TIPS-treated Co-Cr stent showed very effective suppression of restenosis level. The results suggested that the TIPS-treated surface on Co-Cr stent can be a very promising candidate of polymer-free drug eluting stent.

This study suggested that the effectiveness of TIPS-treated surface on various metallic implant can be a promising candidate for the delivery platform of therapeutic agents to improve the ability of metallic bio-implants. For the dental application, the rhBMP-2 and Ag were delivered on Ti implant surface effectively with proper TIPS-structure and process. For the stent application, the paclitaxel was very stably delivered on Co-Cr stent surface. These results support that the TIPS-surface can make a significant improvement of metallic implant application by its excellent delivery property.

References

1. Patrik Schmutz, N.-C.Q.-V., Isabel Gerber, *Metallic Medical Implants: Electrochemical Characterization of Corrosion Processes.* The Electrochemical Society Interface Summer, 2008: p. 35-40.
2. Castellanos, M.I., et al., *Functionalization of CoCr surfaces with cell adhesive peptides to promote HUVECs adhesion and proliferation.* Applied Surface Science, 2017. **393**: p. 82-92.
3. Long, M. and H.J. Rack, *Titanium alloys in total joint replacement - A materials science perspective.* Biomaterials, 1998. **19**(18): p. 1621-1639.
4. Ferrari, M., et al., *3-Year Randomized Controlled Prospective Clinical Trial on Different CAD-CAM Implant Abutments.* Clinical Implant Dentistry and Related Research, 2016. **18**(6): p. 1134-1141.
5. Guo, Y., et al., *Increased osteoblast function in vitro and in vivo through surface nanostructuring by ultrasonic shot peening.* International Journal of Nanomedicine, 2015. **10**: p. 4593-4603.
6. Ou, K.L., et al., *Osseointegration of titanium implants with SLAffinity treatment: a histological and biomechanical study in miniature pigs.* Clinical Oral Investigations, 2016. **20**(7): p. 1515-1524.
7. Xu, J.Y., et al., *Improved bioactivity of selective laser melting titanium: Surface modification with micro-/nano-textured hierarchical topography and bone regeneration performance evaluation.* Materials Science and Engineering C, 2016. **68**: p. 229-240.
8. Balshi, T.J. and G.J. Wolfinger, *Dental Implants in the Diabetic Patient: A Retrospective Study.* Implant Dentistry, 1999. **8**(4): p. 355-359.
9. Mellado-Valero, A., et al., *Effects of diabetes on the osseointegration of dental implants.* Medicina oral, patología oral y cirugía bucal, 2007. **12**(1): p. E38-43.
10. Larsson, C., et al., *Bone response to surface modified titanium implants: Studies on the early tissue response to machined and electropolished implants with different oxide thicknesses.* Biomaterials, 1996. **17**(6): p. 605-616.
11. Le Guehennec, L., et al., *Surface treatments of titanium dental implants for rapid osseointegration.* Dent Mater, 2007. **23**(7): p. 844-54.

12. He, D., et al., *Preparation of hydroxyapatite-titanium dioxide coating on Ti6Al4V substrates using hydrothermal-electrochemical method.* Journal Wuhan University of Technology, Materials Science Edition, 2016. **31**(2): p. 461-467.
13. Kim, M.H., et al., *Cell adhesion and in vivo osseointegration of sandblasted/acid etched/anodized dental implants.* International Journal of Molecular Sciences, 2015. **16**(5): p. 10324-10336.
14. Araújo, M., et al., *Glass coatings on zirconia with enhanced bioactivity.* Journal of the European Ceramic Society, 2016. **36**(13): p. 3201-3210.
15. Kang, K., A. Zakiyuddin, and K. Lee, *Electrochemical properties of HA coated titanium dioxide nanotubes.* Journal of Nanoscience and Nanotechnology, 2016. **16**(2): p. 1708-1710.
16. Colone, M., et al. *Drug delivery system and breast cancer cells*. in *AIP Conference Proceedings*. 2016.
17. Li, J., et al., *Total saponins of panaxnotoginseng promotes lymphangiogenesis by activation VEGF-C expression of lymphatic endothelial cells.* Journal of Ethnopharmacology, 2016. **193**: p. 293-302.
18. Li, Y., et al., *Silver Nanoparticle Based Codelivery of Oseltamivir to Inhibit the Activity of the H1N1 Influenza Virus through ROS-Mediated Signaling Pathways.* ACS Applied Materials and Interfaces, 2016. **8**(37): p. 24385-24393.
19. Bae, I.H., et al., *Anodic oxidized nanotubular titanium implants enhance bone morphogenetic protein-2 delivery.* J Biomed Mater Res B Appl Biomater, 2010. **93**(2): p. 484-91.
20. Schliephake, H., et al., *Effect of immobilized bone morphogenic protein 2 coating of titanium implants on peri-implant bone formation.* Clin Oral Implants Res, 2005. **16**(5): p. 563-9.
21. Abarrategi, A., et al., *Gene expression profile on chitosan/rhBMP-2 films: A novel osteoinductive coating for implantable materials.* Acta Biomaterialia, 2009. **5**(7): p. 2633-2646.
22. Chen, F.M., M. Zhang, and Z.F. Wu, *Toward delivery of multiple growth factors in tissue engineering.* Biomaterials, 2010. **31**(24): p. 6279-6308.
23. Tayalia, P. and D.J. Mooney, *Controlled growth factor delivery for tissue*

engineering. Advanced Materials, 2009. **21**(32-33): p. 3269-3285.

24. Liu, Y., et al., *The influence of BMP-2 and its mode of delivery on the osteoconductivity of implant surfaces during the early phase of osseointegration.* Biomaterials, 2007. **28**(16): p. 2677-86.
25. Teng, F.Y., et al., *Effects of Osseointegration by Bone Morphogenetic Protein-2 on Titanium Implants In Vitro and In Vivo.* Bioinorg Chem Appl, 2016. **2016**: p. 3837679.
26. Kim, N.H., et al., *Effects of rhBMP-2 on Sandblasted and Acid Etched Titanium Implant Surfaces on Bone Regeneration and Osseointegration: Spilt-Mouth Designed Pilot Study.* Biomed Res Int, 2015. **2015**: p. 459393.
27. Mei, S., et al., *Antibacterial effects and biocompatibility of titanium surfaces with graded silver incorporation in titania nanotubes.* Biomaterials, 2014. **35**(14): p. 4255-65.
28. Zheng, Y., et al., *Antimicrobial and osteogenic effect of Ag-implanted titanium with a nanostructured surface.* Int J Nanomedicine, 2012. **7**: p. 875-84.
29. Campoccia, D., et al., *Antibiotic-loaded biomaterials and the risks for the spread of antibiotic resistance following their prophylactic and therapeutic clinical use.* Biomaterials, 2010. **31**(25): p. 6363-6377.
30. Bai, L., et al., *Nanostructured titanium–silver coatings with good antibacterial activity and cytocompatibility fabricated by one-step magnetron sputtering.* Applied Surface Science, 2015. **355**: p. 32-44.
31. Kaba, S.I. and E.M. Egorova, *In vitro studies of the toxic effects of silver nanoparticles on HeLa and U937 cells.* Nanotechnol Sci Appl, 2015. **8**: p. 19-29.
32. Vrcek, I.V., et al., *Comparison of in vitro toxicity of silver ions and silver nanoparticles on human hepatoma cells.* Environ Toxicol, 2016. **31**(6): p. 679-92.
33. Wang, T., et al., *Paclitaxel drug-eluting tracheal stent could reduce granulation tissue formation in a canine model.* Chinese Medical Journal, 2016. **129**(22): p. 2708-2713.
34. Nguyen, V.D., et al., *Feasibility study of dual-targeting paclitaxel-loaded*

magnetic liposomes using electromagnetic actuation and macrophages. Sensors and Actuators, B: Chemical, 2017. **240**: p. 1226-1236.

35. Parry, T.J., et al., *Drug-eluting stents: sirolimus and paclitaxel differentially affect cultured cells and injured arteries.* Eur J Pharmacol, 2005. **524**(1-3): p. 19-29.
36. Bundhun, P.K., Z.J. Wu, and M.H. Chen, *Is There Any Significant Difference in Stent Thrombosis Between Sirolimus and Paclitaxel Eluting Stents?: A Systematic Review and Meta-Analysis of Randomized Controlled Trials.* Medicine (Baltimore), 2016. **95**(5): p. e2651.
37. Tsujino, I., et al., *Drug delivery via nano-, micro and macroporous coronary stent surfaces.* Expert Opin Drug Deliv, 2007. **4**(3): p. 287-95.
38. van der Giessen, W.J., et al., *Lowering the dose of sirolimus, released from a nonpolymeric hydroxyapatite coated coronary stent, reduces signs of delayed healing.* JACC Cardiovasc Interv, 2009. **2**(4): p. 284-90.
39. Alexis, F., et al., *In vitro study of release mechanisms of paclitaxel and rapamycin from drug-incorporated biodegradable stent matrices.* J Control Release, 2004. **98**(1): p. 67-74.
40. Byrne, R.A., et al., *Paclitaxel-eluting balloons, paclitaxel-eluting stents, and balloon angioplasty in patients with restenosis after implantation of a drug-eluting stent (ISAR-DESIRE 3): a randomised, open-label trial.* The Lancet, 2013. **381**(9865): p. 461-467.
41. Mani, G., N. Torres, and S. Oh, *Paclitaxel delivery from cobalt-chromium alloy surfaces using self-assembled monolayers.* Biointerphases, 2011. **6**(2): p. 33-42.
42. Livingston, M. and A. Tan, *Coating Techniques and Release Kinetics of Drug-Eluting Stents.* Journal of Medical Devices, 2015. **10**(1): p. 010801.
43. Han, L., et al., *BMP2-encapsulated chitosan coatings on functionalized Ti surfaces and their performance in vitro and in vivo.* Mater Sci Eng C Mater Biol Appl, 2014. **40**: p. 1-8.
44. Jun, S.H., et al., *Bone morphogenic protein-2 (BMP-2) loaded hybrid coating on porous hydroxyapatite scaffolds for bone tissue engineering.* J Mater Sci Mater Med, 2013. **24**(3): p. 773-82.
45. Pan, C.J., et al., *Preparation and characterization of rapamycin-loaded*

PLGA coating stent. J Mater Sci Mater Med, 2007. **18**(11): p. 2193-8.

46. Takahisa Masaki, W.Z. and A.K.C. Steven E. Kern, *In-vitro Release of Rapamycin from a Thermosensitive Polymer for the Inhibition of Vascular Smooth Muscle Cell Proliferation.* Journal of Bioequivalence & Bioavailability, 2009. **01**(01).
47. Schmidmaier, G., et al., *Local application of growth factors (insulin-like growth factor-1 and transforming growth factor-β1) from a biodegradable poly(D,L-lactide) coating of osteosynthetic implants accelerates fracture healing in rats.* Bone, 2001. **28**(4): p. 341-350.
48. Han, L., et al., *BMP2-encapsulated chitosan coatings on functionalized Ti surfaces and their performance in vitro and in vivo.* Materials Science and Engineering C, 2014. **40**: p. 1-8.
49. GhavamiNejad, A., et al., *Immobilization of silver nanoparticles on electropolymerized polydopamine films for metal implant applications.* Colloids and Interface Science Communications, 2015. **6**: p. 5-8.
50. Qureshi, A.T., et al., *Biocompatible/bioabsorbable silver nanocomposite coatings.* Journal of Applied Polymer Science, 2011. **120**(5): p. 3042-3053.
51. Kothwala, D., et al., *Paclitaxel drug delivery from cardiovascular stent.* Trends in Biomaterials and Artificial Organs, 2006. **19**(2): p. 88-92.
52. Jabara, R., et al., *Evaluation of a Novel Slow-Release Paclitaxel-Eluting Stent With a Bioabsorbable Polymeric Surface Coating.* JACC: Cardiovascular Interventions, 2008. **1**(1): p. 81-87.
53. Barfeie, A., J. Wilson, and J. Rees, *Implant surface characteristics and their effect on osseointegration.* Br Dent J, 2015. **218**(5): p. E9.
54. Costa, R.A., et al., *Polymer-Free Biolimus A9-Coated Stents in the Treatment of De Novo Coronary Lesions: 4- and 12-Month Angiographic Follow-Up and Final 5-Year Clinical Outcomes of the Prospective, Multicenter BioFreedom FIM Clinical Trial.* JACC Cardiovasc Interv, 2016. **9**(1): p. 51-64.
55. Jia, H., et al., *A novel polymer-free paclitaxel-eluting stent with a nanoporous surface for rapid endothelialization and inhibition of intimal hyperplasia: Comparison with a polymer-based sirolimus-eluting stent and bare metal stent in a porcine model.* J Biomed Mater Res A, 2011.

98(4): p. 629-37.

56. Kim, H.S., et al., *Fabrication and characterization of functionally graded nano-micro porous titanium surface by anodizing.* J Biomed Mater Res B Appl Biomater, 2009. **88**(2): p. 427-35.
57. Wu, S., X. Liu, and C. Gao, *Role of adsorbed proteins on hydroxyapatite-coated titanium in osteoblast adhesion and osteogenic differentiation.* Science Bulletin, 2015. **60**(7): p. 691-700.
58. Miletić, A., et al., *Influence of substrate roughness on adhesion of TiN coatings.* Journal of the Brazilian Society of Mechanical Sciences and Engineering, 2013. **36**(2): p. 293-299.
59. Varacalle, D.J., et al., *Effect of Grit-Blasting on Substrate Roughness and Coating Adhesion.* Journal of Thermal Spray Technology, 2006. **15**(3): p. 348-355.
60. Huh, J.B., et al., *Alveolar ridge augmentation using anodized implants coated with Escherichia coli-derived recombinant human bone morphogenetic protein 2.* Oral Surg Oral Med Oral Pathol Oral Radiol Endod, 2011. **112**(1): p. 42-9.
61. Huh, J.B., et al., *Effects of anodized implants coated with Escherichia coli-derived rhBMP-2 in beagle dogs.* Int J Oral Maxillofac Surg, 2012. **41**(12): p. 1577-84.
62. Orozco Carmona, V., et al., *Effect of silver nanoparticles in a hydroxyapatite coating applied by atmospheric plasma spray.* International Journal of Electrochemical Science, 2014. **9**(12): p. 7471-7494.
63. van der Giessen, W.J., et al., *Lowering the Dose of Sirolimus, Released From a Nonpolymeric Hydroxyapatite Coated Coronary Stent, Reduces Signs of Delayed Healing.* JACC: Cardiovascular Interventions, 2009. **2**(4): p. 284-290.
64. Wieneke, H., et al., *Synergistic Effects of a Novel Nanoporous Stent Coating and Tacrolimus on Intima Proliferation in Rabbits.* Catheterization and Cardiovascular Interventions, 2003. **60**(3): p. 399-407.
65. Wheeler, S.L., *Eight-year clinical retrospective study of titanium plasma-sprayed and hydroxyapatite-coated cylinder implants.* International

Journal of Oral and Maxillofacial Implants, 1996. **11**(3): p. 340-350.

66. Tinsley, D., C.J. Watson, and J.L. Russell, *A comparison of hydroxylapatite coated implant retained fixed and removable mandibular prostheses over 4 to 6 years.* Clinical Oral Implants Research, 2001. **12**(2): p. 159-166.
67. Kollum, M., et al., *Particle debris from a nanoporous stent coating obscures potential antiproliferative effects of tacrolimus-eluting stents in a porcine model of restenosis.* Catheterization and Cardiovascular Interventions, 2005. **64**(1): p. 85-90.
68. Lamichhane, S., et al., *Interaction of endothelial and smooth muscle cells with cobalt-chromium alloy surfaces coated with paclitaxel deposited self-assembled monolayers.* Langmuir, 2013. **29**(46): p. 14254-64.
69. Mani, G., et al., *Delivery of paclitaxel from cobalt-chromium alloy surfaces without polymeric carriers.* Biomaterials, 2010. **31**(20): p. 5372-5384.
70. Jang, T.-S., et al., *Large-scale nanopatterning of metal surfaces by target-ion induced plasma sputtering (TIPS).* Rsc Advances, 2016. **6**(28): p. 23702-23708.
71. Zhang, K., M. Brötzmann, and H. Hofsäss, *Surfactant-driven self-organized surface patterns by ion beam erosion.* New Journal of Physics, 2011. **13**(1): p. 013033.
72. Hofsäss, H., et al., *The role of phase separation for self-organized surface pattern formation by ion beam erosion and metal atom co-deposition.* Applied Physics A, 2012. **111**(2): p. 653-664.
73. Pham, V.-H., et al., *Creation of nanoporous tantalum (Ta)-incorporated titanium (Ti) surface onto Ti implants by sputtering of Ta in Ar under extremely high negative substrate biases.* Journal of Materials Chemistry, 2012. **22**(47): p. 24798.
74. Tengvall, P. and I. Lundström, *Physico-chemical considerations of titanium as a biomaterial.* Clinical Materials, 1992. **9**(2): p. 115-134.
75. Cochran, D.L., et al., *The use of reduced healing times on ITI® implants with a sandblasted and acid-etched (SLA) surface: Early results from clinical trials on ITI® SLA implants.* Clinical Oral Implants Research, 2002.

13(2): p. 144-153.

76. Oates, T.W., et al., *Enhanced implant stability with a chemically modified SLA surface: A randomized pilot study.* International Journal of Oral and Maxillofacial Implants, 2007. **22**(5): p. 755-760.
77. Bornstein, M.M., et al., *Early loading of nonsubmerged titanium implants with a sandblasted and acid-etched (SLA) surface: 3-Year results of a prospective study in partially edentulous patients.* International Journal of Oral and Maxillofacial Implants, 2003. **18**(5): p. 659-666.
78. Gu, Y.X., et al., *The roles of PI3K/Akt signaling pathway in regulating MC3T3-E1 preosteoblast proliferation and differentiation on SLA and SLActive titanium surfaces.* J Biomed Mater Res A, 2013. **101**(3): p. 748-54.
79. Rupp, F., et al., *Enhancing surface free energy and hydrophilicity through chemical modification of microstructured titanium implant surfaces.* Journal of Biomedical Materials Research - Part A, 2006. **76**(2): p. 323-334.
80. Huh, J.B., et al., *Physical stability of arginine-glycine-aspartic acid peptide coated on anodized implants after installation.* J Adv Prosthodont, 2013. **5**(2): p. 84-91.
81. Chang, Y.C., et al., *Fibronectin-Grafted Titanium Dental Implants: An in Vivo Study.* BioMed Research International, 2016. **2016**.
82. Jiang, Q.H., et al., *Bone response to the multilayer BMP-2 gene coated porous titanium implant surface.* Clin Oral Implants Res, 2013. **24**(8): p. 853-61.
83. Wang, J., et al., *BMP-functionalised coatings to promote osteogenesis for orthopaedic implants.* Int J Mol Sci, 2014. **15**(6): p. 10150-68.
84. Kim, H., et al., *The biocompatibility of SLA-treated titanium implants.* Biomed Mater, 2008. **3**(2): p. 025011.
85. Muthukuru, M., *Bone morphogenic protein-2 induces apoptosis and cytotoxicity in periodontal ligament cells.* J Periodontol, 2013. **84**(6): p. 829-38.
86. Kim, J.E., et al., *The effect of anodized implants coated with combined rhBMP-2 and recombinant human vascular endothelial growth factors*

on vertical bone regeneration in the marginal portion of the peri-implant. Oral Surg Oral Med Oral Pathol Oral Radiol, 2013. **115**(6): p. e24-31.

87. Chirico, G., et al., *Dynamics of green fluorescent protein mutant2 in solution, on spin-coated glasses, and encapsulated in wet silica gels.* Protein Sci, 2002. **11**(5): p. 1152-61.
88. Han, C.M., H.E. Kim, and Y.H. Koh, *Creation of hierarchical micro/nano-porous TiO2 surface layer onto Ti implants for improved biocompatibility.* Surface & Coatings Technology, 2014. **251**: p. 226-231.
89. Yang, H.S., et al., *Comparison between heparin-conjugated fibrin and collagen sponge as bone morphogenetic protein-2 carriers for bone regeneration.* Exp Mol Med, 2012. **44**(5): p. 350-5.
90. Shah, A.K., et al., *Mechanism of BMP-2 stimulated adhesion of osteoblastic cells to titanium alloy.* Biology of the Cell, 1999. **91**(2): p. 131-142.
91. Lavenus, S., G. Louarn, and P. Layrolle, *Nanotechnology and dental implants.* Int J Biomater, 2010. **2010**: p. 915327.
92. Lee, I.-K., et al., *Analysis of attachment, proliferation and differentiation response of human mesenchymal stem cell to various implant surfaces coated with rhBMP-2.* The Journal of Korean Academy of Prosthodontics, 2012. **50**(1): p. 44.
93. Gautschi, O.P., et al., *Apoptosis induction and reduced proliferation in human osteoblasts by rhBMP-2, -4 and -7.* Journal of Musculoskeletal Neuronal Interactions, 2009. **9**(1): p. 53-60.
94. Ogasawara, T., et al., *Bone morphogenetic protein 2-induced osteoblast differentiation requires Smad-mediated down-regulation of Cdk6.* Mol Cell Biol, 2004. **24**(15): p. 6560-8.
95. Warashina, H., et al., *Biological reaction to alumina, zirconia, titanium and polyethylene particles implanted onto murine calvaria.* Biomaterials, 2003. **24**(21): p. 3655-61.
96. Simchi, A., et al., *Recent progress in inorganic and composite coatings with bactericidal capability for orthopaedic applications.* Nanomedicine: Nanotechnology, Biology, and Medicine, 2011. **7**(1): p. 22-39.

97. Aughenbaugh, W., S. Radin, and P. Ducheyne, *Student research award in the undergraduate degree candidate category, 27th annual meeting of the society for biomaterials, St. Paul, Minnesota, April 24-29, 2001: Silica sol-gel for the controlled release of antibiotics. Ii. The effect of synthesis parameters on the in vitro release kinetics of vancomycin.* Journal of Biomedical Materials Research, 2001. **57**(3): p. 321-326.
98. Gómez-Florit, M., J.M. Ramis, and M. Monjo, *Anti-fibrotic and anti-inflammatory properties of melatonin on human gingival fibroblasts in vitro.* Biochemical Pharmacology, 2013. **86**(12): p. 1784-1790.
99. MÃ¼ller, N., P. Schmidlin, and M. Ã–zcan, *Adhesive durability of bone cements containing gentamicin or gentamicin/clindamycin-based antibiotics on titanium used for oral implants.* Journal of Adhesion Science and Technology, 2016. **30**(19): p. 2130-2145.
100. Agnihotri, S., S. Mukherji, and S. Mukherji, *Size-controlled silver nanoparticles synthesized over the range 5–100 nm using the same protocol and their antibacterial efficacy.* RSC Adv., 2014. **4**(8): p. 3974-3983.
101. Franci, G., et al., *Silver nanoparticles as potential antibacterial agents.* Molecules, 2015. **20**(5): p. 8856-74.
102. Wijnhoven, S.W.P., et al., *Nano-silver – a review of available data and knowledge gaps in human and environmental risk assessment.* Nanotoxicology, 2009. **3**(2): p. 109-138.
103. Tran, H.V., et al., *Synthesis, characterization, antibacterial and antiproliferative activities of monodisperse chitosan- based silver nanoparticles.* Colloids and Surfaces A: Physicochemical and Engineering Aspects, 2010. **360**(1-3): p. 32-40.
104. Abdelgawad, A.M., S.M. Hudson, and O.J. Rojas, *Antimicrobial wound dressing nanofiber mats from multicomponent (chitosan/silver-NPs/polyvinyl alcohol) systems.* Carbohydrate Polymers, 2014. **100**: p. 166-178.
105. Reidy, B., et al., *Mechanisms of Silver Nanoparticle Release, Transformation and Toxicity: A Critical Review of Current Knowledge and Recommendations for Future Studies and Applications.* Materials, 2013.

6(6): p. 2295-2350.

106. Nguyen, V.Q., et al., *Development of antimicrobial biomaterials produced from chitin-nanofiber sheet/silver nanoparticle composites.* Journal of Nanobiotechnology, 2014. **12**(1).
107. Duran, N., et al., *Silver nanoparticle protein corona and toxicity: a mini-review.* J Nanobiotechnology, 2015. **13**: p. 55.
108. Zhu, Y., et al., *Hierarchical micro/nanostructured titanium with balanced actions to bacterial and mammalian cells for dental implants.* Int J Nanomedicine, 2015. **10**: p. 6659-74.
109. Park, J.K., et al., *Development of a novel drug-eluting stent consisting of an abluminal and luminal coating layer dual therapy system.* RSC Advances, 2015. **5**(51): p. 40700-40707.
110. Livingston, M. and A. Tan, *Coating techniques and release kinetics of drug-eluting stents.* Journal of Medical Devices, Transactions of the ASME, 2016. **10**(1).
111. Kipshidze, N., et al., *Role of the endothelium in modulating neointimal formation: Vasculoprotective approaches to attenuate restenosis after percutaneous coronary interventions.* Journal of the American College of Cardiology, 2004. **44**(4): p. 733-739.
112. Lamichhane, S., et al., *Interaction of endothelial and smooth muscle cells with cobalt-chromium alloy surfaces coated with paclitaxel deposited self-assembled monolayers.* Langmuir, 2013. **29**(46): p. 14254-14264.
113. Cheneau, E., et al., *Time course of stent endothelialization after intravascular radiation therapy in rabbit iliac arteries.* Circulation, 2003. **107**(16): p. 2153-2158.
114. Khan, W., et al., *Carrier free rapamycin loaded drug eluting stent: in vitro and in vivo evaluation.* J Control Release, 2013. **168**(1): p. 70-6.
115. Xi, T., et al., *In vitro and in vivo changes to PLGA/sirolimus coating on drug eluting stents.* Biomaterials, 2010. **31**(19): p. 5151-8.
116. Abizaid, A. and J.R. Costa, Jr., *New drug-eluting stents: an overview on biodegradable and polymer-free next-generation stent systems.* Circ Cardiovasc Interv, 2010. **3**(4): p. 384-93.
117. Chen, W., et al., *Polymer-Free Drug-Eluting Stents: An Overview of*

Coating Strategies and Comparison with Polymer-Coated Drug-Eluting Stents. Bioconjug Chem, 2015. **26**(7): p. 1277-88.

118. Lamichhane, S., A. Gallo, and G. Mani, *A polymer-free Paclitaxel eluting coronary stent: effects of solvents, drug concentrations and coating methods.* Ann Biomed Eng, 2014. **42**(6): p. 1170-84.

119. Alpaslan, E., B. Ercan, and T.J. Webster, *Anodized 20 nm diameter nanotubular titanium for improved bladder stent applications.* International journal of nanomedicine, 2011. **6**: p. 219-225.

초 록

오늘날 금속 임플란트는 그 물리, 화학, 생물학적 안정성을 바탕으로 치과용, 정형외과용 임플란트, 심혈관용 스텐트 등 다양한 의료 응용분야에 널리 사용되고 있다. 하지만 충분치 못한 생체 활성, 감염에 대한 취약함, 등 부작용들을 해결하기 위해 여전히 금속 임플란트의 기능개선에 대한 연구가 필요로 되는 실정이다. 최근 연구에 의하면 금속 임플란트에 부가적인 기능을 부가하기 위해 임플란트에 치료제를 전달하는 연구가 활발하게 이루어지고 있다. 이 때, 원하는 성능을 얻기 위해서는 충분한 양의 치료제가 안정적으로 전달이 되어야 하기 때문에 다양한 전달 플랫폼이 연구되었다. 그 예로, 고분자 코팅층, 다공성 세라믹 코팅층, 그리고 그 외 화학적 결합방식 등이 연구되었는데 특정 임플란트 분야에서는 생물학적, 기계적 안정성의 한계로 인해 그 사용이 제한되고 있다. 본 연구에서는 금속 임플란트 표면에 생물학적, 기계적으로 안정한 나노-/마이크로- 수준의 다공성의 금속층을 Target-ion Induced Plasma Sputtering (TIPS)이라는 식각에 기반한 공정을 통해 형성하고, 이 표면층을 통해 다양한 치료제를 전달, 그 효과를 평가하여 TIPS 공정을 통한 금속층의 치료제의 전달 플랫폼으로써 가능성을 확인하고자 한다.

먼저, 치과용 임플란트의 Fixture 부분의 골유착능 향상을 위해 Sandblasting with large-grit and acid etching (SLA) 처리가 된 티타늄 표면에 TIPS 공정을 진행하여, 마이크로-/나노- 수준이 공존하는 표면적이 극대화 된 이중층을 형성하고, Bone morphogenetic protein-2 (BMP-2)를 그 표면에 코팅하여 전달하였다. 형성된 구조로 인해 증가된 친수성과 표면적으로 인하여, BMP-2 의 코팅량이 확연히 증가되는 것을 확인할 수 있었고, 조골모세포를 통한 세포 실험을 통하여, 형성된 이중층에 BMP-2 를 코팅할 경우 코팅량 증가 효과에 의해 가장 뛰어난 세포

부착특성과 세포 분화 특성을 보이는 것을 확인할 수 있었다. 반면, 세포의 증식은 BMP-2 의 유무보다는 구조 자체에 의한 증가 효과가 더 큰 것을 확인할 수 있었다. 이를 통해, 구조적인 효과와 BMP-2 코팅량 증가효과의 시너지 효과로 실제 골유착능의 향상이 이루어 질 것이라 예측할 수 있었고, 잡견 하악 모델 이용한 동물실험을 통해 확인해본 결과 실제로 SLA 단일층에 BMP-2 를 코팅한 임플란트 표면대비 이중층 구조에 BMP-2 를 코팅한 임플란트 표면에서 더 높은 수준의 골유착능이 나타나는 것을 Bone in contact 값과 New bone volume 값의 향상을 통해 확인할 수 있었다. 부가적으로, 치과용 임플린트 abutment 부분에 항균 특성을 부여하기 위해 티타늄 표면 TIPS 공정을 진행하여 나노 수준의 기공층을 형성하고, sputtering 을 통해 그 표면에 은을 소량 코팅하여 전달하였다. 나노 기공층의 상단부에 은이 집중적으로 코팅이 되었으며, 공정 시간 증가에 따라 은의 함량이 증가하고 은 이온의 방출량이 증가되는 것을 확인할 수 있었다. 그 후, 대장균을 이용해 은 함량에 따른 항균 성능 평가를 진행하였는데, 은이 존재할 경우 그 함량에 상관없이 뛰어난 항균 특성을 보이는 것을 확인할 수 있었다. 반면, 섬유아세포를 통한 세포독성 평가에서는 은의 함량이 높아질수록 세포 증식이 억제되는 것을 확인하였고, 은을 10 초간 코팅한 경우 순수 티타늄과 비슷한 수준의 세포 증식수준을 보이면서도 뛰어난 항균특성을 보였기 때문에, 이를 최적조건으로 선정하였다.

마지막으로, 혈관 재협착을 방지용 고분자층이 없는 약물 방출 스텐트를 개발하기 위해 코발트-크롬 합금 표면에 TIPS 처리를 하여 Paclitaxel 을 전달하는 연구를 진행하였다. TIPS 공정의 기판 바이어스를 조절하여 크기와 깊이가 다른 두 기공구조를 형성하였고, Paclitaxel 을 담지 하였다. 표면과 단면 관찰을 통해 Paclitaxel 이 균일하게, 그리고 기공구조의 내부까지 잘 담지가 되었음을 확인할 수 있었다. 그 후, 약물의 담지 안정성을 평가하기 위해 기판에 변형을 가하고, 담지 된

약물층의 변화를 관찰하였는데, 처리가 되지 않은 코발트-크롬 합금 표면에서는 약물 층이 탈락하는 것이 관찰되는 반면, TIPS 처리가 된 코발트-크롬 합금표면에서는 약물 층의 탈락이 전혀 관찰되지 않는 것을 확인할 수 있었다. 단면을 관찰하였을 때, 기공 내부로 침투된 약물에 의해 약물층이 강하게 고정되어있는 것을 확인할 수 있었다. 약물 방출거동 평가도 진행하였는데, 처리 되지 않은 표면에서는 7 일 이내에 대부분의 약물이 방출되는데 반해, 처리가 된 경우 최대 28 일이 지난 후에도 80% 정도의 약물만이 방출된 것을 확인할 수 있었다. 약물 방출거동에 기반하여, 방출 후 남은 약물의 세포 증식효과를 혈관 근육세포를 통해 확인하였다. 7 일 과 21 일의 약물 방출을 진행한 후, 약물이 남아있는 시편 표면에 세포를 배양한 결과, 처리가 되지 않은 시편에서는 세포 부착이 잘 일어나고 증식도 잘 일어나는데 반면, 약물이 많이 남아있는 처리가 된 시편에서는 세포의 부착과 증식이 모두 억제되는 것을 확인할 수 있었다. 최종적으로, 죽상동맥경화증을 일으킨 토끼 장골동맥 모델을 통해 스텐트의 효과를 평가해보니, TIPS 처리를 하여 Paclitaxel 을 전달한 스텐트가 비교군에 비해 확연하게 재협착 증상을 억제하는 것을 확인할 수 있었다.

본 연구를 통해서 TIPS 구조층 표면에 다양한 치료제를 전달하고 그 효과를 확인할 수 있었다. TIPS 구조를 필요에 맞게 형성하고, 이를 통해 적절한 치료제 전달을 할 수 있음을 확인함으로써, TIPS 구조의 치료제 전달 플랫폼으로써의 응용가능성을 입증하였다.

주요어 : 금속 임플란트, 치과용 임플란트, 약물 전달 스텐트, 치료제 전달, 표면 기공구조, 골유착능 향상, 항균, 재협착 방지

학번 : 2011-20628

Curriculum Vitae

BIBLIOGRAPHY

Name: Sungwon Kim

Date of Birth: May, 29th, 1987

Nationality: Republic of Korea

EDUCATION

Integrated M.S./Ph.D. in Department of Materials Science and Engineering,

Seoul National University, Seoul, Korea Feb. 2017

Thesis: Therapeutic Agent coating on Structure Modified Metallic Bio-implant Surface to Improve Biological Activity.

Advisor: Professor Hyoun-Ee Kim

B.S. in Department of Materials Science and Engineering, Seoul National University, Seoul, Korea Feb. 2011

RESEARCH FIELDS

Seoul National University, Seoul, Korea

Doctoral Thesis research Mar. 2011 – Feb. 2017

Advisor: Professor Hyoun-Ee Kim

- Powder Metallurgy : Fabrication of porous Ti scaffold
- Surface treatment of metal : Silver coating by sputtering, Polymer coating, Fabrication of nano-patterned surface by Target-ion Induced Plasma Sputtering (TIPS)
- Therapeutic agent delivery : Bone morphogenetic protein, Silver, Paclitaxel delivery
- Biological evaluations : *In-vitro* cell test, *In vivo* animal test, bacterial test

PUBLICATIONS

1. **Sungwon Kim**, Hyun-Do Jung, Min-Ho Kang, Hyoun-Ee Kim, Young-Hag Koh, Yuri Estrin, Fabrication of porous titanium scaffold with controlled porous structure and net-shape using magnesium as spacer, Materials Science and Engineering: C 33(5) 2808-2815, 2013/ 8

2. Min-Ho Kang, Hyun-Do Jung, **Sungwon Kim**, Sung-Mi Lee, Hyoun-Ee Kim,Yuri Estrin, Young-Hag Koh, Production and bio-corrosion resistance of porous magnesium with hydroxyapatite coating for biomedical applications, Materials Letters 108 122-124 2013/ 10

3. Tae-Sik Jang, **Sungwon Kim**, Hyun-Do Jung, Jin-Wook Chung, Hyoun-Ee Kim, Young-Hag Koh, and Juha Song, Large-scale nanopatterning of metal surfaces by target-ion induced plasma sputtering (TIPS), RSC Advances 6 23702-23708 2016/ 2

4. Min-Ho Kang, Tae-Sik Jang, **Sungwon Kim**, Hui-Sun Park, Juha Song, Hyoun-Ee Kim, Kyung-Hwan Jung, Hyun-Do Jung, MgF2-coated porous magnesium/alumina scaffolds with improved strength, corrosion resistance, and biological performance for biomedical applications, Materials Science and Engineering C 62 634-642 2016/ 3

5. Jaeuk Baek, Hyun-Do Jung, Tae-Sik Jang, **Sungwon Kim**, Min Ho Kang, Hyoun-Ee Kim, Young-Hag Koh, Synthesis and evaluation of bone morphogenetic protein(BMP)-loaded hydroxyapatite microsphere for enhanced bone regeneration, Ceramics International 42 7748-7756 2016/ 3

6. Cheonil Park, **Sungwon Kim**, Hyoun-Ee Kim, Tae-Sik Jang, Mechanical stable tantalum coating on a nano-roughened NiTi stent for enhanced radiopacity and biocompatibility, Surface & Coatings Technology 305 (2016) 139-145 2016/ 8

7. **Sungwon Kim**, Cheonil Park, Byeong-Seok Moon, Hyoun-Ee Kim, Tae-Sik Jang, Enhancement of osseointegration by direct coating of rhBMP-2 on target-ion induced plasma sputtering treated SLA surface for dental application, Journal of Biomaterials Applications 31 (6) 807-818 2017/ 1

8. Byeong-Seok Moon, **Sungwon Kim**, Hyoun-Ee Kim, Tae-Sik Jang, Hierarchical micro-nano structured Ti6Al4V surface topography via two-step etching process for enhanced hydrophilicity and osteoblastic responses, Materials Science and Engineering:C 73 90-98 2017/ 4

KOREA PATENTS

1. Hyoun-Ee Kim, Tae-Sik Jang, **Sungwon Kim**, et al., A method for preparation of

metal alloy with nanostructured surface comprising heavy metal using selective plasma etching and use thereof, Oct 2016, 10-166672 B1

PRESENTATIONS

1. **Sungwon Kim**, Hyun-Do Jung, Hyoun-Ee Kim, Fabrication of Porous Ti Implants with Complex Shape, Oral presentation, 9th World Biomaterials Congress, Jun 2012. China

2. **Sungwon Kim**, Hyun-Do Jung, Hyoun-Ee Kim, Fabrication of Porous Ti Implants with Complex Shape, Oral presentation, IUMRS-ICA 2012, Aug 2012, Korea

3. Hyun-Do Jung, Tae-Sik Jang, Min-Ho Kang, **Sungwon Kim**, Hyoun-Ee Kim, Young-Hag Koh, Yuri Estrin, Fabrication of Customized Porous Hydroxyapatite (HA) implants for Osteotomy, Poster presentation, 2013 Annual Meeting and Exposition, Apr 2013, USA

4. Min-Ho Kang, Hyun-Do Jung, Se-Won Yook, **Sungwon Kim**, Yuri Estrin, Hyoun-Ee Kim, Hydroxyapated Coated Porous Magnesium for Biomedical Applications, Oral presentation, 2013 Annual Meeting and Exposition, Apr 2013, USA

5. Hyun-Do Jung, Hui-Sun, Park, **Sungwon Kim**, Min-Ho Kang, Hyoun-Ee Kim, Yuri Estrin, Mechanical and biological analysis of compression molded polyetheretherketone-titanium (PEEK-Ti) composites, Oral presentation, Mechanical and biological analysis of compression molded polyetheretherketone-titanium (PEEK-Ti) composites, Apr 2013, USA

6. Tae-Sik Jang, **Sungwon Kim**, Hyoun-Ee Kim, Creation of Nanoporous Surface onto Co-Cr by Selective Plasma Ethching Method for Vascular Stent Application, Poster presentation, 2014 Annual Meeting and Exposition, Apr 2014, USA

7. Min-Ho Kang, Sae-Mi Kim, **Sungwon Kim**, Juha Song, Hyoun-Ee Kim, Hyun-Do Jung, Hybridized PEI/Silica and Hydroxyapatite Dual Coating on Porous Magnesium for Enhanced Corrosion Resistance, Poster presentation, 2014 Annual Meeting and Exposition, Apr 2014, USA

8. **Sungwon Kim**, Tae-Sik Jang, Juha Song, Hyoun-Ee Kim, Nanoporous Metal Surface via Selective Plasma Etching for Application of Polymer-Free Drug Eluting Stent, Oral presentation, 2014 Annual Meeting and Exposition, Apr 2014, USA

9. Jae-Uk Beak, Hyun-Do Jung, Tae-Sik Jang, **Sungwon Kim**, Min-Ho Kang, Juha Song, Hyoun-Ee Kim, Sustained Release Behavior of Drug-Loaded Calcium Phosphate Microspheres, Oral presentation, 2014 Annual Meeting and Exposition, Apr 2014, USA

10. **Sungwon Kim**, Tae-Sik Jang, Byeong-Seok Moon, Juha Song, Hyoun-Ee Kimg, Surface modification of Ti with micro/nano multi-scale roughness for the growth factor loaded implant, Oral presentation, 2015 Annual Meeting and Exposition, Apr 2015, USA

11. Min-Ho Kang, **Sungwon Kim**, Juha Song, Hyoun-Ee Kim, Application of Corrosion-Resistive Polyetherimide Coating to Vascular Magnesium Stent, Oral presentation, 2015 Annual Meeting and Exposition, Apr 2015, USA

12. Jae-Uk Beak, Hyun-Do Jung, Tae-Sik Jang, **Sungwon Kim**, Min-Ho Kang, Juha Song, Hyoun-Ee Kim, Accelerated Bone Regeneration of BMP-2 Loaded Hydroxyapatite Microspheres for Bone Filler Applications, Oral presentation, 2015 Annual Meeting and Exposition, Apr 2015, USA

13. Byeong-Seok Moon, Tae-Sik Jang, **Sungwon Kim**, Juha Song, Hyoun-Ee Kim, Multi-Scale Surface Modification on Ti-6Al-4V alloy by SPE process, Poster presentation, 2015 Annual Meeting and Exposition, Apr 2015, USA

14. Tae-Sik Jang, **Sungwon Kim**, Byeong-Seok Moon, Juha Song, Hyoun-Ee Kim, Multi-Scale Surface Modification of Ti for Orthopedic Implant Application, Oral presentation, 2015 Annual Meeting and Exposition, Apr 2015, USA